ATMOSPHERIC POLLUTANT DISPERSION MODELING FROM MULTIPLE STACKS USING GAUSSIAN PLUME MODEL

by

YUSRI BIN YUSUP

Thesis submitted in fulfillment of the requirements for the degree of Master of Science

May 2003

ACKNOWLEDGEMENTS

I would like to begin by expressing my gratitude to God Almighty Allah S.W.T. for His blessings on me and giving me the ability to complete this project.

First and foremost, I thank my supervisor and mentor **Prof. Dr. Mohd. Omar Abdul Kadir** for his support and encouragement. My co-supervisor Prof. Madya Dr. Nik Norulaini Abdul Rahman, I thank for her understanding nature and patience, making it possible for this project to run smoothly.

I greatly appreciate the assistance given to me by **Prof. Koh** who shared invaluable advice as well as ideas to proceed with my project. I also thank **Wai Fon** for all the thoughts and help that she gave me throughout my modeling work. Thanks to Mr. K. M. Chew from Toray Plastics (Malaysia) Sdn. Bhd. for providing information gravely needed regarding my work.

I also thank all my colleagues in the environmental laboratory, **Mrs. Norli, Mrs. Norhuda, Mr. Budi, Ms. Pang** for their friendship and support.

Last but not least, I thank my family for always being there for me, through the good and the bad.

TABLE OF CONTENTS

LIST OF TABLES AND FIGURES

Fig. 4.80 3-D plot of particulate concentration distribution for a 300 g/cm3 particulate density and 30 μm particulate diameter

NOMENCLATURE

A	Linear decay term for vertical dispersion in Schulman-Scire downwash (dimensionless)
A_e	Effective area for open pit emissions (dimensionless)
D	Exponential decay term for Gaussian plume equation (dimensionless)
D_B	Brownian diffusivity (cm/s)
D_r	Relative pit depth (dimensionless)
d_p	Particle diameter for particulate emissions (μm)
d_s	Stack inside diameter (m)
F_b	Buoyancy flux parameter (m^4/s^3)
F_m	Momentum flux parameter (m^4/s^2)
g	Acceleration due to gravity (9.80616 m/s^2)
h_b	Building height (m)
h_e	Plume (or effective stack) height (m)
h_s	Physical stack height (m)
h_s'	Release height modified for stack-tip downwash (m)
h_w	Crosswind projected width of building adjacent to a stack (m)
L_y	Initial plume length for Schulman-Scire downwash sources with enhanced lateral plume spread (m)
L_b	Lesser of the building height and crosswind projected building width (m)
p	Wind speed power law profile exponent (dimensionless)
Q_s	Pollutant emission rate (g/s)
R	Precipitation rate (mm/hr)
R_o	Initial plume radius for Schulman-Scire downwash sources (m)
r	Radial distance range in a polar receptor network (m)
s	Stability parameter = $g\frac{\partial\theta/\partial z}{T_a}$
S_{CF}	Splip correction factor (dimensionless)
Sc	Schmidt number = υ / D_B (dimensionless)

St	Stokes number = $(v_g/g)\ \ (u_*^2/\upsilon)$ (dimensionless)
T_a	Ambient temperature (K)
T_s	Stack gas exit temperature (K)
u_{ref}	Wind speed measured at reference anemometer height (m/s)
u_s	Wind speed adjusted to release height (m/s)
u_*	Surface friction velocity (m/s)
v_d	Particle deposition velocity (cm/s)
v_g	Gravitational settling velocity for particles (cm/s)
v_s	Stack gas exit velocity (m/s)
X	X-coordinate in a Cartesian grid receptor network (m)
Y	Y-coordinate in a Cartesian grid receptor network (m)
θ	Direction in a polar receptor network (degrees)
x	Downwind distance from source to receptor (m)
x_y	Lateral virtual point source distance (m)
x_z	Vertical virtual point source distance (m)
x_f	Downwind distance to final plume rise (m)
x^*	Downwind distance at which turbulence dominates entrainment (m)
y	Crosswind distance from source to receptor (m)
z	Receptor/terrain height above mean sea level (m)
z_r	Receptor height above ground level (i.e. flagpole) (m)
z_{ref}	Reference height for wind speed power law (m)
z_s	Stack base elevation above mean sea level (m)
z_i	Mixing height (m)
z_0	Surface roughness height (m)
β	Entrainment coefficient used in buoyant rise for Schulman-Scire downwash sources = 0.6
β_j	Jet entrainment coefficient used in gradual momentum plume rise calculations $= \frac{1}{3} + \frac{u_s}{v_s}$
Δh	Plume rise (m)
$\partial\theta/\partial z$	Potential temperature gradient with height (K/m)
Λ	Precipitation scavenging ratio (s^{-1})

λ	Precipitation rate coefficient $(s\text{-}mm/hr)^{-1}$
π	pi = 3.14159
ψ	Decay coefficient = $0.693/T_{1/2}$ (s^{-1})
ψ_H	Stability adjustment factor (dimensionless)
φ	Fraction of mass in a particular settling velocity category for particulates (dimensionless)
ρ	Particle density (g/cm^3)
ρ_{AIR}	Density of air (g/cm^3)
σ_y	Horizontal (lateral) dispersion parameter (m)
σ_{yo}	Initial horizontal dispersion parameter for virtual point source (m)
σ_{ye}	Effective lateral dispersion parameter including effects of buoyancy-induced dispersion (m)
σ_z	Vertical dispersion parameter (m)
σ_{zo}	Initial vertical dispersion parameter for virtual point source (m)
σ_{ze}	Effective vertical dispersion parameter including effects of buoyancy-induced dispersion (m)
υ	Viscosity of air = 0.15 cm^2/s
μ	Absolute viscosity of air = 1.81×10^{-4} g/cm/s
χ	Concentration $(\mu g/m^3)$
χ_d	Concentration with dry deposition effects $(\mu g/m^3)$

ABSTRAK

PEMODELAN PENYEBARAN PENCEMAR UDARA DARIPADA BEBERAPA CEROBONG MENGGUNAKAN MODEL PLUM GAUSSIAN

Satu model penyebaran pencemar udara jangka pendek berasaskan Gaussian yang seimbang telah dibina. Model in dinamakan HAWA. HAWA ditulis seperti Model Industrial Source Complex Short Term 3 (ISCST3) yand diprogram oleh Environmental Protection Agency (EPA). Model in boleh digunakan untuk memodel penyebaran pencemar udara daripada 10 cerobong dalam kawasan yang agak rata. Model in mempunyai ciri-ciri deposisi kering partikel, deposisi basah partikel, kesan bangunan ke atas plum, reputan pencemar udara tahap pertama dan kenaikan plum berdasarkan jarak. HAWA menghasilkan fail berbentuk text juga fail yang berbentuk Matlab©. Microsoft Visual C++© 6.0 telah digunakan untuk menulis model ini berbanding dengan model-model yang lain yang biasanya ditulis menggunakan bahasa FORTRAN©. Visual C++© digunakan supaya dapat menghasilkan suatu model yang senang diguna oleh pengguna.

Beberapa kes studi telah dijalankan untuk menunjuk kebolehan HAWA memodel pelbagai jenis keadaan atmosfera dan konfigurasi penempatan cerobong. HAWA telah memodel setiap kelas kestabilan Pasquill-Gifford (A hingga F) untuk menunjukkan kesan atmosfera ke atas plum. Konfigurasi cerobong yang berbeza telah dimodel menggunakan HAWA seperti konfigurasi selari dengan paksi x, konfigurasi selari dengan paksi y, konfigurasi berbentuk L. Kesan suatu bangunan terhadap plum juga telah dimodel oleh HAWA. Di samping itu, suatu model purata 24 jam kepekatan pencemar udara dan kesan deposisi kering penyebaran partikel-partikel yang besar telah disimulasikan oleh HAWA.

ABSTRACT

ATMOSPHERIC POLLUTANT DISPERSION MODELING FROM MULTIPLE STACKS USING GAUSSIAN PLUME MODEL

A short term steady state Gaussian-based air pollutant dispersion model has been developed. It is named HAWA. It follows closely to U.S. Environmental Protection Agency (EPA) Industrial Source Complex Short Term 3 (ISCST3) model. This model can be used to evaluate pollutant concentrations from elevated point sources (e.g. stacks) for up to 10 sources in moderate terrain. This model incorporates dry deposition of particles, wet deposition of particles, building downwash, first order decay of pollutant, and plume rise as a function of downwind distance. HAWA generates text file and Matlab© file as output. Microsoft Visual C++© 6.0 was used in writing the model in contrast to FORTRAN© that was used to programmed ISCST3. The former was used to develop a more user friendly model compared to other models that are difficult for use.

Case studies were conducted using HAWA to demonstrate its' ability to model various atmospheric conditions and stack configurations. Atmospheric conditions were changed using Pasquill-Gifford stability classes (A to F) to show the effect of the atmosphere to the behavior of a plume. Different stack configurations like X-aligned, Y-aligned, L-shaped configurations were used to show HAWA's capability in handling various stack arrangements. The affect of a building height to a plume was also modeled using HAWA. A 24-hour average dispersion of a pollutant from a stack in urban terrain together with the affect of dry deposition to pollutant dispersion was modeled using HAWA.

1. INTRODUCTION

1.1 Concept of modeling

Modeling is to represent real-world processes using simplified mathematical formulation. It is done to make it easier to understand and to predict the process that is being modeled. A model is always validated to ensure its accuracy. This includes taking note of the assumptions, the information used, the results produced by the model, and the conclusions inferred (Scotney, 2002).

In this case, mathematics is used to represent air dispersion in the atmosphere from multiple stacks.

1.2 Definition of air pollution

"Air pollution may be defined as the presence in the outdoor atmosphere of one or more contaminants or combinations thereof in such quantities and of such duration as may be or may tend to be injurious to human, plant, or animal life, or property or which unreasonably interferes with the comfortable enjoyment of life or property or the conduct of business" (Wark and Warner, 1976). Brunner defines air pollution as "the presence of matter or energy whose nature, location, or quantity produces undesirable environmental effects" (Brunner, 1985).

1.3 Types of air pollutants

Air pollutants are divided to primary pollutants and secondary pollutants. Primary pollutants are pollutants that are directly emitted from sources. Secondary pollutants are pollutants that are formed in the atmosphere by the reaction of primary pollutants with atmospheric gases (Seinfeld, 1976).

Primary pollutants are listed below:

1. Particulate matter
2. Sulfur compounds
3. Organic compounds

4. Nitrogen compounds
5. Carbon compounds
6. Halogen compounds
7. Radioactive compounds

(Wark and Warner, 1976)

The major classes of air pollutants would be inorganic compounds, organic compounds, and particulate matter (Brunner, 1985). The specific criteria pollutants would be particulate matter (PM), sulfur oxides (SO_x), nitrogen oxides (NO_x), volatile organic compounds (VOCs), and carbon monoxide (CO) (Cooper and Alley, 1994).

1.4 Impacts of air pollution to the environment

Air pollution has an affect on human beings and animals, vegetation, soils, and materials. In addition to this list come the climate, visibility, and solar radiation. Air pollution also poses a risk to production processes and safety. Due to the difficulty in acquiring quantitative measure of the effect of air pollution there were numerous debates on the actual effect of air pollution (Seinfeld, 1975).

One of the impacts of air pollution to the environment is visibility reduction, fog formation and precipitation, solar radiation reduction, and temperature and wind distribution alteration. The most readily observed effect of air pollution would be the reduction of visibility (Seinfeld, 1975). Besides visibility, air pollutants can also absorb radiation which would cause environment deterioration (Wark and Warner, 1976). One such phenomenon is known as global warming.

The second impact would be the effect of air pollution to materials. Dark smoke and high concentration of particulates would stain clothing and structures. Acid and alkaline particles (containing sulfur) would dissolve materials such as paint, masonry, electrical contacts, and textiles. Ozone, on the other hand would deteriorate rubber (Seinfeld, 1975).

Chlorophyll and photosynthesis in vegetation would be affected by air pollution, specifically by phytotoxicants (e.g. Sulfur dioxide, peroxyacetyl nitrate, ethylene, etc.). The plant would have growth defects or ultimately die (Seinfeld, 1975). Fluorides would cause plant damage and magnesium oxides would result in poor plant growth (Wark and Warner, 1976).

Last but not least effect of air pollution is on human beings. Common pollutants from air pollution such as carbon monoxide, oxides of sulfur, oxides of nitrogen, photochemical oxidants, and lead have different effects on human beings depending on concentration and period of exposure. Each pollutant causes different reaction in the human body ranging from eye and lung diseases to death (Seinfeld, 1975). It is extremely difficult to relate air pollutant concentrations to human health. The exposure time frame and also combination with other pollutants causes severe health deterioration (Wark and Warner, 1976).

1.5 Sources of air pollution

Air pollution can come from natural and unnatural sources. Furthermore, sources of air pollution can be divided into 2 major categories. The first category is stationary sources and the second category is mobile sources. The main concern of this work is the pollution that comes from stationary sources. Generally, the highest stationary source contributor to air pollution is power plants through burning of fossil fuel (Brunner, 1985). Manufacturing processes such as grinding, smelting, crushing, and grain milling and drying with industries that implement burning of fossil fuels also causes air pollution (Wark and Warner, 1976).

Different pollutants originate from different sources. Major sources of particulates are industrial sources, coal-burning and oil-burning electric power plants, and residential fuel combustion (Cooper and Alley, 1994).

Sulfur oxides (SO_x) come from burning sulfur or any material containing sulfur. Fossil-fuel combustion for electric power generation and nonferrous metal smelting are the major contributor. Furnaces also produce sulfur dioxide (Cooper and Alley, 1994).

Nitrogen oxides (NO_x) form when fuel is burned in air. Fuel-dependent industries would be the major sources of nitrogen oxides (Cooper and Alley, 1994).

Photochemical oxidants and VOCs (volatile organic compounds) would react with NO_x under sunlight to produce ozone (a strong oxidizing agent). Major sources of VOCs are petrochemical processes, surface coating, printing, and other processes involving organic solvents (Cooper and Alley, 1994).

Carbon monoxide (CO) comes mostly from incomplete combustion of carbonaceous fuel. Residential heating and industrial processes emit CO (Cooper and Alley, 1994).

1.6 Air pollution modeling

Air pollution modeling can be conducted in two methods; one is the use of a physical model and the second using computational techniques. The physical model includes the use of wind tunnels or water tanks to simulate the atmosphere at a smaller scale. This requires a high level of technical expertise and specialized facilities, resulting in considerable cost and time (Patrick, 1994).

Computational techniques, on the other hand, are categorized into two parts. The first category is the empirical model and the second category is the deterministic model. The empirical model needs the user to measure both the source and receptor locations to estimate the distribution of the source at receptor locations (Patrick, 1994).

The deterministic model is used in this project. This model uses simplified mathematical equations to represent the processes of the atmosphere along with emission source data to predict the impact of the source to the atmosphere.

The screening model and the refined model are categorized under the deterministic models. The screening model is able to model a limited amount of atmospheric conditions with simple assumptions made to reduce calculation time. The refined model, by contrast, has a broader range of atmospheric conditions that could be modeled (Patrick, 1994).

The initial emission characteristics, climatology, and topography are important in creating a dispersion profile from a source. It is dependent on ambient air temperature and pressure, presence of sunlight and/or clouds, and wind speed and direction. Topography plays a part in formulating a dispersion profile in terms of the presence of nearby obstacles (e.g. buildings, hills) that would yield different profile compared to a flat plain or absence of tall buildings (Brunner, 1985).

The dispersion of pollutants depends entirely on meteorological conditions such as wind speed and direction, and atmospheric stability. When wind is strong or good vertical mixing is present in the atmosphere, pollutants will be spread out quickly into a large volume of air, resulting in low concentrations. When the wind is low and an inversion is there, then pollutant concentrations will increase (Cooper & Alley, 1994).

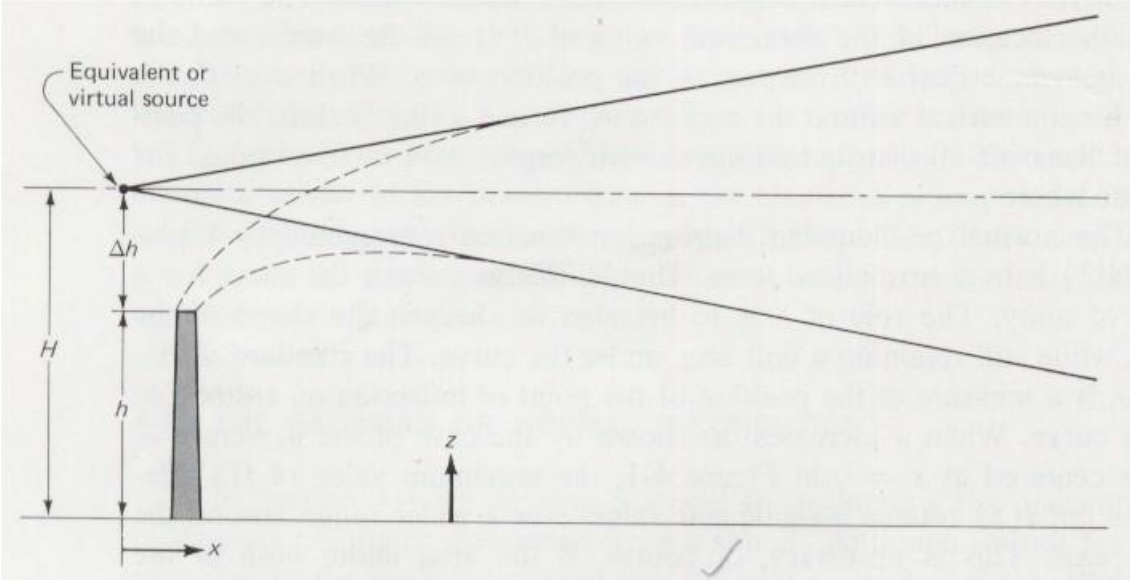

Fig. 1.1 A dispersion model with virtual source at an effective stack height, H.

A continuous emission of pollutants vented into constant wind of the atmosphere will initially rise. Then slopes down and travel with the average wind. This will dilute the pollutants and carry them away from the source. This is shown in Fig. 1.1. The plume will spread in both directions: horizontally and vertically from its centerline. This condition of distribution is defined as bi-normal. A way to model this situation is

to assume the wind as being constant and the plume is distributed by eddy diffusivities. It is also assumed that the pollutants are the same density as air.

The most common solution to this problem is to use the statistical nature of the dispersion process known as the Gaussian dispersion equation. The equation is as follows:

$$C = \frac{Q}{2\pi u_s \sigma_y \sigma_z} \exp\left[-\left(\frac{y^2}{2\sigma_y^2}\right)\right]\left\{\exp\left[\frac{-(z-H)^2}{2\sigma_z^2}\right] + \exp\left[\frac{-(z+H)^2}{2\sigma_z^2}\right]\right\}$$

where

C	=	steady state concentration at a location (x, y, z), µg/m^3
Q	=	emission rate, µg/s
σ_y, σ_z	=	horizontal and vertical distribution parameters, m
u	=	mean wind speed at stack height, m/s
y	=	horizontal distance from plume centerline, m
z	=	vertical distance from ground level, m
H	=	effective stack height, m

This equation is valid for aerosols, gases, particulate matter, and radioactive material. The calculations would be conservative, giving higher concentration results compared to observation concentration (Brunner, 1985).

Many different models have been tried with the same amount of success and failure. The most widely used model is nonetheless the Gaussian-based model. It is chosen because of two main advantages:

1. Simple and easily understandable.
2. The mathematical equations are relatively simple to apply in computer programs.

Some general relationships are needed to take notice of by using this equation. The downwind concentrations are directly proportional to the source, Q. The downwind ground-level concentrations are inversely proportional to wind speed. Ground-level concentration also generally increases until it has reached a maximum before decreasing. This is because the pollutants require time to spread to ground-level. Due to reflections of the ground, the pollutant concentration will increase until all the pollutants are spread upwards and outwards. Typically, unstable conditions of the atmosphere will decrease downwind concentrations. Lastly, the higher the effective stack height, H, the further away the maximum concentration will occur from the source (Cooper & Alley, 1994).

This fundamental equation is the basis for almost all United States Environmental Protection Agency (USEPA) computer program models. Sophistication is introduced in the model by adding modifications to this equation to model different situations such as adjustment to wind speed according to height, adjustments to the point of origin of the source using Briggs' plume rise equations, and adjustments according to buoyancy-induced dispersion. Dispersion coefficients are determined using atmospheric stability classes. The conditions of the surrounding area of interests to be modeled are also important by specifying the dispersion coefficients by determining whether it is an urban or rural area. Other modifications include stack-tip downwash, building downwash, effect of wet deposition on the plume, and effect of dry deposition on the plume. The equations used to add these modifications are stated in the following chapters.

The Gaussian model approximation will take on a normal bell-shaped curve when the distribution of values is plotted as shown in Fig. 1.2. The height of the curve is the maximum value in the distribution, and the square root of the variance represents the width of the curve. The dispersion coefficients are used to define the standard deviation of the concentration distribution. Meteorological conditions, surface characteristics, and distance from the source define the dispersion coefficients used in the Gaussian model (Patrick, 1994).

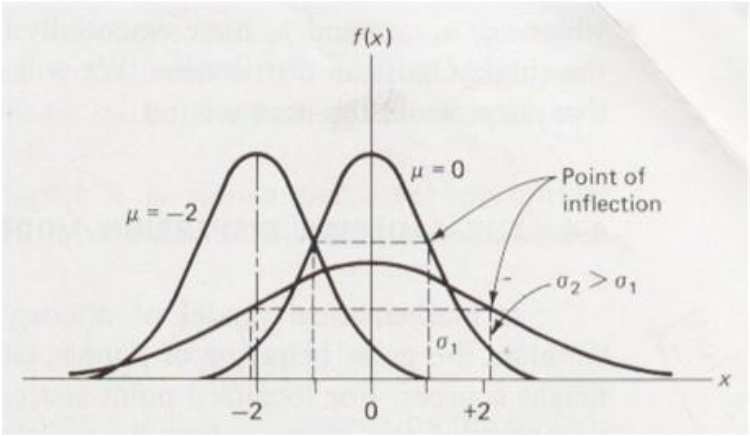

Fig. 1.2 The Gaussian distribution function of different values of μ and σ.

1.6.1 Adjustment of wind speed with height

Most wind measurements are taken near ground level. Wind speed typically increases with height. Wind speed can be adjusted according to height using a simple power law. The equation is presented in the coming chapter. The exponent coefficient is related to the stability class as well as whether is a rural or urban terrain (Cooper & Alley, 1994).

1.6.2 Briggs' plume rise

Plume rise is the initial rise of the plume before reaching its steady-state. The origin of this steady state is required to determine the effective stack height (stack height added with the height of the plume rise) to be used in the Gaussian model. The Briggs' plume rise formulas are currently recommended by the EPA to model thermally dominated plumes. The rise of the hot plumes is due to the higher temperature of the gases. Three parameters influence plume rise. They are meteorological conditions, stack characteristics, and physical and chemical nature of the gas (Wark & Warner, 1976). Thermal buoyancy makes the plume continue to rise even after it has bent over by the wind. This depends on a buoyancy flux term, wind speed, and distance downwind. (Cooper & Alley, 1994)

1.6.3 Dispersion coefficients

One method used to determine the dispersion coefficients is the use of stability classes that range from stability class A to stability class F. Stability class A is the most unstable class and has the greatest dispersion potential. Stability class F would be the most stable class and has the lowest dispersion ability. Classes A to C is used to model daytime while classes E and F, nighttime. Class D is known as the neutral class and can be used in both day and nighttime.

1.6.4 Urban/Rural dispersion coefficient

Most air models also allow the user to specify the use of urban or rural terrain dispersion coefficients. EPA has set up a guideline in determining if the terrain is rural or urban.

1.6.5 Stack-tip downwash

Stack-tip downwash is a phenomenon where the velocity of the effluent from stack is less than sufficient to counter the wind speed at stack height, resulting in lower effective stack height. The stack gas velocity would need to be at least twice the speed of the wind to prevent stack-tip downwash (Wark & Warner, 1976).

1.6.6 Building downwash

The presence of nearby buildings can cause an aerodynamic turbulence that will result in higher pollutant concentrations near to the source. Stacks that are near buildings that are less than 0.8 km from the source are required to include building downwash in process of modeling (USEPA, 1992).

1.6.7 Buoyancy-induced dispersion

Buoyancy-induced dispersion happens when velocity differences of the plume and the ambient air will result in turbulences at the edges of the plume.

1.6.8 Dry deposition and wet deposition

Dry deposition and chemical transformation assuming exponential decay simulate the removal and dilution of the plume because of gravitational settling of particles to the ground. The removal of particles due to precipitation is also modeled known as wet deposition (Cooper & Alley, 1994).

1.7 Objectives

The objectives of this research are as follows:

1. To develop a Gaussian-based air dispersion model computer program.
2. To conduct a case study using the above-mentioned program.
3. To validate the developed computer program model using Industrial Complex Source Short-Term (ISCST3).

2.0 LITERATURE REVIEW

2.1 The importance of air pollution modeling

Atmospheric pollutant dispersion modeling is important because it is needed to understand the impact of stacks emitting pollutants to the surrounding environment. Modeling has been known to evaluate the impact economically and swiftly compared to experimental analysis. Study of the impacts of air pollution emissions requires determination of the resulting ambient air quality because of these stacks. This could be achieved using two different approaches: field studies or modeling studies.

Modeling studies have long been an accepted method in studying the impact of pollutant emitting stacks. The ability to predict the impact of a proposed stack on the air quality and air pollution reduction plan is one of modeling strongest point. "The goal of any air modeling project is to predict ambient air concentrations at a particular location or receptor" (Patrick, 1994). Another point would be that is highly cost-effective method compared to field monitoring studies. Modeling also provide the only method to analyze the impact of a proposed new emission source, planning air pollution reduction, and planning emergency response plans for accidental releases. Models are important tools help us make better decisions concerning air pollution (Cheremisinoff, 1989).

It was said "[t]he ability to model atmospheric dispersion and to predict pollutant concentrations from a proposed new source are important parts of air pollution engineering." Recently, a lot of innovation and work were put on developing more sophisticated model although the accuracy is questionable. As long as the user is aware of the limitations, the model usage would be successful (Cooper & Alley, 1994).

Some of the uses of a model are:

1. Establishment of emission control legislation.
2. Evaluation of proposed emission control techniques and strategies.
3. Planning of locations of future sources of air contaminants.
4. Planning for the control of air pollution episodes.

5. Assessment of responsibility for existing levels of air pollution. (Seinfeld, 1975)

An example problem that requires the use of atmospheric dispersion modeling is to generally determine the stacks that are particularly responsible for unacceptable levels of pollution on the environment. Conducting experiments and tests to conclude this problem need costly technical expertise and problems in management between the companies involve. Modeling is needed to solve the problem quickly and inexpensively. The main objective of this work is to achieve that.

2.2 Models in general

Recently there are 3 types of model families that can be used for atmospheric dispersion modeling. The first is the Gaussian dispersion model (which most of the models are based on), the second is the integral-type model, and the third is the three-dimensional models.

The advantages of the Gaussian dispersion model are simple and derivatives option to take the obstacles and surface roughness into account. The gas is assumed to be same density as air (known as passive pollutants) and this model cannot compute extreme meteorological conditions. Atmospheric pollutant dispersion modeling follows the Gaussian model which assumes that the dispersion of pollutants depend on standard deviations (depending from the distance of the source) and the state of the atmosphere. The disadvantages are, it does not take obstacles or relief into account, only valid beyond 100 meters, cannot be adjusted, and requires correction for observation time, non-point source, surface roughness, and obstacles. (European Process Safety Centre, 1999)

The integral-type model is needed to model quite large heavy gas emissions. It still cannot model extreme meteorological conditions. The simulation can only be valid for the range covered by Gaussian dispersion. The advantages include reasonable cost and the model needed to be adjusted according to experience. The disadvantages are the same as the Gaussian model with no insufficient quantity of pollutant emitted, no high emission temperature, no emission at altitude, no deposition or absorption or the pollutant, obstacles and relief not taken into account, and no high surface roughness.

The three-dimensional model takes into account atmospheric turbulence, extreme meteorological conditions, all obstacles, light and heavy gases, initial conditions of the emission, and area close to the source. It is also verified by experiments and incident reports. The disadvantages are that this model is expensive to conduct, only limited from 0 to 500 meters, and uses simplifying hypothesis beyond 500 meters (European Process Safety Centre, 1999).

2.3 Models recommended by the EPA

These are some computer models that the US Environmental Protection Agency (EPA) suggests:

1. Industrial Source Complex (ISC)
2. COMPLEX 1
3. Rough Terrain Diffusion Model
4. CRSTER
5. RAM
6. CDM
7. MPTER
8. BLP
9. FDM

The ISC model is the model that I based my program on as stated before. This model is for most flat or moderately rolling terrains. There are 2 versions of this model, one is the Short-Term model and the other is the Long-Term model.

COMPLEX 1 model is screening model used for complex terrain. It is a Gaussian plume-based model. For terrains that are below the stack height, this model is similar to ISC. For terrains that are above the stack height, a correction factor is employed. There is no atmospheric deposition consideration for this model.

The Rough Terrain Diffusion model is a follow up screening model of COMPLEX 1. This model adds the ability to define a critical plume height, sloping, and plume reflection at the critical plume height. It uses a

reflection factor R to overcome unrealistically high concentration of pollutants using other models (Rafson, 1998).

The CRSTER model is the suggested simple terrain model for simulating a single point source located in a rural area as well as urban areas, for short term and annual average concentrations. CRSTER is a Gaussian plume model that calculates up to 19 individual point sources in a single run.

The RAM model can evaluate single or multiple point and area sources in an urban surroundings both short-term and long-term concentrations. RAM is also a Gaussian based plume dispersion model requiring input by the user.

CDM (Climatological Dispersion Model) model is specifically for the long-term concentration modeling in urban surroundings for limited amount sources. It can calculate seasonal or annual long-term concentrations.

The Multiple Gaussian Dispersion Algorithm with Terrain Adjustment (MPTER) is like the rest a Gaussian based model for multiple point sources (short-term and long-term) in a rural and urban environment. The MPTER model adjusts the plume height with terrain to simulate terrain changes.

The Buoyant Line and Point Source (BLP) model was coded to model emission from line source in a rural environment for short-term and long-term concentrations. This case is usually for buoyant emission vented through the roof (e.g. aluminum reduction plants). It can also model building downwash.

Fugitive Dust Model (FDM) is a refined model dealing with particulate matter emissions from fugitive sources in urban or rural areas with simple terrain. It still follows Gaussian model with both short and long term concentrations.

2.4 Air dispersion modeling studies

"A study of atmospheric dispersion of radionuclides at a coastal site using a modified Gaussian model and a mesoscale sea breeze model" is a paper that discusses ground level concentration and sky-shine dose due to radioactive emissions from a nuclear power plant at a coastal site using the standard Gaussian Plume Model (GPM) and the modified GPM suggested by Misra (Atmospheric Environment 14 (1980) 397), which incorporates fumigation effect under sea breeze condition. The difference in results between these two models is analyzed in order to understand their significance and errors that would occur if proper choice were not made. Radioactive sky-shine dose from 41Ar, emitted from a 100m stack of the nuclear plant is continuously recorded by environmental gamma dose monitors and the data is used to validate the modified GPM. It is observed that the dose values increase by a factor of about 2 times than those of the standard GPM estimates, up to a downwind distance of 6km during sea breeze hours. In order to examine the dispersion of radioactive effluents in the mesoscale range, a sea breeze model coupled with a particle dispersion model is used. The deposited activity, thyroid dose and sky-shine radioactive dose are simulated for a range of 30km. In this range, the plume is found to deviate from its straight-line trajectory, as otherwise assumed in GPM. A secondary maximum in the concentration and the sky-shine dose is also observed in the model results. These results are quite significant in realistically estimating the area affected under any unlikely event of an accidental release of radioactivity (Venkatesan et al., 2002).

A comparison of direct gamma dose rates from a stationary Gaussian plume using Lagrangian dose model (LDM), Gaussian plume model (GPM), and uniform cloud model (UCM). The comparison of the LDM results with the GPM indicated that both models predict comparable results in a homogeneous atmosphere. The UCM also compared well for ground releases; however, it cannot be used for elevated releases and short downwind distances (Raza and Avila, 2002).

"Dispersion modeling considerations for transient emissions from elevated point sources" was written in 2002 concerning air pollution dispersion modeling of tall stacks that emit infrequently during periods of a year. One of the problems of cases like this is that the predictions of maximum concentrations become increasingly influenced by the prevailing meteorology as the amount of time a source emits during a year shortens. A probabilistic approach has been used by randomly sampling the predicted concentrations at

different receptor locations over 5 different years. This approach is used to explore how source-operating time affects high-percentile concentration predictions of SO_2 from a single stack and a network of four stacks. For locations that are usually not downwind of sources and for low operational times, the inter-annual variability of predicted concentrations is shown to be high. Furthermore, the range of possible concentrations for a particular year is wide and suggests that model results under such conditions could easily be atypical, even when several years of meteorological data are used. The modeling also highlights how the probability distributions are affected by plant operating patterns for two cases: first, where sources are assumed to emit simultaneously and second, where they emit independent of one another. By considering ensembles in this manner, it is possible to derive median predicted concentrations and information concerning the probability of exceeding a certain concentration, thus providing decision makers with a richer source of information (Carslaw et al. 2002).

There was work done on modeling the benefits of a power plant emission control in Massachusetts in 2002. The paper "Modeling the benefits of power plant emission control in Massachusetts" discusses the results of combining emissions information, dispersion modeling, and epidemiologic evidence. They have developed an analytical modeling to evaluate the health benefits of controlling emissions on two power plants. They used the CALPUFF atmospheric dispersion model to estimate the impact of using Best Available Control Technology (BACT). With these results they estimated that there would be deaths of 70 per year in a population of 33 million individuals. The authors concluded these results could help decision makers to make the proper choice in different scenarios (Levy et al. 2002).

"Numerical study of atmospheric dispersion of a substance released from an industrial complex in the southern coast of Korea" was written in 2001 describing pollutant dispersion in a complex terrain with a shoreline in the summer and winter. RAMS (Regional Atmospheric Modeling System) was used. The assumptions made were that the wind was horizontally homogeneous with speeds below 2 ms^{-1}. They have discovered that with complicated wind fields and low wind speeds, the pollutant concentrations in the surroundings were high. When the wind field was uniform, the terrain effects were not significant and a mixing layer developed (Oh and Ghim, 2001).

The dispersion of contaminants under the wake of an obstacle was investigated in the paper "Experimental investigation of the residence of contaminants in the wake of an obstacle under different stability conditions". The decay duration, which is the time required for the contaminants to exit the wake region, is greater in stable atmospheric conditions because of lower wind speeds with higher concentration observed. It was also concluded that the decay duration was independent of atmospheric stability. The results matched with values calculated using empirical formulas from wind tunnel experiments (Mavroidis et al., 1999).

A study on comparing plume dispersion results from scaled field and wind tunnel on arrays of obstacles was done by Macdonald, Griffiths, and Hall. The results were that, at short distances from the source, the concentration profiles in the obstacle arrays were quite variable. At distances beyond two rows, the concentration profiles were well approximated by a Gaussian distribution laterally and a reflected Gaussian vertically. Plumes in the arrays were typically 2-4 times as wide compared to field results. At short to intermediate distances the plume width was approximate to the width of the obstacles. Typically, about one building height was the effective vertical displacement. This resulted in a total vertical growth of the plume which was 2-3 times larger than that in the open terrain at similar distances from the source. In the arrays of obstacles with width/height > 1, significant bodily deflection of the plume occurred for non-orthogonal wind directions. Compared to the wind tunnel, there was more variability in the field results, and some effects of the larger scales of turbulence were observed. However, the field results were qualitatively and in most cases quantitatively the same as those from the wind tunnel (Macdonald et at., 1998).

Hao, Raman, and Sethu held out a study on elevated accidental release from a space shuttle tower at the Kennedy Space Center in Florida with the influence of a stratified onshore flow. The temperature difference between land and ocean can generate a local sea-land circulation and a thermal internal boundary layer. Both play an important role in coastal dispersion. Results from a Gaussian dispersion model and those from numerical simulations show that the concentrations obtained from these two very different methods are of the same magnitude and patterns. Numerical simulations were performed by combining the Advanced Regional Prediction System with an Eulerian pollutant dispersion model. Numerical sensitivity experiments were conducted to investigate the effects of upwind stability, coastal topography, and calm

wind condition. Numerical results also show that the dispersion pattern from a continuous release is significantly different from that of a finite release (Hao et al., 1996).

A paper was written entitled “Field experiments of dispersion through regular arrays of cubic structures” in 1997. A scaled field measurements have been made on the dispersion of a plume released straight through arrays of cubes of various placement. It was discovered that the lateral concentration profiles were Gaussian in all cases. Close to the source, the lateral dispersion parameter increased, compared to that of a plume in open terrain and was highest for the most packed cubic structures placement. Even so the plume dimensions increased in the array, the reduction in advection velocity resulted in ground-level concentrations that were not too different from those of a plume in open terrain. This behavior can be modeled by a Gaussian-plume-type expression for time-averaged concentration (Macdonald et al., 1997).

Predictions of hydrogen sulfide and ammonia were made using a modified Pasquill-Gifford model. Two approaches were done, the first using empirical corrections to the Gaussian model for direct downwind distances with neutral atmospheric stability conditions. The second was based on improved procedures for estimation of the dispersion coefficients. The new dispersion coefficients were obtained from experimental data under neutral and stable atmospheric conditions (Rege et al., 1996).

Jin and Chang wrote a paper on a method of estimating the dispersion coefficients used in the Gaussian model from experimental data without prior data on the change of wind direction. The value of the lateral dispersion coefficient can be determined by solving the Gaussian model with a concentration ratio while the vertical dispersion coefficient determined using a dimensionless concentration ratio. This method can be used on the field as well as model calibration and validation (Jin & Chang, 1996).

Another study on dispersion on group of structures was conducted by Davidson, Snyder, and Lawson in 1996. The paper entitled “Wind tunnel simulations of plume dispersion through group of obstacles” confirmed that the mean structure of a plume has a Gaussian form as it passes through an array of obstacles. Thus, the mean lateral spread and decay of mean concentration of the plume with downstream distance resemble that of a plume released under identical conditions where the obstacle array is not present. High-

strength turbulence rapidly mixes the plume internally, reducing the strength of concentration changes within the plume (Davidson et al., 1996).

The paper "Plume dispersion through large groups of obstacles – a field investigation" discusses the behavior of neutrally buoyant plumes released below the height of the obstacles as well as alongside the obstacles. Certain average concentrations of the plume stay the same even when it is passing the obstacles like the lateral growth and decay along the center line with downwind distance. Meanwhile, the vertical growth increased by 40 to 50 percent. The r.m.s. variations of concentration within the plume are reduced. A clipped Gaussian distribution is proven to be appropriate for the concentration fluctuations within the array plume (Davidson et al., 1995).

Wind-tunnel tests were conducted to examine how the standard Gaussian dispersion parameters might be expected to vary with source height and downwind distance, both with and without the presence of several building configurations. For isolated sources, there was no obvious effect of release height on the lateral dispersion coefficient, on the other hand, there appeared to be a dependence of the vertical dispersion coefficient on source height. The effect of buildings was dependent on the particular configuration, and in general the lateral and vertical dispersion coefficient appeared to be affected differently. Particularly significant effects were observed for cases when the plume was directed at an oblique angle to the buildings. For releases less than the building height there was no effect of release height on the dispersion coefficient. It was also observed that for a stack 3.5 times the average building height, the lateral dispersion coefficient was still significantly affected by the presence of the building array (Singh et al., 1994).

A study was done comparing air dispersion modeling results with ambient air sampling data at Tacoma Landfill. Dispersion modeling was performed with measured stack emission data using Industrial Source Complex (ISC) to determine the groundlevel concentrations of VOCs from the air stripper, flares, and active portion of the landfill for comparison with the measured ambient air data collected during 1992 (Griffin et al., 1994).

A paper discusses the importance of pollutant dispersion along the nominal wind direction written by Straja. From the statistical point of view, the author concluded that for the case of a continuous point source there

is no significant difference between the predictions of the Gaussian plume and dispersion model. The author also states that the Gaussian plume model is useful just for continuous source, while the dispersion model can be used to estimate pollutant concentration from multiple sources and both continuous and instantaneous (Straja, 1994).

Equations were derived from the Gaussian plume model to describe the critical downwind distance, wind speed, and plume rise values that result in maximum ground-level concentrations under downwash conditions. The result of higher ground-level concentrations with respect to downwind distance and wind speed under downwash conditions shows the relationship between critical parameters, the physical parameters of a source, and the dimensions of a nearby building. The results are meant to a better understanding of the dispersion process and its mathematical representation. Examples for Schulman-Scire and Huber-Snyder downwash treatments for enhanced and regular sigmas are provided (Bowman, 1994).

2.5 Air dispersion model development

A paper was written on the development of a model to estimate concentrations from a source in a complex terrain. The model uses the assumptions that the concentration at a receptor is the combination of concentrations cause by two asymptomatic states. The first is that the plume remains horizontal and the second is that the plume climbs over a hill. A function of the fractional mass above the dividing streamline height weights the two states. The model works as good as a well-known model CTDMPLUS designed for use in complex terrain (Venkatram et al., 2001).

In 1998, an urban Gaussian dispersion model was developed for application in urban air quality management in London. It was called Ambient Background Model (ABM). Hourly meteorological data for the whole year are combined with a detailed gridded emission inventory, covering traffic and non-traffic point and area source emissions, to predict annual average air quality at a central urban background monitoring site. A odeling domain of 100 km by 100 km around the city were calculated for the components Nox, PM10, C6H6, NMVOC and CO. The impact of sources outside the odeling domain is estimated using EMEP European long-range model. The results of the odeling exercise are compared to measured ambient data at the central urban background site London Bloomsbury for 1993. The

comparisons show that the ABM model gives good predictions of annual average concentrations, and is capable of odeling hourly fluctuations in air quality with acceptable results (Seika et al., 1998).

A review of AIRSCAPE was written by Kumar, Madasu, and Mahurkar. An interface to the Industrial Source Complex Model was developed by Alpha Terra, Kohler, Wisconsin. AIRSCAPE is a Windows-based program for developing ISC2 input files using a graphical user interface in Windows. The hardware required to run AIRSCAPE is as follows: an 80386-, an 80486-, or a Pentium-based IBM or compatible; a minimum of 4 MB RAM; 1.44 MB, 3.5-inch floppy disc-drive; and Microsoft Windows 3.1. The software is found to be a very useful tool to run the ISC2 model, and it can be used to train new employees on air quality modeling process (Kumar et al., 1995).

2.6 Wind speed in air dispersion modeling

The paper "A mathematical model for the dispersion of air pollutants in low wind conditions" was wrote by Sharan, Yadav, and Singh. This study assumes constant eddy diffusivity coefficients in the advection-diffusion equation. The solution simplified to the standard Gaussian plume equation when thin plume approximation is used. The solution also matches the solution of Gaussian plume equation for ground-level concentration at the plume centerline. The model uses the data collected from experiments conducted at the Indian Institute of Technology, Delhi (India). The results are reasonable good when the limitations of the model were considered for 30 min and 3 min averaging (Sharan et al., 1996).

A general method for determining the effective transport wind speed, u, in the Gaussian plume equation is discussed in the paper "Determination of transport wind speed in the Gaussian plume diffusion equation for low-lying point sources. Physical arguments are given for using the generalized u instead of the often adopted release-level wind speed with the plume diffusion equation. Simple analytical expressions for u applicable to low-level point releases and a wide range of atmospheric conditions are developed. A non-linear plume kinematic equation was derived using these expressions (Wang, 1996).

The dispersion coefficients schemes were compared for air pollutant dispersion in low winds. Specifically, schemes viz., standard, split sigma, split sigma theta, segmented plume (I) and (II), short-term averaging

and U min approach are studied through inter-comparison. The concentration formula used in this inter-comparison is obtained from the steady-state advection-diffusion equation. The results show that with hourly data of wind velocity and standard deviation of horizontal wind direction (sj) split sigma and split sigma theta schemes perform much better than the traditional standard method as they take into account the wind direction fluctuations for the horizontal dispersion. On the other hand, with high-frequency data of wind velocity and sj, schemes like segmented plume (I) and (II) and short-term averaging simulate the observations much better especially in terms of the multiple peak nature of the concentration distribution. The influence of wind fluctuations from instantaneous plumes is captured by the high-frequency data. Further, short-term averaging scheme has the advantage of not requiring sj and still performing well. The difference in these results and those obtained from the Gaussian plume solution has been found to be marginal (Sharan et al., 1995).

2.7 Wet deposition

"Wet removal of pollutants from Gaussian plumes: Basic linear equations and computational approaches" was written by Hales. The paper presents a procedure that can be used as a guide to improve the formulation of the wet removal of pollutants from Gaussian plumes. The approach takes the form of a set of analytical equations that correspond to five kinds of Gaussian plume formulations: standard bivariate-normal point-source plumes, line-source plumes, unrestricted instantaneous puffs, and point-source plumes and puffs that experience reflection from inversion layers aloft. These equations represent the concentration of scavenged pollutants in falling raindrops and are the same in complexity to their associated gas-phase plume equations. They are strictly linear, thus allowing superposition of wet-deposition contributions by multiple plumes. It preserves linearity by assuming that pollutant-gas solubility and mass-transport parameters are concentration independent – a convenient feature for multi-source Lagrangian models, which usually rely on superposition to compute collective plume behavior. This assumption is reasonably well justified for gaseous pollutants whose water solubility obeys Henry's law, and it can be extended to moderately deviant systems by linearization of the associated equations, although it can produce radically incorrect results for strongly nonlinear systems. The approach assumes negligible vertical redistribution of the plume by "washdown" caused by absorption and subsequent desorption of pollutant from the falling rain. This assumption is justified under most practical conditions because vertical transport by atmospheric

mixing largely obscures washdown effects. The approach also assumes vertical rainfall and no aqueous-phase reaction, a constraint that can be removed for simple, linear reacting systems by appropriate adaptation of the associated equations. The procedure also assumes that interactions between the plume and clouds are negligible – a situation that often can be justified in the case of gas scavenging but can become problematic for suspended particulate matter, where in-cloud capture mechanisms tend to dominate (Hales, 2002).

2.8 Industrial Source Complex (ISC)

In the year 2000, there was developmental work done on the existing Gaussian plume model called PRIME. PRIME (plume rise model enhancements) was evaluated and discussed in the paper "Development and evaluation of the PRIME plume rise building downwash model". The paper presented the formulation and compared the results of the model with field and wind-tunnel observation (Schulman et al., 2000).

A program called SAFE_AIR was developed and evaluated with air pollution and laboratory experiments. This program simulates the transport and diffusion of airborne pollutants using Gaussian plume segments as well as puff. This model can deal with non-stationary and in-homogeneous conditions. The model was evaluated using field data (convectively unstable and neutral conditions from KNRC Katrex experiments on flat terrain) and wind tunnel observation from EPA Rushil experiments wind tunnel with two-dimensional schematic hill under neutral conditions. The conclusions of the paper are that the model works better simulating the wind-tunnel experiments compared to the open air experiment, the model gives relatively accurate results under stable conditions, model results are better for elevated sources, and the most important function is the Igl function of the program (Canepa et al. 2000).

A paper was written in 1997 about the improvements of the EPA industrial source complex dispersion model. The paper states that since its development in the 1970s by the U.S. Environmental Protection Agency, this widely used model has been updated as state-of-the-science techniques have become available. Some of the recent modifications to the ISC2 model include a dry-deposition algorithm that can account for a full range of particle size distributions and an algorithm for calculating wet-deposition flux using the scavenging coefficient approach. These modifications, which are part of the current ISCST3 model, are

described in detail within this paper. In addition, a plume depletion model demonstration was performed to compare observed and estimated crosswind integrated concentrations of a depositing tracer as functions of travel time and stability (Atkinson et al., 1997).

Another paper was written on ISC entitled Sensitivity of the Industrial Source Complex model to input deposition parameters. This study checks the sensitivity of the maximum model predictions due to changes in input parameters controlling deposition, for example the shape of the particle size distribution, resolution of the size distribution, and scavenging coefficients. The modeled deposition values are more sensitive because of the changes in these parameters than the concentrations. The model is particularly sensitive to the use of the plume depletion option, with deposition values lowered by up to 40% when the depletion option is selected. Changes in the specification of the particle size distribution affected the highest deposition values by as much as 25%. Neither concentration nor deposition seems particularly sensitive to the use of gridded terrain data (Schwede and Paumier, 1997).

3.0 METHODOLOGY

3.1 HAWA

The Gaussian plume model is used in HAWA to calculate the concentration of pollutants at selected places of interests, better known as receptors. A circular grid can also be set up to roughly determined the highest concentration of pollutants. The equations used are based from EPA Model Industrial Source Complex (ISC3), widely used around the world for modeling atmospheric dispersion. Modifications to the Gaussian model are plume height, stack-tip downwash, buoyancy-induced dispersion, building downwash, dry deposition, and wet deposition. HAWA could calculate up to 10 different point sources. The equations used would be explained in detail later in the chapter. HAWA is a Windows based program and could run on any computer with Windows 95 and above.

HAWA is based on Industrial Source Complex (ISC) Short Term Model and it uses a straight-line, steady state Gaussian plume equation with modifications. It is widely used worldwide to simulate pollutant dispersion in a typical industrial source complex. It is coded using FORTRAN language. The usage of the program is fairly complex where the input file requires a bit of programming knowledge and specific keywords and spacing. Although this allow a lot of flexibility of the program, it causes the modeling process to be more time consuming and difficult. HAWA has been coded the same equations used in ISC3 but used a more recent programming language Visual C++ 6. This allows the program to be able to run on any windows installed computer and the interface is user friendly. I made it able to calculate pollutant dispersion for 10 different elevated sources (e.g. stacks) on 10 receptor points.

HAWA is developed to show quickly and cheaply the effect of stacks on the environment. The stacks responsible on the highest concentration on a given receptor would be able to be identified. Ten stacks are deemed enough to picture a typical industrial site for this case and ten receptors to depict the quality of the air surrounding the industrial site.

The features available in HAWA are as follows. Receptor could be placed anywhere according to their x, y coordinates. The z-coordinate is the height from sea-level. The origin is assumed to be (0,0). Stacks are also placed this way, where the user is needed to input the location of the stacks.

Atmospheric data like, atmospheric pressure, ambient temperature, wind speed and direction (the direction is from where the wind is coming from), averaging time (up to 5 hours), and mixing height (the mixing height is the maximum allowable height the pollutant would disperse) are needed for the program to run. The user also needs to determine whether the site is rural or urban. HAWA can also calculate stack-tip downwash. Precipitation rate is used if wet deposition is needed to be modeled. Stability class with the options of Stability A, B, C, D, E, and F is also considered. Stability class A is very unstable, B moderately unstable, C slightly unstable, D neutral, E slightly stable, and F stable.

The data needed by the user for the stacks are stack gas temperature, inner diameter of stack, stack gas velocity, volumetric flowrate of the gas, molecular weight of the gas (it is usually 28.9 g/g-mol for combustion sources), heat emission rate of the stack, and stack height. These are needed to calculate the plume rise. Choices of plume rise are Briggs plume rise and the Schulman plume rise.

Half life is needed if the half life of the pollutant modeled is known. If the stack gas is buoyancy induced (where the gas moves upward because of the momentum before it reaches a steady state) then the user is needed to check the box titled “buoyancy-induced”.

Building-downwash is used when a building is directly in the plume of the gas causing the gas to disperse. The height and width of the building concerned is required with box checked titled “building-downwash”. “Building location” means the location of the building, whether it is at the side of the plume or right in the middle of the plume. The Schulman-Scire plume rise is used when modeling building downwash.

Dry deposition is used when modeling particulates in the exhaust of the stack. Particle density and particle diameter are needed.

Instead of using the 10 receptors, the user can also use the receptor grid to initially determine the location of the highest concentration of pollutants. The receptor grid will construct a circular grid around the origin of (0,0). The length between rings is needed with the amount of receptors on each ring. The receptors are equally distributed around the ring. The amount of circular grid is also required. The height from sea level is the height of the receptor from the sea level.

Bar graphs could be displayed to show the distribution of pollutants on 10 receptors. Meanwhile the pie chart will show the percentage contribution of pollutants on receptor 1 from different stacks.

The accuracy of these data is pertinent for a viable estimate of the pollutant dispersion. It is often said that the data and not the equations that causes the wrong simulation of pollutant dispersion.

3.2 The equations

3.2.1 Plume rise equations

Stack-tip downwash is first considered before calculating plume rise. Stack-tip downwash occurs when the velocity of the stack is insufficient compared to the wind speed causing plume downwash at the stack exit. This can be prevented by increasing the stack gas velocity at least 1.5 times higher than the wind speed (Wark and Warner, 1976). The conditions of stack-tip downwash is as follows,

$$h_s' = h_s + 2d_s\left[\frac{v_s}{u_s}\right] \quad \text{for } v_s < 1.5u_s$$

or

$$h_s' = h_s \quad \text{for } v_s \geq 1.5u_s$$

This option is available for use in HAWA if the user requires it. It must be noted that the following plume rise equations assume no stack-tip downwash.

HAWA uses Briggs' plume rise equations to simulate plume rise from an elevated source (e.g. stack). The buoyancy flux parameter, F_b (m^4/s^3), is first calculated. The equation is as follows,

$$F_b = g v_s d_s^2 \left(\frac{\Delta T}{4 T_s} \right)$$

The temperature difference of the stack temperature and the ambient temperature is needed to determine the type of plume release flux, $\Delta T = T_s - T_a$. The temperatures are in Kelvin (K). They are they buoyancy and momentum fluxes. The momentum flux parameter, F_m (m^4/s^2), is calculated using the following equation,

$$F_m = v_s^2 d_s^2 \frac{T_a}{4 T_s}$$

There are 3 types of atmospheric conditions that dictate the equations used to calculate plume rise height. They are the unstable, neutral, and stable conditions. Unstable condition stands for the A, B, and C stability classes. The neutral condition denotes the D stability class, while stable condition denotes the E and F stability class. The following charts describe the procedure of calculating the plume rise height for these 3 different conditions.

Jet entrainment is a constant needed in some of the equations included with the plume rise equations. The jet entrainment equation is as follows,

$$\beta_j = \frac{1}{3} + \frac{u_s}{v_s}$$

$(\Delta T)_c$ is a number that determines whether a plume rise is buoyancy dominated or momentum dominated. If $(\Delta T)_c \geq \Delta T$ the plume rise is buoyancy dominated and if $(\Delta T)_c < \Delta T$ the plume rise is momentum

dominated. The buoyancy flux parameter, Fb, determines the $(\Delta T)_c$ equation used as shown in the following flowchart.

The distance of final rise denoted as x_f and x_{max} (x_f used for buoyancy dominated plume rise and x_{max} used for momentum dominated plume rise) is the distance where the plume has reached the final rise height. Other equations are used to calculate the height before this distance is reached for both the buoyancy dominated plume rise and the momentum dominated plume rise.

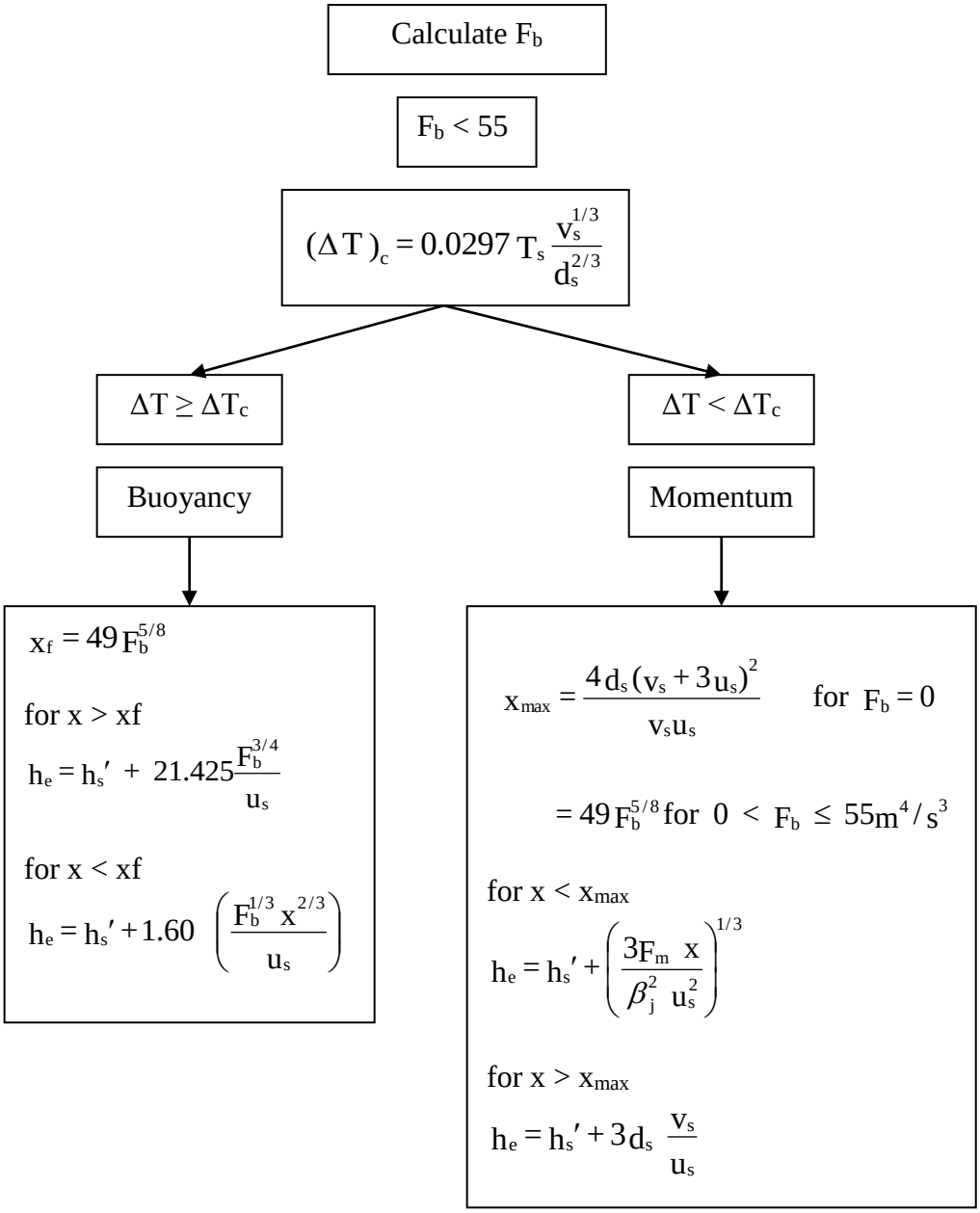

Fig. 3.1 Flowchart calculating Briggs' plume rise for unstable/neutral atmospheric conditions if $F_b < 55$

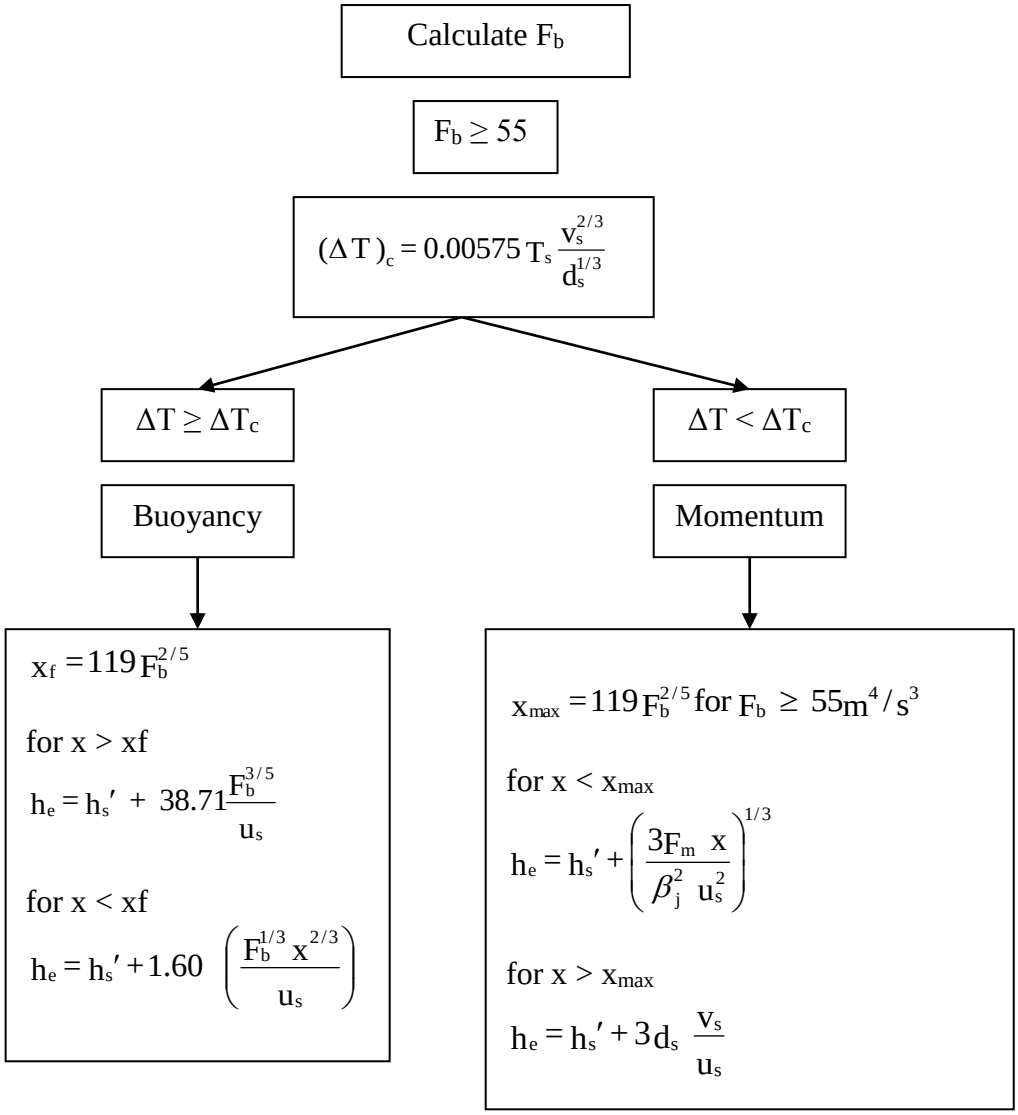

Fig. 3.2 Flowchart calculating Briggs' plume rise for unstable/neutral atmospheric conditions if $F_b \geq 55$

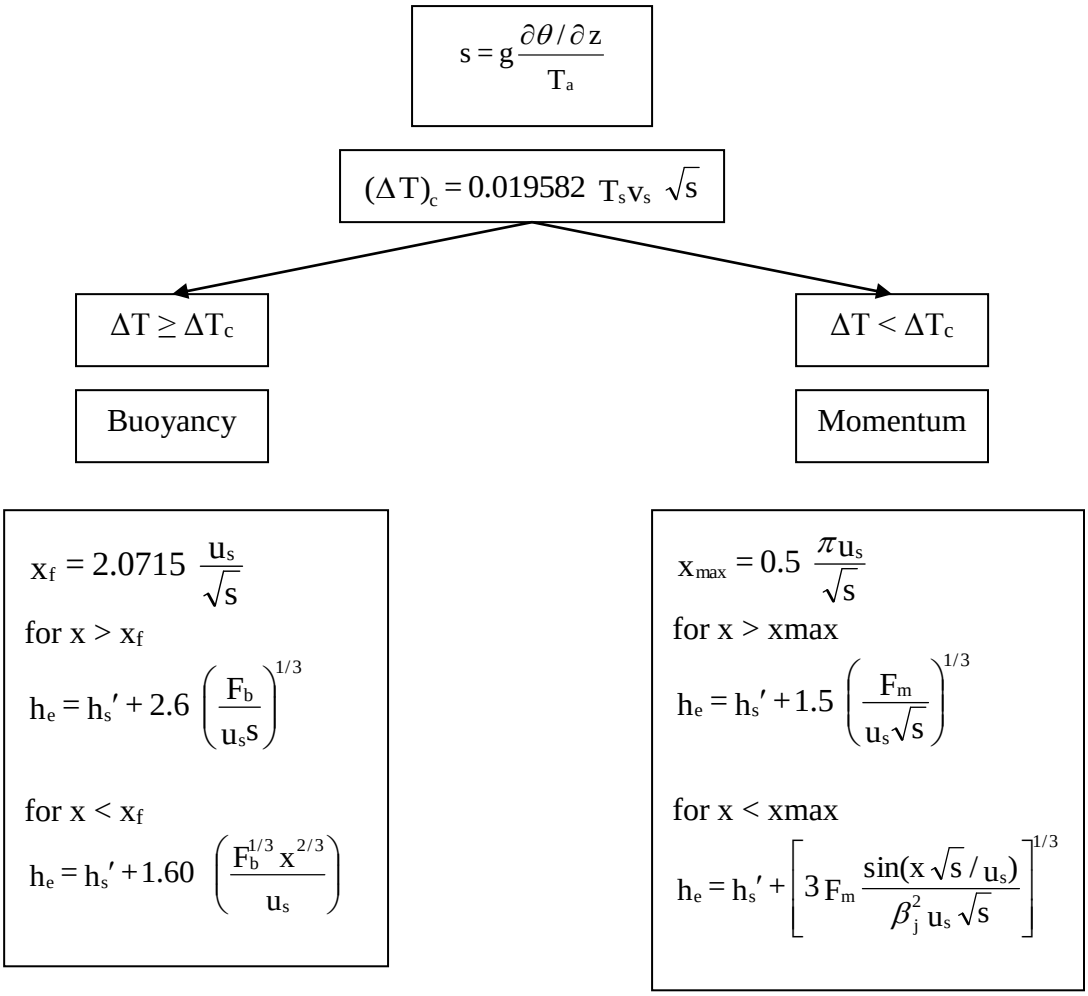

Fig. 3.3 Flowchart calculating Briggs' plume rise for stable atmospheric conditions

Stability class E has a $\partial\theta/\partial z$ of 0.020 K/m and stability class F has a $\partial\theta/\partial z$ of 0.035 K/m.

These equations have been coded in Visual C++ 6.0 in the class StackHeight(double). There are 10 classes of StackHeight(double), one class for each stack for 10 stacks.

3.2.2 The Dispersion Parameters

HAWA implements Pasquill-Gifford curves to calculate the dispersion parameters, σ_y and σ_z for both rural and urban terrain. The lateral, σ_y, dispersion parameters are as follows,

$$\sigma_y = 465.11628(x)\tan(TH)$$

$$TH = 0.017453293[c - d\ln(x)]$$

The vertical dispersion parameter, σ_z, is represented as,

$$\sigma_z = ax^b$$

The constants a, b, c, d, are listed in the following tables,

Table 3.1 Constants c and d used in obtaining lateral dispersion parameters, σ_y

Pasquill Stability Category	c	d
A	24.1670	2.5334
B	18.3330	1.8096
C	12.5000	1.0857
D	8.3330	0.72382
E	6.2500	0.54287
F	4.1667	0.36191

Table 3.2 Constants a and b used in obtaining vertical dispersion parameters, σ_z

Pasquill Stability Category	x (km)	a	b
A*	<.10	122.800	0.94470
	0.10 – 0.15	158.080	1.05420
	0.16 – 0.20	170.220	1.09320
	0.21 – 0.25	179.520	1.12620
	0.26 – 0.30	217.410	1.26440
	0.31 – 0.40	258.890	1.40940
	0.41 – 0.50	346.750	1.72830
	0.51 – 3.11	453.850	2.11660
	>3.11	**	**
B*	<.20	90.673	0.93198
	0.21 – 0.40	98.483	0.98332
	>0.40	109.300	1.09710
C*	All	61.141	0.91465
D	<.30	34.459	0.86974
	0.31 – 1.00	32.093	0.81066
	1.01 – 3.00	32.093	0.64403
	3.01 – 10.00	33.504	0.60486
	10.01 – 30.00	36.650	0.56589
	>30.00	44.053	0.51179

*The maximum value of σ_z must be 5000 m

**σ_z is equal to 5000 m.

Pasquill Stability Category	x (km)	a	b
E	<.10	24.260	0.83660
	0.10 – 0.30	23.331	0.81956
	0.31 – 1.00	21.628	0.75660
	1.01 – 2.00	21.628	0.63077
	2.01 – 4.00	22.534	0.57154
	4.01 – 10.00	24.703	0.50527
	10.01 – 20.00	26.970	0.46713
	20.01 – 40.00	35.420	0.37615
	>40.00	47.618	0.29592
F	<.20	15.209	0.81558
	0.21 – 0.70	14.457	0.78407
	0.71 – 1.00	13.953	0.68465
	1.01 – 2.00	13.953	0.63227
	2.01 – 3.00	14.823	0.54503
	3.01 – 7.00	16.187	0.46490
	7.01 – 15.00	17.836	0.41507
	15.01 – 30.00	22.651	0.32681
	30.01 – 60.00	27.074	0.27436
	>60.00	34.219	0.21716

Urban terrain uses different types of equations to determine the lateral and vertical dispersion parameter. The equations are the result of the studies conducted by McElroy-Pooler. The equations are shown in the following tables.

Table 3.3 McElroy-Pooler equations to determine the lateral dispersion parameter, σ_y

Pasquill Stability Category	σ_y(meters)*
A	$0.32 \text{ x } (1.0 + 0.0004 \text{ x})^{-1/2}$
B	$0.32 \text{ x } (1.0 + 0.0004 \text{ x})^{-1/2}$
C	$0.22 \text{ x } (1.0 + 0.0004 \text{ x})^{-1/2}$
D	$0.16 \text{ x } (1.0 + 0.0004 \text{ x})^{-1/2}$
E	$0.11 \text{ x } (1.0 + 0.0004 \text{ x})^{-1/2}$
F	$0.11 \text{ x } (1.0 + 0.0004 \text{ x})^{-1/2}$

Table 3.4 McElroy-Pooler equations to determine the lateral dispersion parameter, σ_z

Pasquill Stability Category	σ_z(meters)*
A	$0.24 \text{ x } (1.0 + 0.001 \text{ x})^{1/2}$
B	$0.24 \text{ x } (1.0 + 0.001 \text{ x})^{1/2}$
C	0.20 x
D	$0.14 \text{ x } (1.0 + 0.0003 \text{ x})^{-1/2}$
E	$0.08 \text{ x } (1.0 + 0.0015 \text{ x})^{-1/2}$
F	$0.08 \text{ x } (1.0 + 0.0015 \text{ x})^{-1/2}$

*x is in meters

3.2.3 Lateral and vertical virtual distances

Lateral and vertical virtual distances are used in calculating the modified lateral and vertical dispersion parameters for building downwash.

The lateral virtual distance for rural terrain is

$$x_y = \left(\frac{\sigma_{yo}}{p} \right)^{1/q}$$

The vertical virtual distance for rural terrain is

$$x_z = \left(\frac{\sigma_{zo}}{a} \right)^{1/b}$$

The constants p and q are listed in the following table. The constants a and b are shown in section 3.2.2.

Table 3.5 The constants p and q used in lateral virtual equation

Pasquill Stability Category	p	q
A	209.14	0.890
B	154.46	0.902
C	103.26	0.917
D	68.26	0.919
E	51.06	0.921
F	33.92	0.919

3.2.4 Plume height for wake effects determination

It is recommended to use the Schulman-Scire plume rise when building downwash is concerned instead of the above mentioned Briggs' plume rise equations. It is must be noted that the Schulman-Scire plume rise is used in conjunction with Schulman-Scire refined building downwash. The condition when Schulman-

Scire is used when the stack height is less than the building height plus half of the lesser building height or width.

The plume height is first determined using Briggs' momentum-dominated plume rise at a distance of 2 building heights. The jet entrainment factor and stability factor are also needed.

$$h_e = h_s' + \left[3\,F_m \frac{\sin(x\sqrt{s}/u_s)}{\beta_j^2\, u_s \sqrt{s}} \right]^{1/3}$$ stable condition

$$h_e = h_s' + \left(\frac{3F_m\ x}{\beta_j^2\ u_s^2} \right)^{1/3}$$ unstable/neutral condition

$$s = g\frac{\partial\theta/\partial z}{T_a}$$ stability parameter

$$\beta_j = \frac{1}{3} + \frac{u_s}{v_s}$$ jet entrainment

Plume rise, denoted as z (in meters), equations are shown below depending on different atmospheric conditions,

$$Z^3 + \left(\frac{3L_y}{\pi\beta}\right)Z^2 + \left(\frac{6R_oL_y}{\pi\beta^2} + \frac{3R_o^2}{\beta^2}\right)Z = \frac{3F_bx^2}{2\beta^2u_s^3} + \frac{3F_mx}{\beta_j^2u_s^2}$$ neutral conditions

$$Z^3 + \left(\frac{3L_y}{\pi\beta}\right)Z^2 + \left(\frac{6R_oL_y}{\pi\beta^2} + \frac{3R_o^2}{\beta^2}\right)Z = \frac{3F_bx^2}{2\beta^2u_s^3} + \frac{3F_m\ \sin\left(\frac{x\sqrt{s}}{u_s}\right)}{\beta_j^2\ u_s\sqrt{s}}$$ stable conditions

$$Z^3 + \left(\frac{3L_y}{\pi\beta}\right)Z^2 + \left(\frac{6R_o\ L_y}{\pi\beta^2} + \frac{3R_o^2}{\beta^2}\right)Z = \frac{6F_b}{\beta^2u_ss}$$ maximum stable buoyant rise

Where,

$$R_o = \sqrt{2}A\sigma_z \qquad x = 3L_B$$

$$L_y = \sqrt{2\pi}\,(\sigma_y - \sigma_z) \quad x = 3L_B,\ \sigma_y \geq \sigma_z$$

$$L_y = 0 \qquad x = 3L_B,\ \sigma_y < \sigma_z$$

The linear decay factor, A, is explained in the following section. The linear decay factor is calculated using the refined Schulman-Scire building downwash.

3.2.5 Effects of building wakes on effluent dispersion

Huber and Snyder

Huber and Snyder formulate the procedures to account for effects of building wakes on effluent dispersion by conducting an atmosphere turbulence experiment in a wind-tunnel in between the slightly unstable atmospheric condition (stability class C) and the neutral stability class D.

Huber and Snyder procedure is followed when the stack height is higher than the building height plus the lesser of the building height of width. A building would cause wake effects when the distance between the stacks and the nearest part of the building is less than or equal to 5 times the lesser of the height or width of the building. A building is assumed to cause wake effects if the stack is located in the rectangle shown in Fig. 3.4.

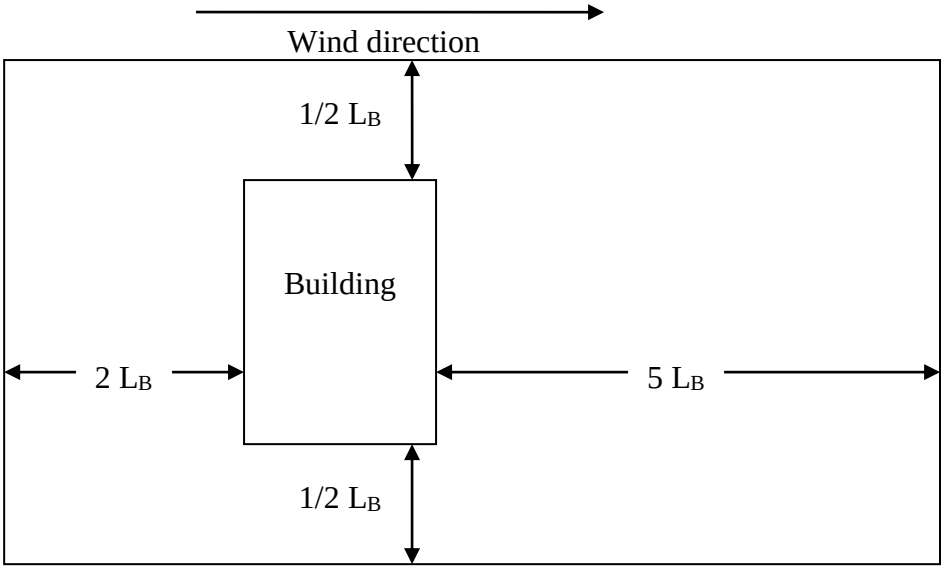

Fig. 3.4 Wake effects would occur if the stack is located in the area around the building shown

σ_y and σ_z is modified to account for building wakes when using the Huber and Snyder procedures. The criteria to determine whether a plume is affected by building wakes is when the plume height to building height ratio is less than or equal to 1.2. Both σ_y and σ_z is modified under this condition. Σ_z is modified when the ratio is more than 1.2 but not greater than 2.5. According to ISC3 model, buildings are categorized into 2 classes, squat (building width is larger than building height) and tall (building width is less than building height). The concentration of pollutants at distances less than 3 building height or width (whichever the lesser) is inconclusive because the air is both highly turbulent and generally re-circulating. For distances more than 3 building height and 3 building width, the estimated concentration is properly modeled by the following equations.

Modifying σ_z,

Squat buildings

The equation to calculate σ_z is as follows,

$$\sigma_z' = 0.7h_b + 0.067(x - 3h_b) \quad \text{for } 3h_b \leq x < 10h_b$$

or

$$= \sigma_z\{x + x_z\} \quad \text{for } x \geq 10h_b$$

Tall buildings

$$\sigma_z' = 0.7h_w + 0.067(x - 3h_w) \quad \text{for } 3h_w \leq x < 10h_w$$

or

$$= \sigma_z\{x + x_z\} \quad \text{for } x \geq 10h_w$$

The vertical virtual distance equations, x_z, for rural terrain are as follows,

$$x_z = \left(\frac{1.2h_b}{a}\right)^{1/b} - 0.01h_b \qquad \text{tall buildings}$$

$$x_z = \left(\frac{1.2h_w}{a}\right)^{1/b} - 0.01h_w \qquad \text{squat buildings}$$

The vertical virtual distance equations (tall buildings), x_y, for urban terrain are as follows,

$0.24x\sqrt{1.0+0.001x}=1.2h_b$ Stability class A and B

$0.2x=1.2h_b$ Stability class C

$\frac{0.14x}{\sqrt{1.0+0.0003x}}=1.2h_b$ Stability class D

$\frac{0.08x}{\sqrt{1.0+0.0015x}}=1.2h_b$ Stability class E and F

The vertical virtual distance equations (squat buildings), x_y, for urban terrain are as follows,

$0.24x\sqrt{1.0+0.001x}=1.2h_w$ Stability class A and B

$0.2x=1.2h_w$ Stability class C

$\frac{0.14x}{\sqrt{1.0+0.0003x}}=1.2h_w$ Stability class D

$\frac{0.08x}{\sqrt{1.0+0.0015x}}=1.2h_w$ Stability class E and F

Modifying σ_y,

Squat buildings

For building width to building height ratio is less than or equal to 5,

$$\sigma_y' = 0.35h_w + 0.067(x - 3h_b) \quad \text{for } 3h_b \leq x < 10h_b$$

or

$$= \sigma_y\{x + x_y\} \quad \text{for } x \geq 10h_b$$

For building width to building height ratio is more than 5 with the stack is located near the center of the building,

$$\sigma_y' = 0.35h_b + 0.067(x - 3h_b) \quad \text{for } 3h_b \leq x < 10h_b$$

or

$$= \sigma_y\{x + x_y\} \quad \text{for } x \geq 10h_b$$

A stack which is located at the end of the building,

$$\sigma_y' = 1.75h_b + 0.067(x - 3h_b) \quad \text{for } 3h_b \leq x < 10h_b$$

or

$$= \sigma_y\{x + x_y\} \quad \text{for } x \geq 10h_b$$

Tall buildings

To account for influence of tall buildings on wake effect, the following equations are used.

$$\sigma_y' = 0.35 h_w + 0.067(x - 3h_w) \quad \text{for } 3h_w \leq x < 10h_w$$

or

$$= \sigma_y \{x + x_y\} \quad \text{for } x \geq 10h_w$$

3.2.6 Schulman and Scire refined building downwash

The Schulman and Scire method is used when the physical stack height is less than the building height plus half of the lesser of building height or building width. This is because it accounts for reduced plume rise due to initial plume dilution. It also considers an enhanced vertical plume spread as a linear function of the effective plume height. The specification of building dimensions as a function of wind direction is also needed.

The refined building downwash method is used with the Schulman and Scire plume rise.

A linear decay factor, A, is introduced to be calculated with the equations used in Huber and Snyder building downwash procedure. The vertical dispersion parameter is modified using this procedure,

$$\sigma_z'' = A\sigma_z'$$

$$A = 1 \qquad \text{if } h_e \leq h_b$$

$$A = \frac{h_b - h_e}{2L_B} + 1 \qquad \text{if } h_b < h_e \leq h_b + 2L_B$$

$$A = 0 \qquad \text{if } h_e > h_b + 2L_B$$

The stack height with the plume rise, h_e, is calculated using the momentum-dominated plume rise at the distance of 2 building heights.

3.2.7 Buoyancy-induced dispersion

Buoyancy-induced dispersion is defined as turbulent motion of the plume and turbulent entrainment of ambient air. The lateral and vertical dispersion parameters are modified to account for this phenomena.

The lateral dispersion parameter, σ_y,

$$\sigma_{ye} = \left[\sigma_y^2 + \left(\frac{\Delta h}{3.5} \right)^2 \right]^{1/2}$$

The lateral dispersion parameter, σ_y,

$$\sigma_{ze} = \left[\sigma_z^2 + \left(\frac{\Delta h}{3.5} \right)^2 \right]^{1/2}$$

The Δh is the distance-dependent plume rise for receptors before the final plume rise distance, and final plume rise for receptors after the final plume rise distance. It must be noted that buoyancy-induced dispersion is not used in conjunction with Schulman-Scire downwash option.

3.2.8 Vertical dispersion

The vertical term accounts for effects of source elevation, receptor elevation, plume rise, limited mixing in the vertical, and gravitational settling and dry deposition of particulates.

The vertical term without dry deposition

Dry deposition should not be considered when the pollutants are gaseous or very small particulates. The vertical term without dry deposition,

$$V = \exp\left[-\frac{1}{2}\left(\frac{z_r - h_e}{\sigma_z}\right)^2\right] + \exp\left[-\frac{1}{2}\left(\frac{z_r + h_e}{\sigma_z}\right)^2\right]$$

$$+ \sum_{i=1}^{\infty}\left\{\exp\left[-\frac{1}{2}\left(\frac{H_1}{\sigma_z}\right)^2\right] + \exp\left[-\frac{1}{2}\left(\frac{H_2}{\sigma_z}\right)^2\right]\right.$$

$$\left. + \exp\left[-\frac{1}{2}\left(\frac{H_3}{\sigma_z}\right)^2\right] + \exp\left[-\frac{1}{2}\left(\frac{H_4}{\sigma_z}\right)^2\right]\right\}$$

Where:

$h_e = h_s + \Delta h$

$H_1 = z_r - (2iz_i - h_e)$

$H_2 = z_r + (2iz_i - h_e)$

$H_3 = z_r - (2iz_i + h_e)$

$H_4 = z_r + (2iz_i + h_e)$

z_r = receptor height above ground (flagpole) (m)

z_i = mixing height (m)

The infinite series term is included to model the effects of the boundary layer (mixing layer) on the vertical plume growth. It has also been coded into HAWA that for any plume that exceeds the mixing height, the receptors on ground level would have zero pollutant concentration.

If the σz/zi ratio is greater than or equal to 1.6, the vertical term is reduced to,

$$V = \frac{\sqrt{2\pi}\,\sigma_z}{z_i}$$

The vertical term in elevated simple terrain

Behavior of plume in elevated simple terrain (terrain that exceeds the stack base elevation but below the release height) is assumed to be:

1. The plume axis remains at the plume stabilization height above mean sea level as it passes over elevated or depressed terrain.
2. The mixing height is terrain following.
3. The wind speed is a function of height above the surface.

The modified plume stabilization height, he', replace the effective stack height, he, in the vertical term. The modified plume stabilization equation is as follows,

$$h_e' = h_e + z_s - z|_{(x,y)}$$

It should be noted that for any receptors that exceeds the stack height are automatically cut because the concentration at these levels are under considerable uncertainty.

The vertical term with dry deposition

The vertical term is modified to account for dry deposition using a corrected source-depletion model developed by Horst. This model includes the gravitational settling of the plume and the removal of plume mass at the surface. This would make the plume tilt. The equation is a follows,

$$h_{ed} = h_e - h_v = h_e - \frac{x}{u_s} v_g$$

This new effective stack height is used in the vertical term. v_g stands for gravitational settling velocity for particulates (cm/s). v_g is calculated using the following formula,

$$v_g = \frac{(\rho - \rho_{AIR}) g d_p^2 c_2}{18\mu} S_{CF}$$

Where,

ρ =the particle density (g/cm^3),

ρ_{AIR} =the air density (_ 1.2 x 10^{-3} g/cm^3),

d_p =the particle diameter (μm),

μ =the absolute viscosity of air (_ 1.81 x 10^{-4} g/cm/s),

c_2 =air units conversion constant (1 x 10^{-8} cm^2/μm^2), and

S_{CF} =the slip correction factor, which is computed as:

$$S_{CF} = 1. + \frac{2\,x_2\left(a_1 + a_2\, e^{-\left(a_3 d_p / x_2\right)}\right)}{10^{-4}\, d_p}$$

and, x_2, a_1, a_2, a_3 are constants with values of 6.5 x 10^{-6}, 1.257, 0.4, and 0.55 x 10^{-4}, respectively.

3.2.9 Decay of pollutants

The decay term is used to model pollutant removal by physical or chemical processes. The term is as follows,

$$D = \exp\left(-\psi \frac{x}{u_s}\right) \quad \text{for } \psi > 0$$

or

$$= 1 \qquad \text{for } \psi = 0$$

Where,

ψ = the decay coefficient (s^{-1})

x = downwind distance (m)

ψ can be calculated using the following formula,

$$\psi = \frac{0.693}{T_{1/2}}$$

Where,

$T_{1/2}$ = pollutant half-life (s)

3.2.10 Wind speed profile

The wind power law is used to determine the wind speed at stack height relative to the wind speed observed. The wind speed at stack height is the wind used in the calculation of pollutant dispersion. The power law equation is,

$$u_s = u_{ref}\left(\frac{h_s}{z_{ref}}\right)^p$$

Where,

h_s = stack height (m)

u_{ref} = observed wind at reference height (m/s)

z_{ref} = reference height (m)

Table 3.6 Exponent p used in the power law equation

Stability Category	Rural Exponent	Urban Exponent
A	0.07	0.15
B	0.07	0.15
C	0.10	0.20
D	0.15	0.25
E	0.35	0.30
F	0.55	0.30

3.2.11 Wet Deposition

Wet deposition is a process of removal of gases and particles. A scavenging ratio approach is used in HAWA. The volumetric flowrate, Q, is modified by the equation to account for this process.

$$Q(x) = Q_o e^{-\Lambda x/u} = Q_o e^{-\Lambda t}$$

Where,

t	=	$\Lambda x/u$
Λ	=	$\lambda \times R$
λ	=	scavenging coefficient $((s\text{-}mm/hr)^{-1})$
R	=	precipitation rate (mm/hr)

The above equation would deplete the concentration of the pollutants with downwind distance.

4.0 RESULTS AND DISCUSSION

The following data are plugged into HAWA to calculate the 400 receptor points possible to plot the contour plot and 3-dimensional graph. The plots are possible with the use of Matlab© 6.0. The files necessary to run on Matlab© are generated by HAWA and can be loaded directly into Matlab©.

4.1 Effect of Pasquill-Gifford stability class on the concentration distribution of pollutant (SO_2) for one stack in an urban terrain

The following data are used in HAWA to simulate SO_2 dispersion from one elevated source (stack) under different stability class in urban terrain. The amount of receptor points are 400, which are at ground level.

4.1.1.1 Meteorology Data

The data used shown in Table 4.1 are reasonable estimate of meteorological data of a normal Malaysian atmospheric condition.

Table 4.1 Meteorology data 1

Parameter	**Value**
Wind velocity	2 m/s
Wind direction	3.142 rad
Averaging time	10 min
Atmospheric pressure	1000 mb
Mixing height	6000 m
Height wind is recorded	10 m
Terrain type	Urban
Stack tip downwash	Enabled

4.1.1.2 Emission data from one point elevated source (stack)

The following data in Table 4.2 are similar for all three stacks with the only difference being the stability class. Table 4.3 states the location of the stack in a Cartesian grid.

Table 4.2 Emission data 1

Parameter	**Value**
Stack inner diameter	5 m
Flue gas temperature	450 K
Stack height	50 m
Mass flowrate of pollutant SO_2	5 g/s
Half-life of pollutant SO_2	14400 s
Buoyancy-induced	Enabled

Table 4.3 Stack location 1

Stack	**X (km)**	**Y (km)**	**Z (km)**
Stack 1	0	0	0

4.1.2 Pasquill-Gifford stability class A (very unstable)

Fig. 4.1 and Fig. 4.2 show the concentration distribution of SO_2 under Pasquill-Gifford stability class A. It can be seen that the maximum concentration of SO_2 (100 $\mu g/m^3$) occurs directly downwind from the stack at approximately 100 m from the source at ground level. It can be summarized that the distribution of pollutants under this stability class are contained in a smaller area thus the concentration tend to be higher in this region.

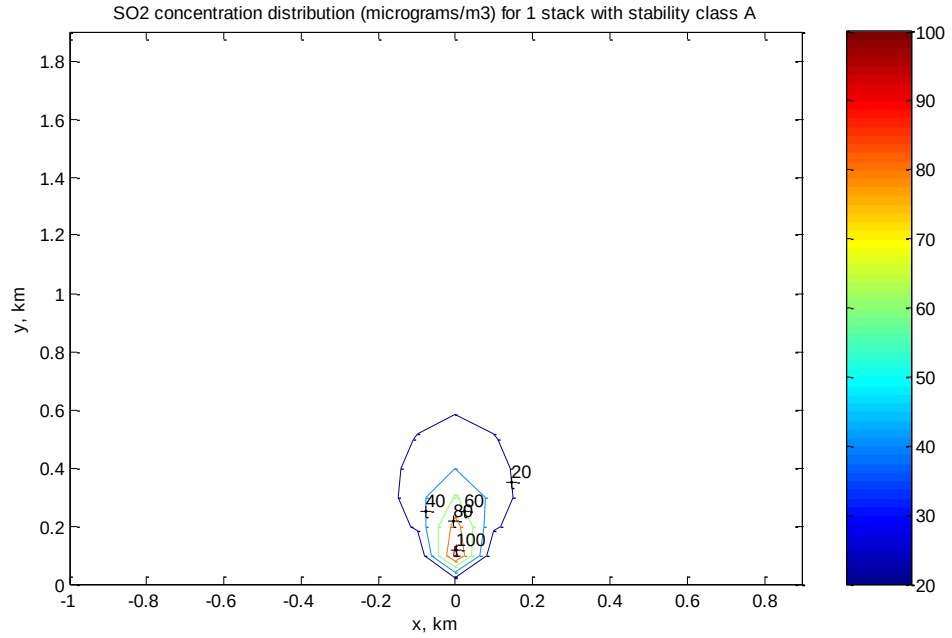

Fig. 4.1 Contour plot of SO_2 concentration distribution ($\mu g/m^3$) for 1 stack with stability class A

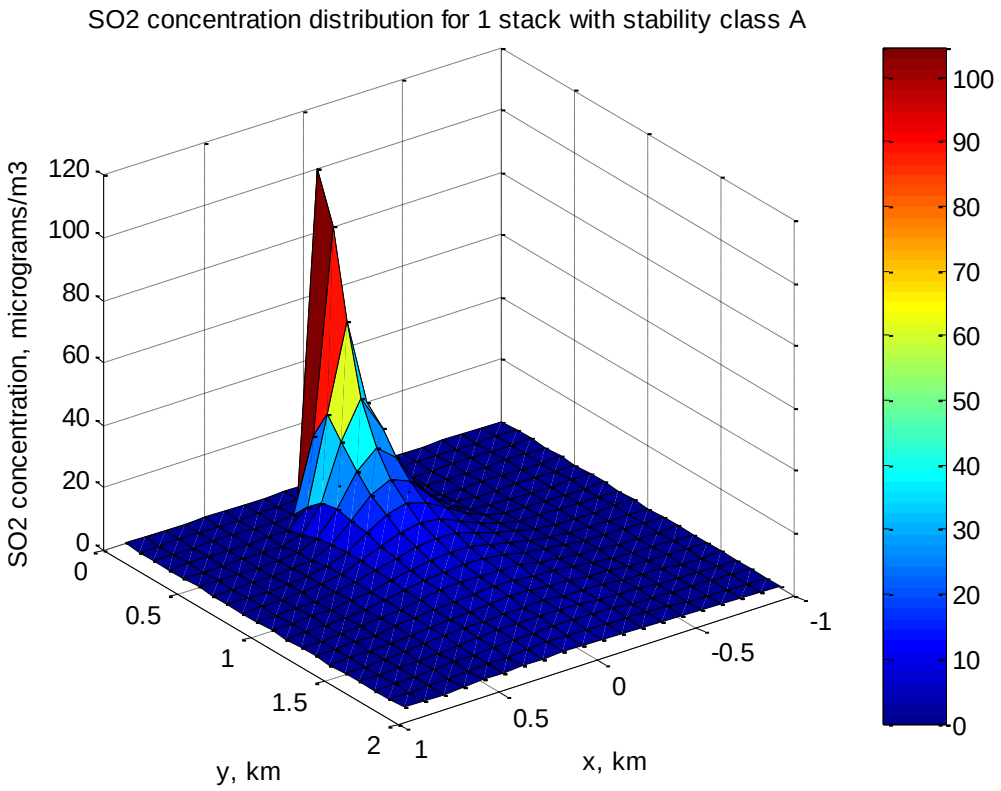

Fig. 4.2 3-D plot of SO_2 concentration distribution for 1 stack with stability class A

4.1.3 Pasquill-Gifford stability class B (moderately unstable)

Fig. 4.3 and Fig. 4.4 show the concentration distribution of SO_2 under Pasquill-Gifford stability class B. The dispersion profile follows closely with Pasquill-Gifford stability class A because both have almost similar lateral and vertical dispersion parameter equation for urban terrain. It can be seen that the maximum concentration of SO_2 (100 µg/m^3) also occurs directly downwind from the stack at approximately 100 m from the source at ground level. Pollutant SO_2, at 20 µg/m^3, occupies a larger area compared to stability class A.

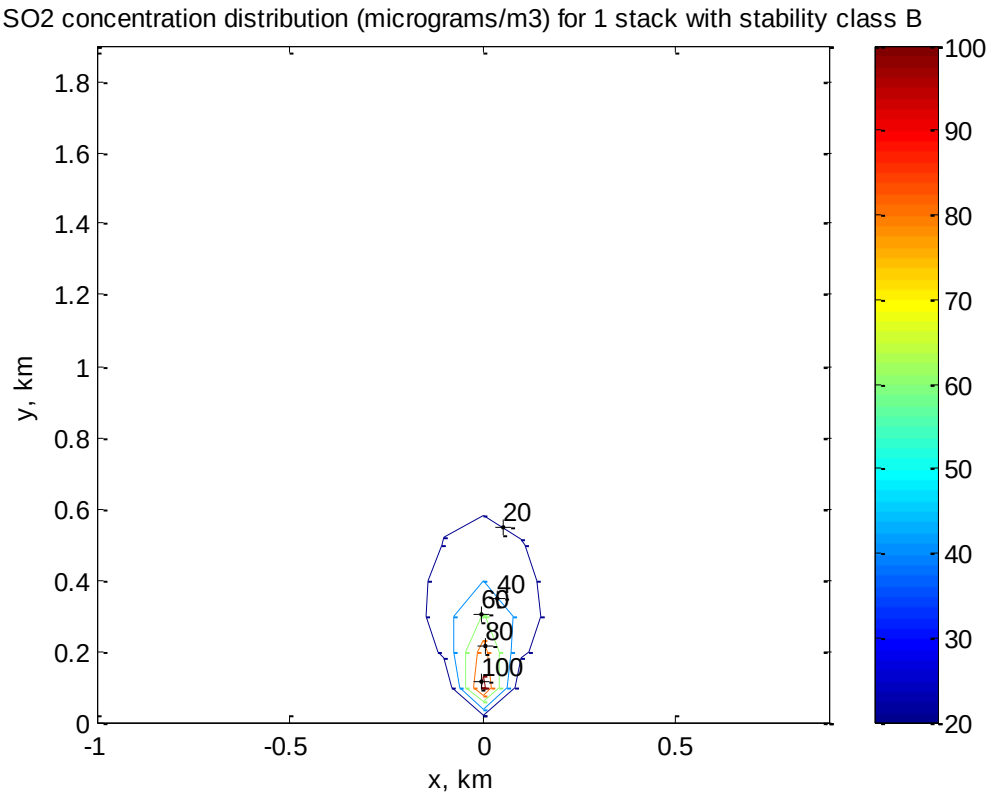

Fig. 4.3 Contour plot of SO_2 concentration distribution (µg/m^3) for 1 stack with stability class B

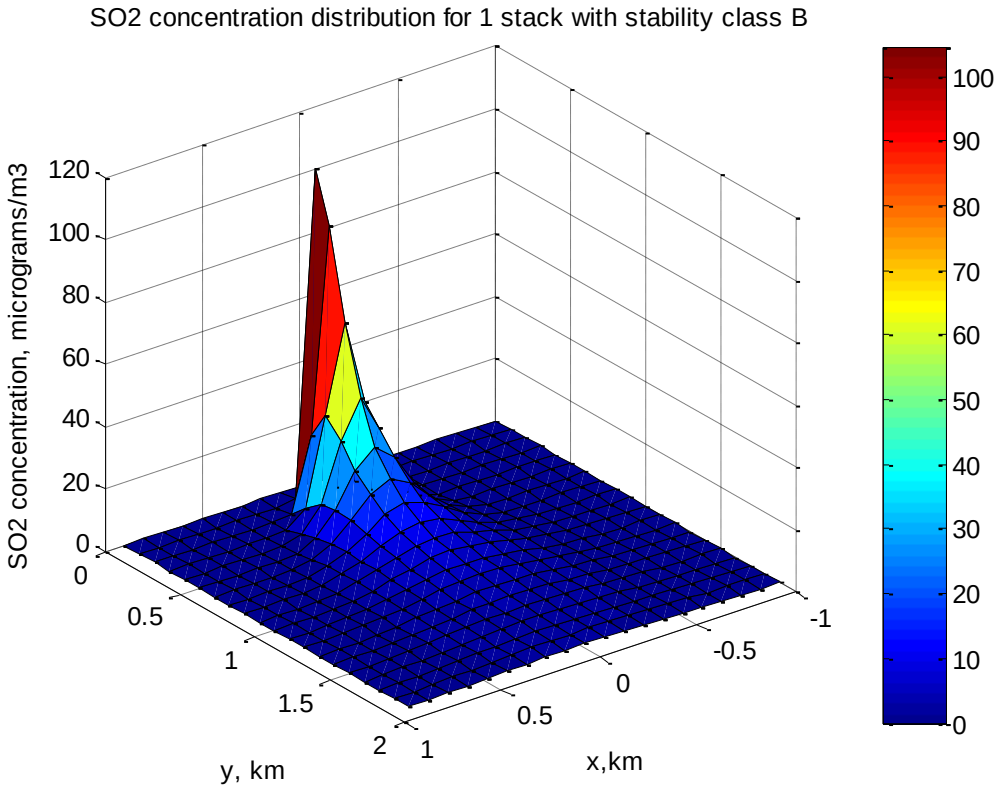

Fig. 4.4 3-D plot of SO_2 concentration distribution for 1 stack with stability class B

4.1.4 Pasquill-Gifford stability class C (slightly unstable)

Fig. 4.5 and Fig. 4.6 show the concentration distribution of SO_2 under Pasquill-Gifford stability class C. It can be seen that the maximum concentration of SO_2 (90 µg/m^3) occurs directly downwind from the stack at approximately 200 m from the source at ground level. The SO_2 pollutants are more dispersed under this stability class resulting in less maximum concentration but wider area occupied with SO_2 extending to 1200 m from the source.

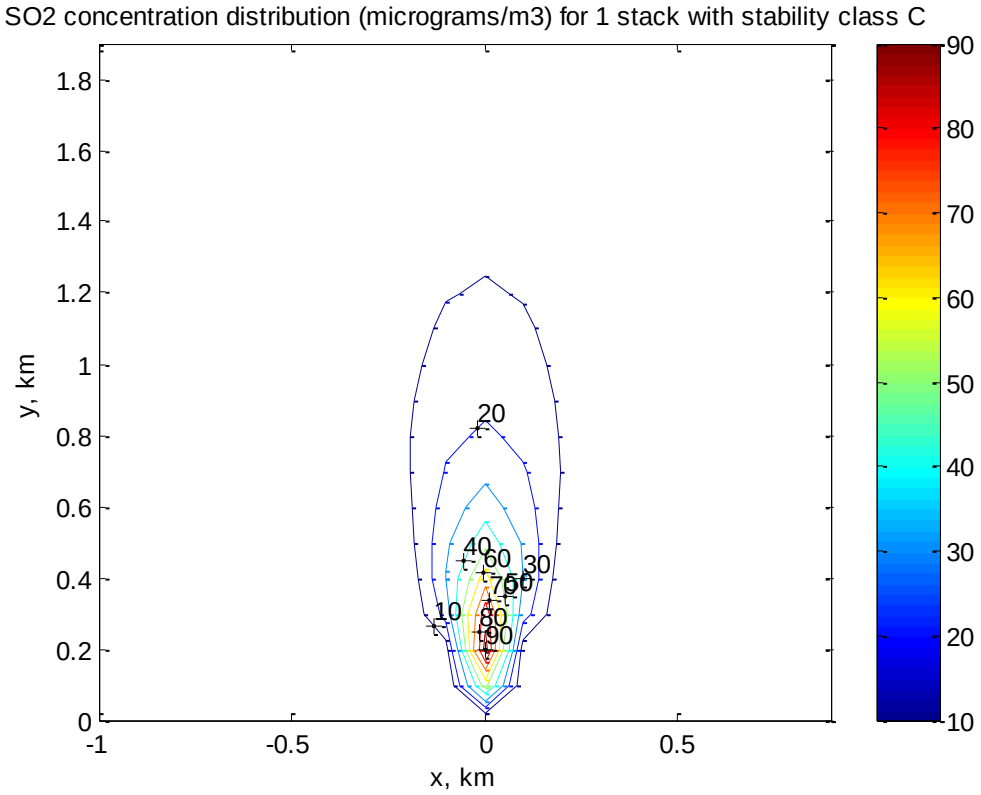

Fig. 4.5 Contour plot of SO_2 concentration distribution ($\mu g/m^3$) for 1 stack with stability class C

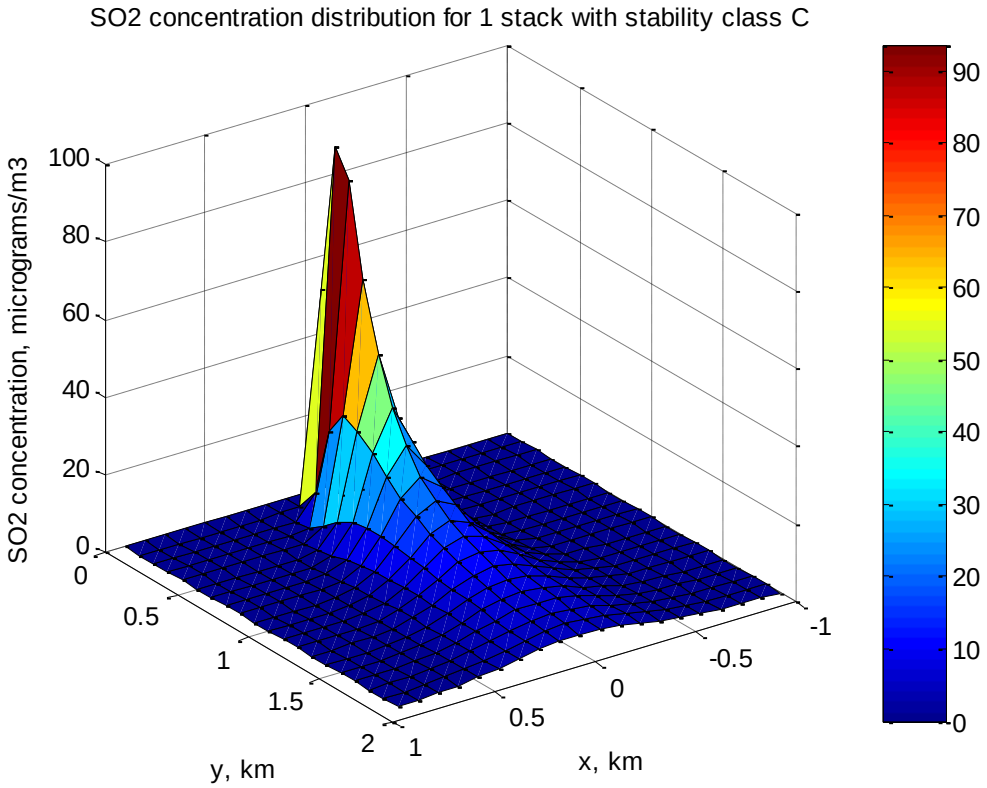

Fig. 4.6 3-D plot of SO_2 concentration distribution for 1 stack with stability class C

4.1.5 Pasquill-Gifford stability class D (neutral)

Fig. 4.7 and Fig. 4.8 show the concentration distribution of SO_2 under Pasquill-Gifford stability class D. It can be seen that the maximum concentration of SO_2 (80 µg/m^3) occurs directly downwind from the stack at approximately 400 m from the source at ground level. As before, the SO_2 pollutants are more dispersed under this stability class resulting in less maximum concentration but wider area occupied with SO_2 extending to 1800 m from the source.

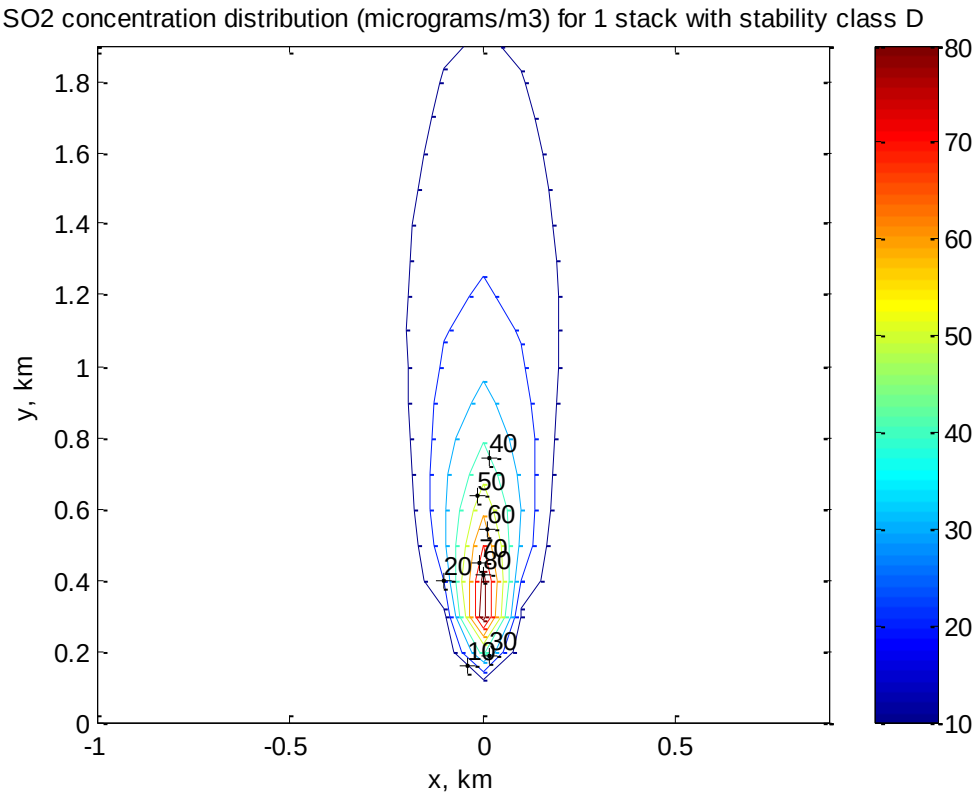

Fig. 4.7 Contour plot of SO_2 concentration distribution (µg/m^3) for 1 stack with stability class D

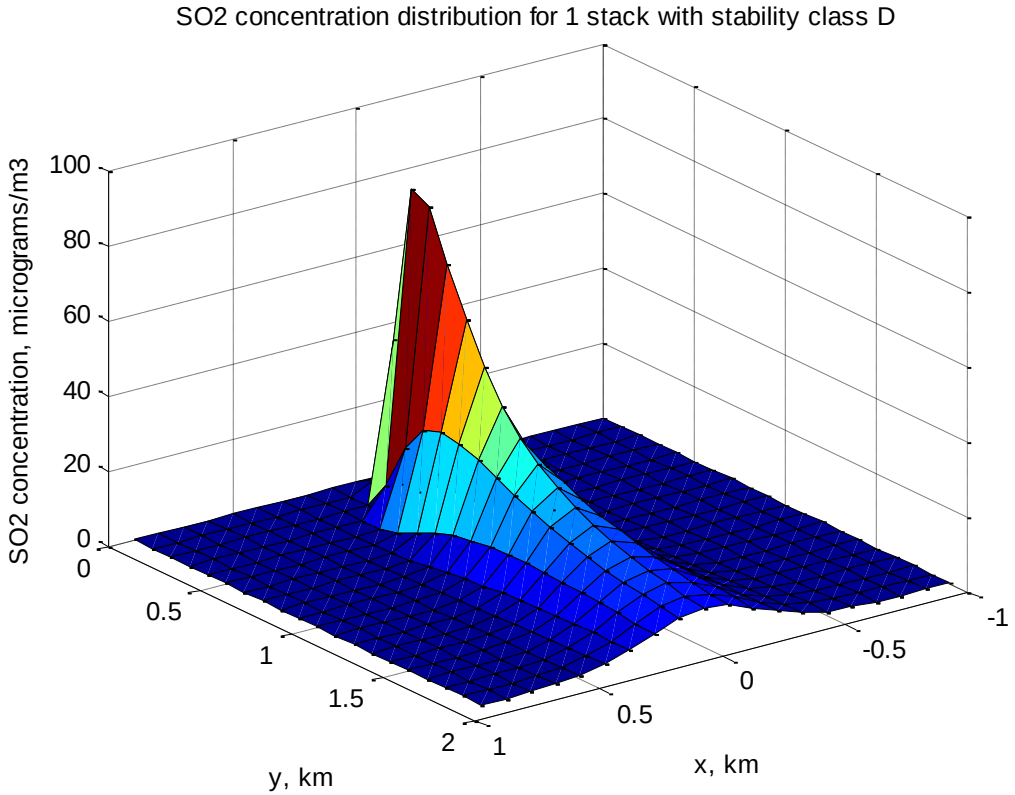

Fig. 4.8 3-D plot of SO_2 concentration distribution for 1 stack with stability class D

4.1.6 Pasquill-Gifford stability class E (slightly stable)

Fig. 4.9 and Fig. 4.10 show the concentration distribution of SO_2 under Pasquill-Gifford stability class E. It can be seen that the maximum concentration of SO_2 decreases to 60 µg/m^3 which occurs directly downwind from the stack at approximately 500 m from the source at ground level. The SO_2 pollutants spread into a wider area with less maximum concentration but wider area occupied with SO_2 extending to more than 2 km from the source.

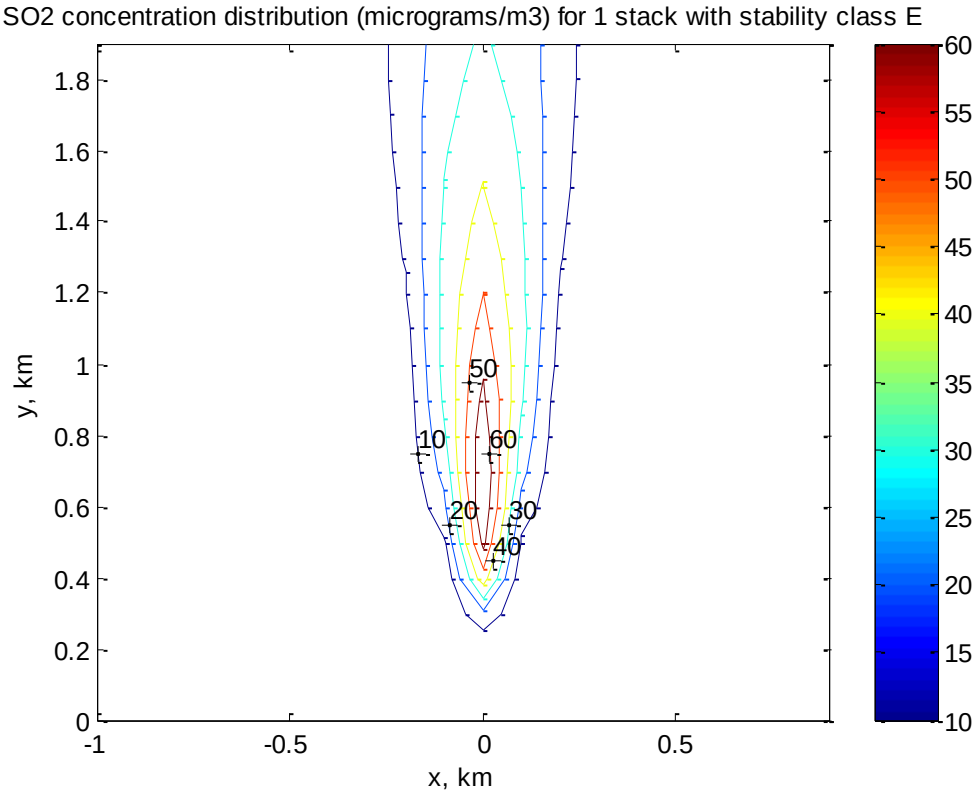

Fig. 4.9 Contour plot of SO_2 concentration distribution ($\mu g/m^3$) for 1 stack with stability class E

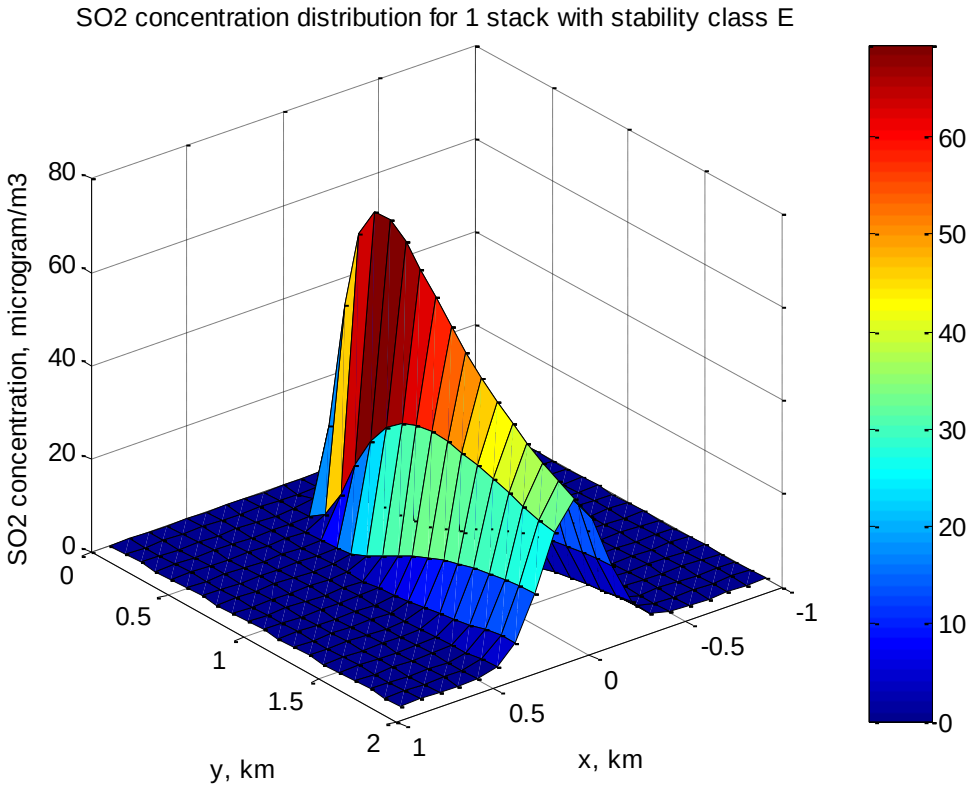

Fig. 4.10 3-D plot of SO_2 concentration distribution for 1 stack with stability class E

4.1.7 Pasquill-Gifford stability class F (stable)

Fig. 4.11 and Fig. 4.12 show the concentration distribution of SO_2 under Pasquill-Gifford stability class F. It is the same compared to stability class E because the equations used for determining the vertical and lateral dispersion parameters are similar.

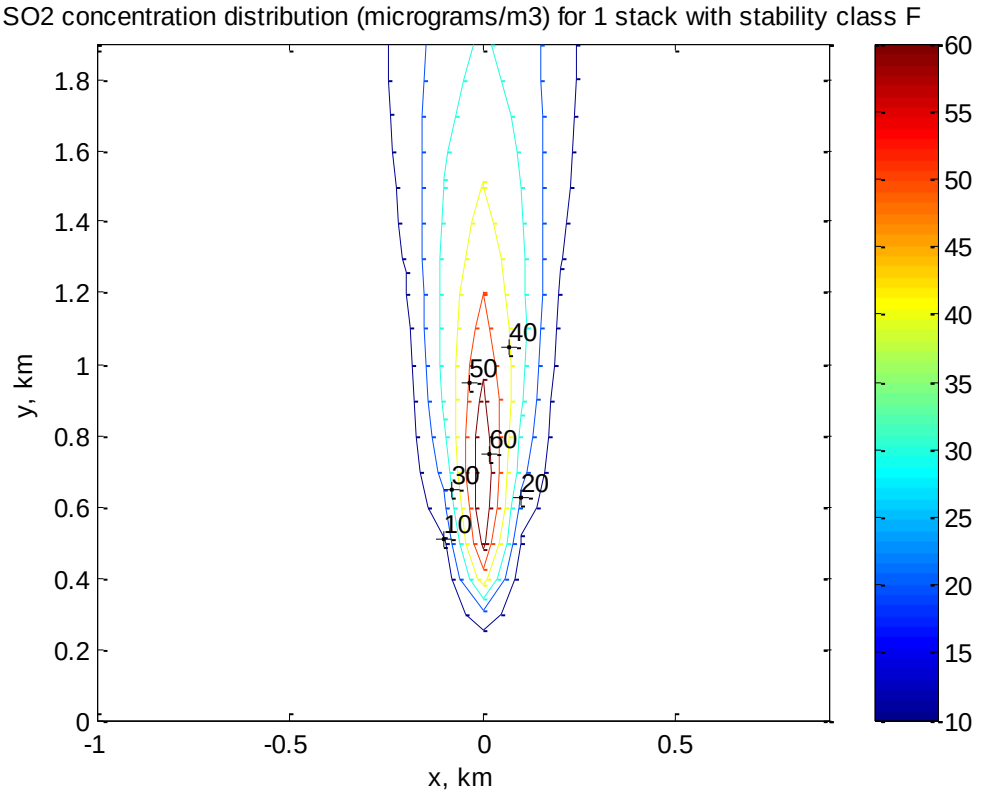

Fig. 4.11 Contour plot of SO_2 concentration distribution ($\mu g/m^3$) for 1 stack with stability class F

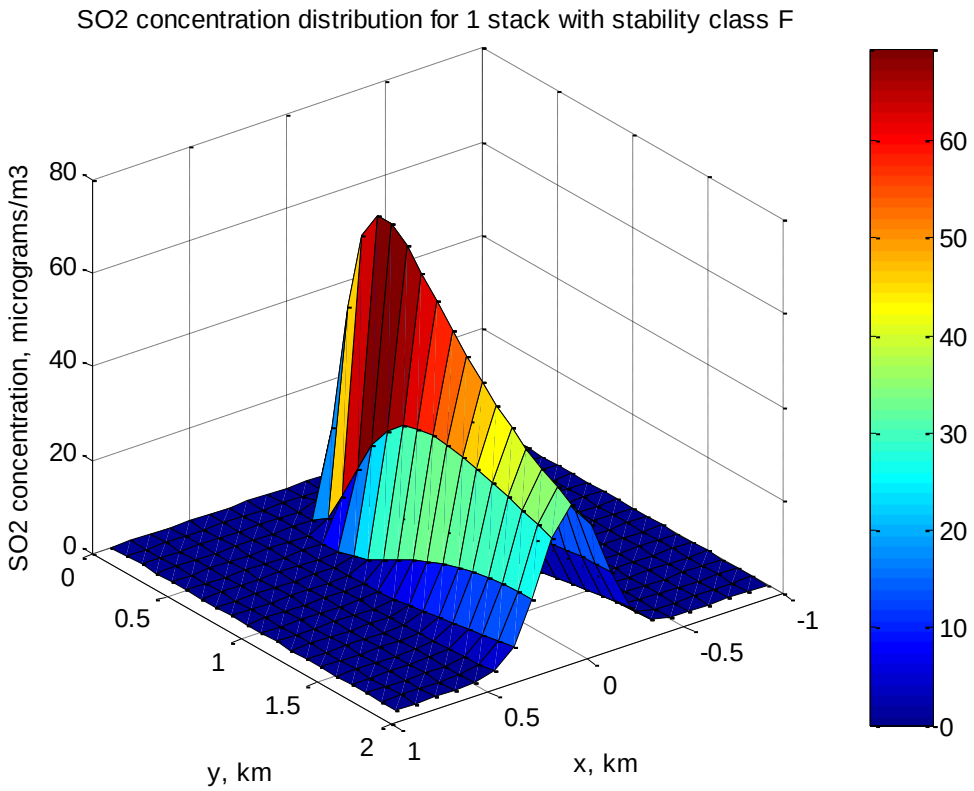

Fig. 4.12 3-D plot of SO_2 concentration distribution for 1 stack with stability class F

Table 4.4 below is used to plot Fig. 4.13.

Table 4.4 Centerline ground level concentration of SO_2 for different stability classes

Downwind distance, km	**A**	**B**	**C**	**D**	**E**	**F**
0.1	104.677719	104.67772	54.593316	2.995121	0	0
0.2	88.952484	88.952484	93.692524	42.943491	0.840852	0.840852
0.3	61.071798	61.071798	86.842214	85.11432	18.40621	18.40621
0.4	39.21184	39.21184	63.89136	83.04793	46.064287	46.064287
0.5	26.36399	26.36399	46.711556	69.917842	63.149872	63.149872
0.6	18.654675	18.654675	35.122359	57.190586	69.42387	69.42387
0.7	13.780944	13.780944	27.233757	46.932538	69.483063	69.483063
0.8	10.542367	10.542367	21.703538	38.992202	66.607471	66.607471
0.9	8.296673	8.296673	17.703589	32.859979	62.569596	62.569596

1	6.682935	6.682935	14.726549	28.076753	58.241967	58.241967
1.1	5.488155	5.488155	12.454459	24.294116	54.028669	54.028669
1.2	4.580968	4.580968	10.682126	21.259342	50.100566	50.100566
1.3	3.877183	3.877183	9.273173	18.79057	46.51502	46.51502
1.4	3.321001	3.321001	8.13444	16.756183	43.275707	43.275707
1.5	2.874349	2.874349	7.200685	15.059851	40.362353	40.362353
1.6	2.510575	2.510575	6.425182	13.630143	37.745421	37.745421
1.7	2.210602	2.210602	5.773787	12.41336	35.393254	35.393254
1.8	1.960498	1.960498	5.221095	11.368598	33.275393	33.275393
1.9	1.749906	1.749906	4.747894	10.464303	31.363981	31.363981
2.0	1.571005	1.571005	4.339443	9.675837	29.634212	29.634212

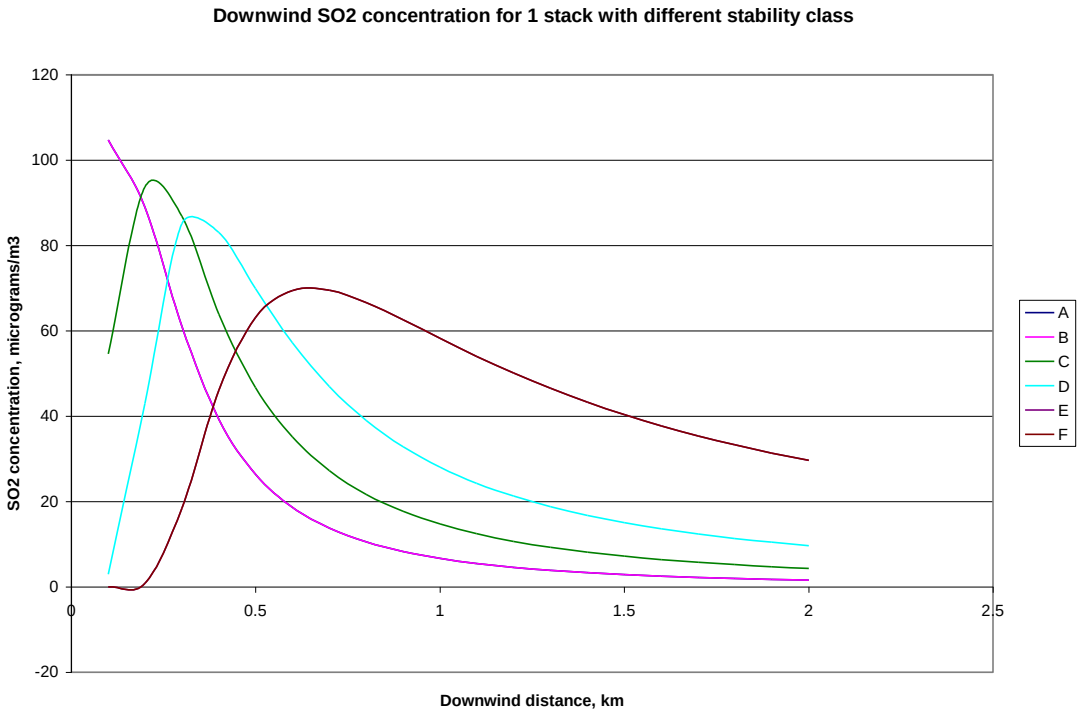

Fig. 4.13 Centerline ground level concentration of SO_2 for different stability classes

Pasquill-Gifford stability class A and B have the same curve profile due to same vertical and lateral dispersion parameter equations. Maximum concentration decreases with stability class from very unstable (A) to stable (F).

4.2 Effect of stack height on the concentration distribution of pollutant for one stack in an urban terrain

Meteorology data and emission data are the same as Table 4.1 and Table 4.2 except that the stack height ranges from 50 m to 100 m. The Pasquill-Gifford stability class used is D (neutral).

4.2.1 Stack height of 50 m

The SO_2 distribution profile for stack height 50 m can be seen in Fig.4.14 and Fig. 4.15 below.

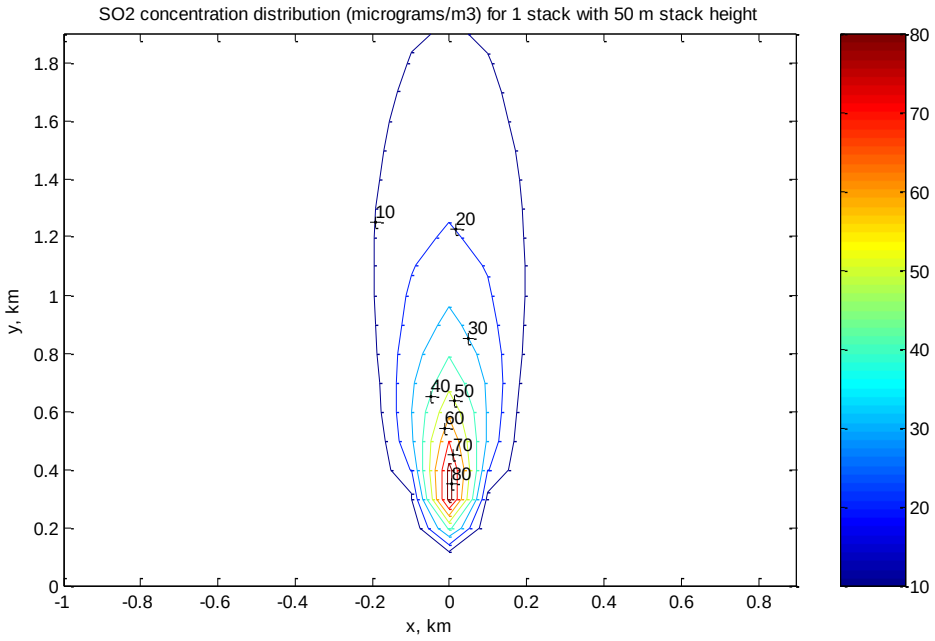

Fig. 4.14 Contour plot of SO_2 concentration distribution ($\mu g/m^3$) for 1 stack with 50 m stack height

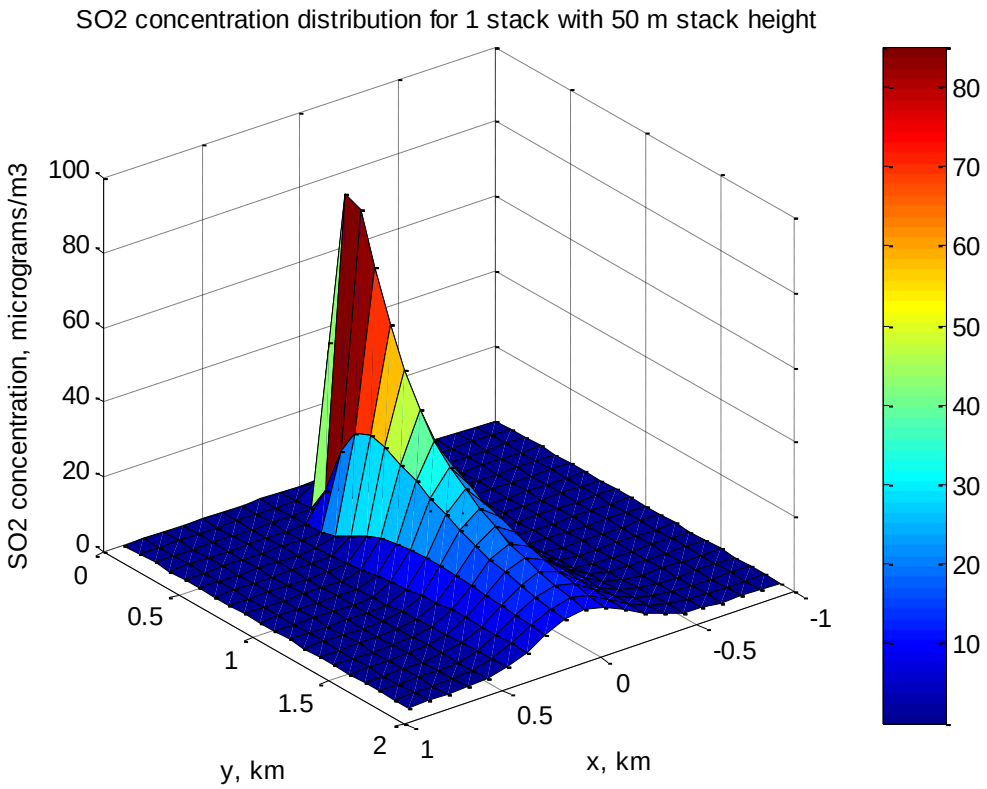

Fig. 4.15 3-D plot of SO_2 concentration distribution for 1 stack with 50 m stack height

4.2.2 Stack height of 60 m

The SO_2 distribution profile for stack height 60 m can be seen in Fig. 4.16 and Fig. 4.17 below.

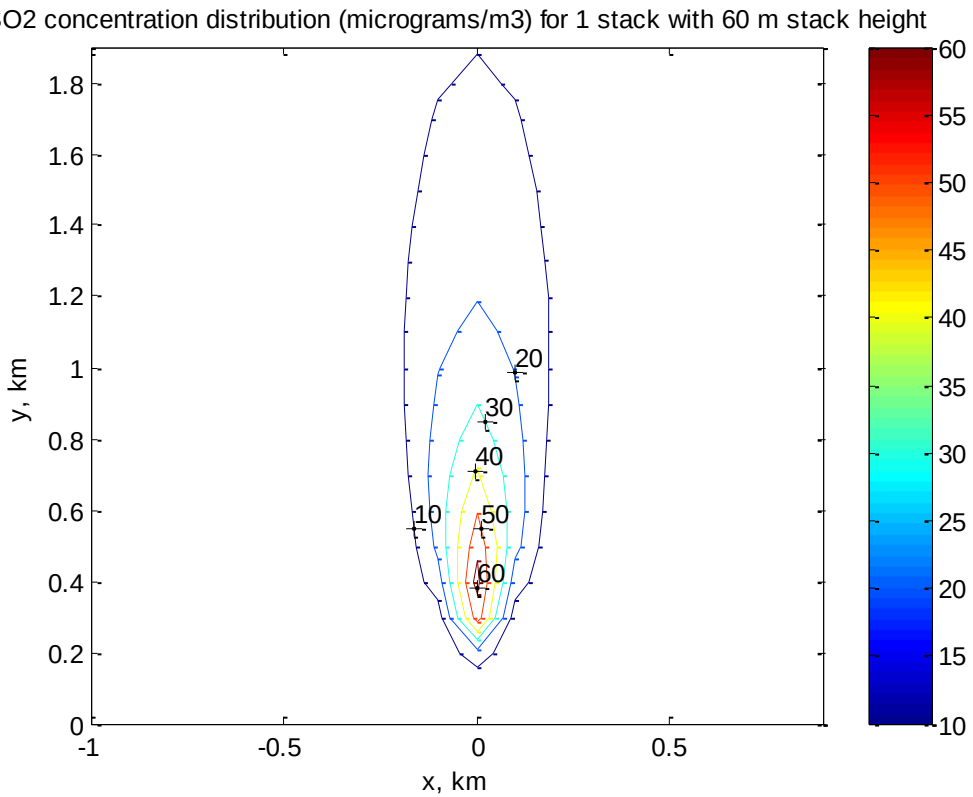

Fig. 4.16 Contour plot of SO_2 concentration distribution ($\mu g/m^3$) for 1 stack with 60 m stack height

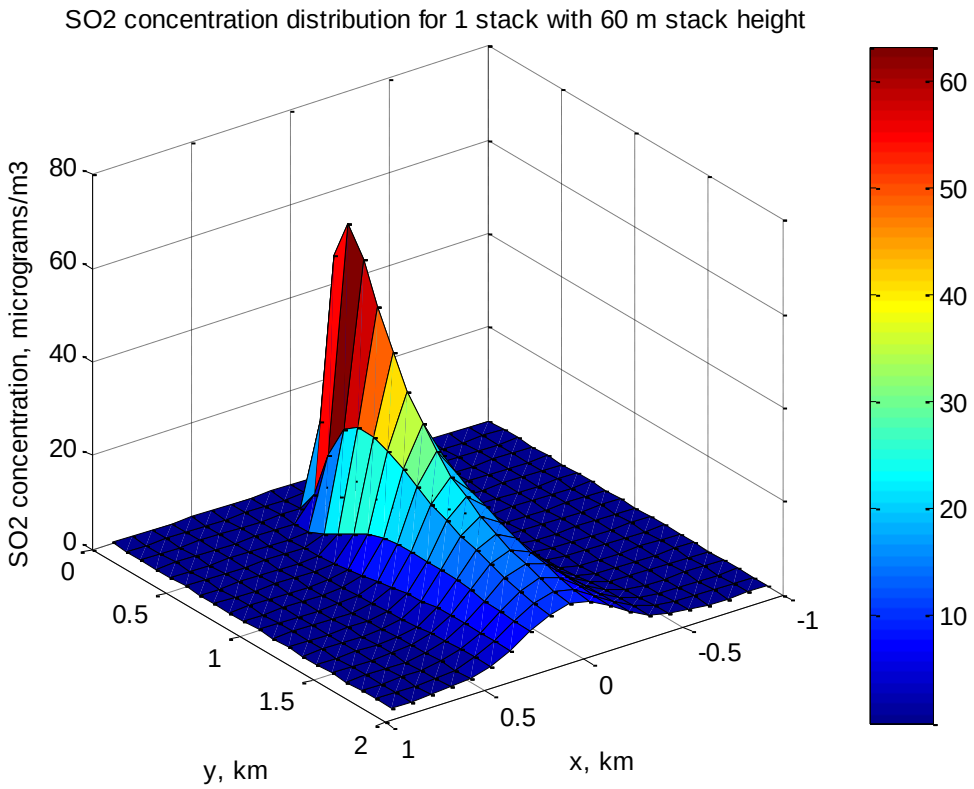

Fig. 4.17 3-D plot of SO_2 concentration distribution for 1 stack with 60 m stack height

4.2.3 Stack height of 70 m

The SO_2 distribution profile for stack height 70 m can be seen in Fig. 4.18 and Fig. 4.19 below.

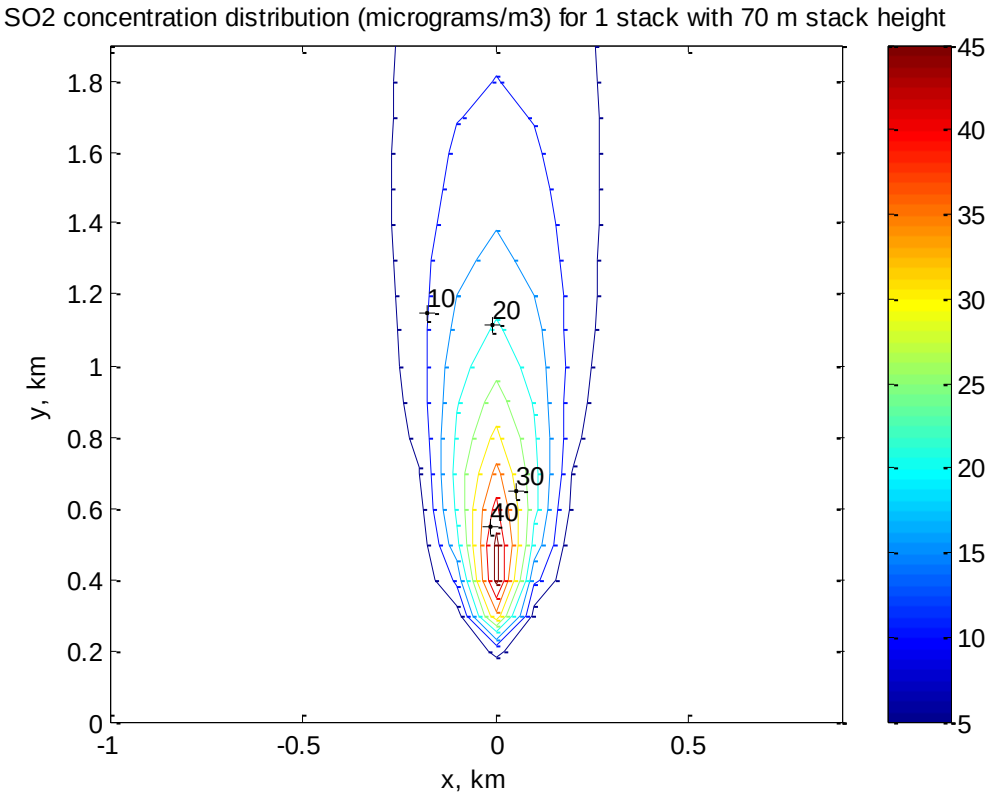

Fig. 4.18 Contour plot of SO_2 concentration distribution ($\mu g/m^3$) for 1 stack with 70 m stack height

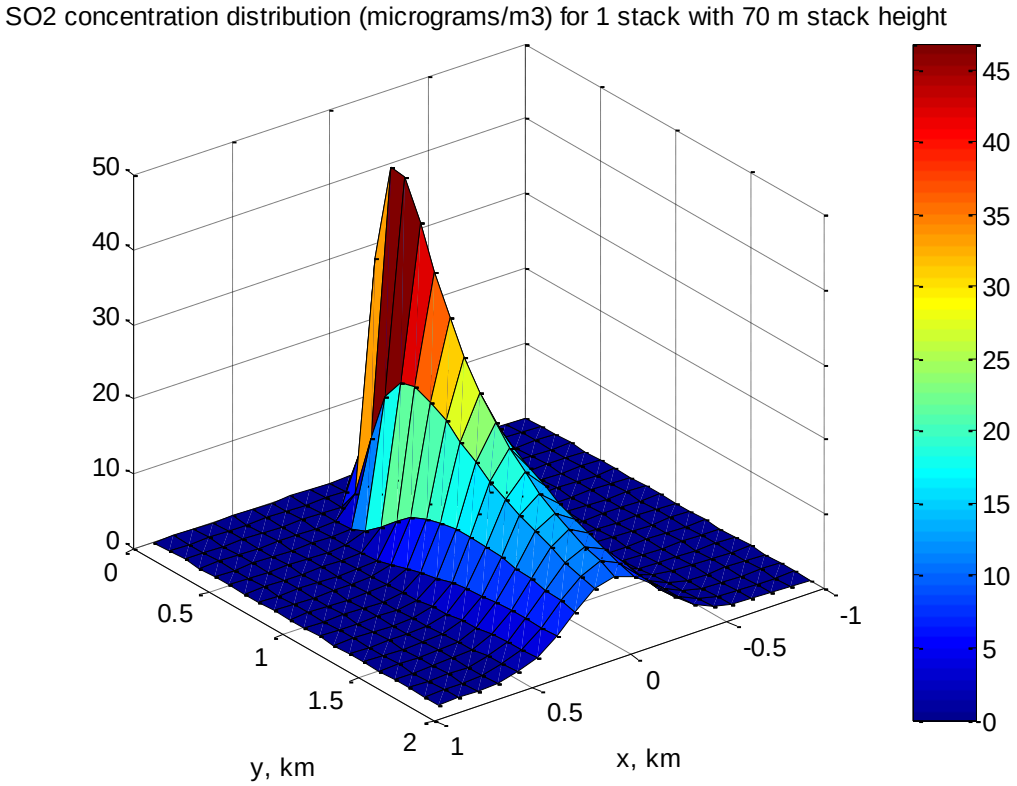

Fig. 4.19 3-D plot of SO_2 concentration distribution for 1 stack with 70 m stack height

4.2.4 Stack height of 80 m

The SO_2 distribution profile for stack height 80 m can be seen in Fig. 4.20 and Fig. 4.21 below.

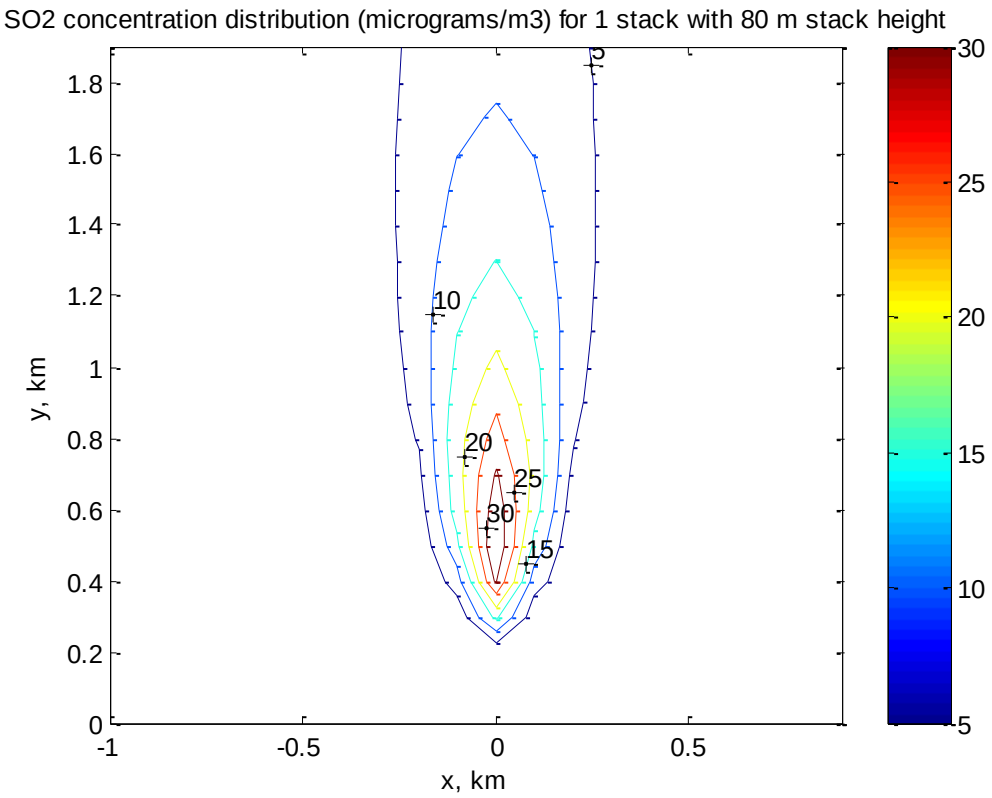

Fig. 4.20 Contour plot of SO_2 concentration distribution ($\mu g/m^3$) for 1 stack with 80 m stack height

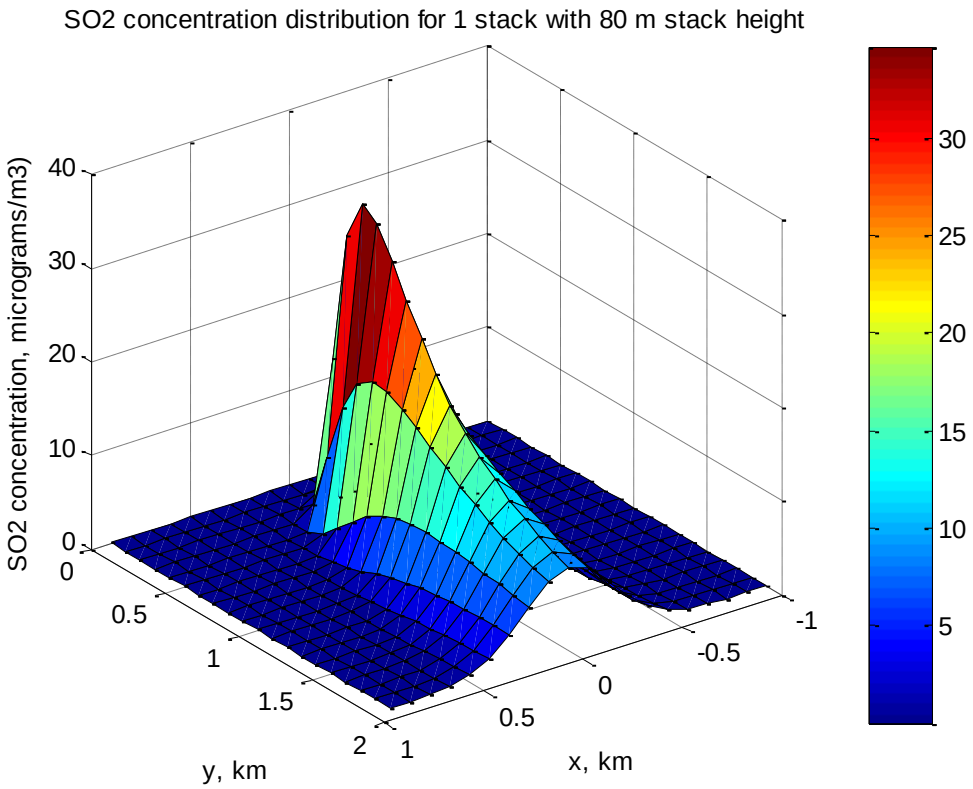

Fig. 4.21 3-D plot of SO_2 concentration distribution for 1 stack with 80 m stack height

4.2.5 Stack height of 90 m

The SO_2 distribution profile for stack height 90 m can be seen in Fig. 4.22 and Fig. 4.23 below.

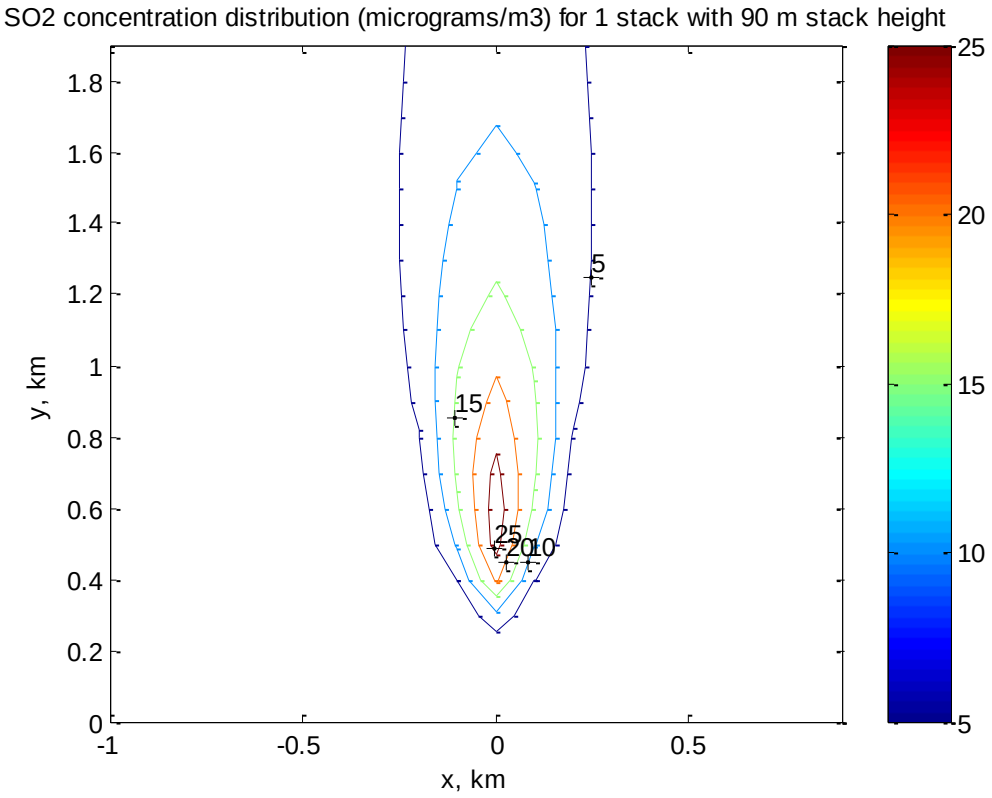

Fig. 4.22 Contour plot of SO_2 concentration distribution ($\mu g/m^3$) for 1 stack with 90 m stack height

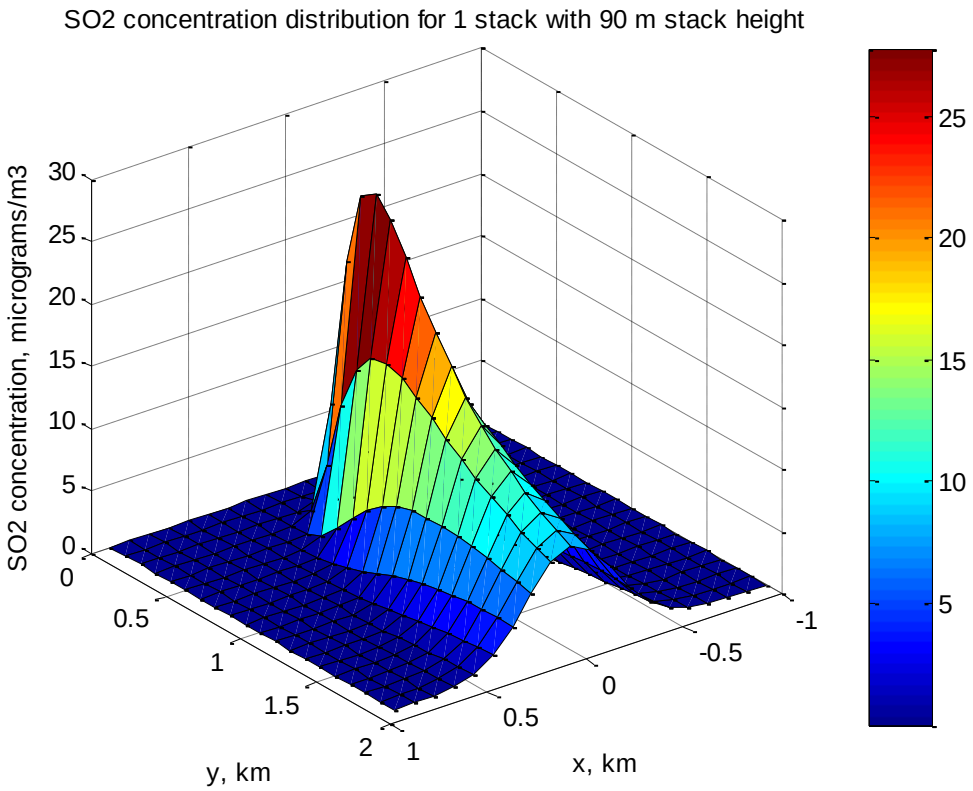

Fig. 4.23 3-D plot of SO_2 concentration distribution for 1 stack with 90 m stack height

4.2.6 Stack height of 100 m

The SO_2 distribution profile for stack height 100 m can be seen in Fig.4.24 and Fig. 4.25 below

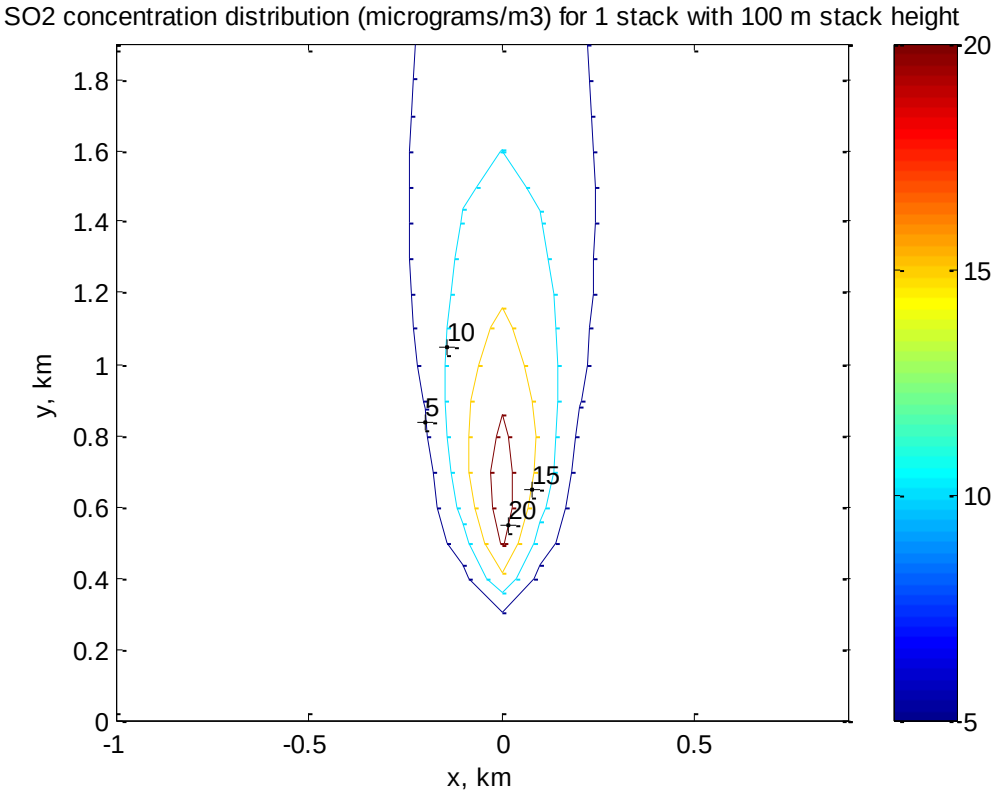

Fig. 4.24 Contour plot of SO_2 concentration distribution ($\mu g/m^3$) for 1 stack with 100 m stack height

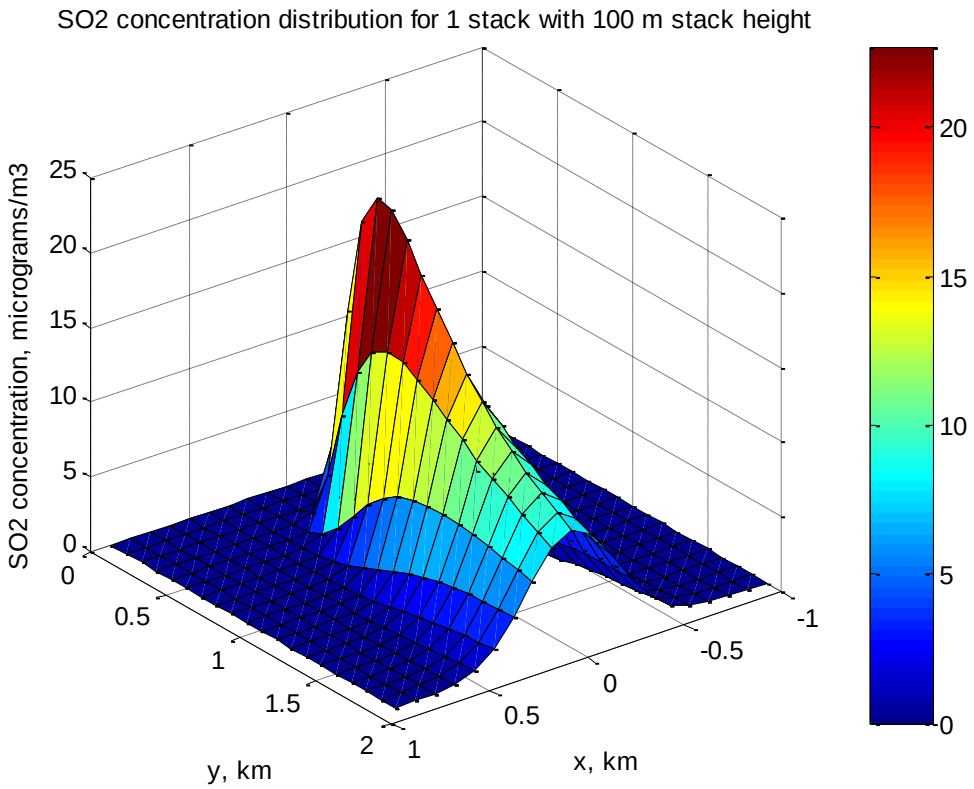

Fig. 4.25 3-D plot of SO_2 concentration distribution for 1 stack with 100 m stack height

A summary of the concentration profile of SO_2 for different stack height is shown in the table and figure 26 below.

Table 4.5 Centerline ground level concentration of SO_2 for different stack heights

Stack height, m	50	60	70	80	90	100
0.1	2.995121	0.155762	0.004827	0.000025	0	0
0.2	42.943491	17.353132	6.185745	1.325841	0.35629	0.084111
0.3	85.11432	54.879509	33.541713	16.292698	8.79499	4.482244
0.4	83.04793	63.214541	46.791578	30.394392	21.020285	14.080354
0.5	69.917842	57.533709	46.593916	34.691602	26.952292	20.52649
0.6	57.190586	49.125333	41.805103	33.556612	27.796205	22.720362
0.7	46.932538	41.386171	36.302303	30.510358	26.2829	22.432575
0.8	38.992202	34.983224	31.3036	27.117103	23.96993	21.04876
0.9	32.859979	29.837438	27.071389	23.949006	21.552214	19.303502

1	28.076753	25.716931	23.568272	21.170012	19.300361	17.53606
1.1	24.294116	22.397805	20.681505	18.790373	17.298465	15.886881
1.2	21.259342	19.698638	18.294931	16.768935	15.553747	14.40323
1.3	18.79057	17.480193	16.308929	15.052626	14.044598	13.090821
1.4	16.756183	15.637354	14.643241	13.590777	12.741025	11.938176
1.5	15.059851	14.090866	13.234702	12.33952	11.612974	10.927888
1.6	13.630143	12.780641	12.033954	11.262386	10.63339	10.041646
1.7	12.41336	11.66074	11.002393	10.329594	9.779031	9.262349
1.8	11.368598	10.695697	10.109691	9.516984	9.030363	8.574847
1.9	10.464303	9.857851	9.331868	8.804973	8.371138	7.96607
2.0	9.675837	9.125417	8.649819	8.17765	7.787889	7.424891

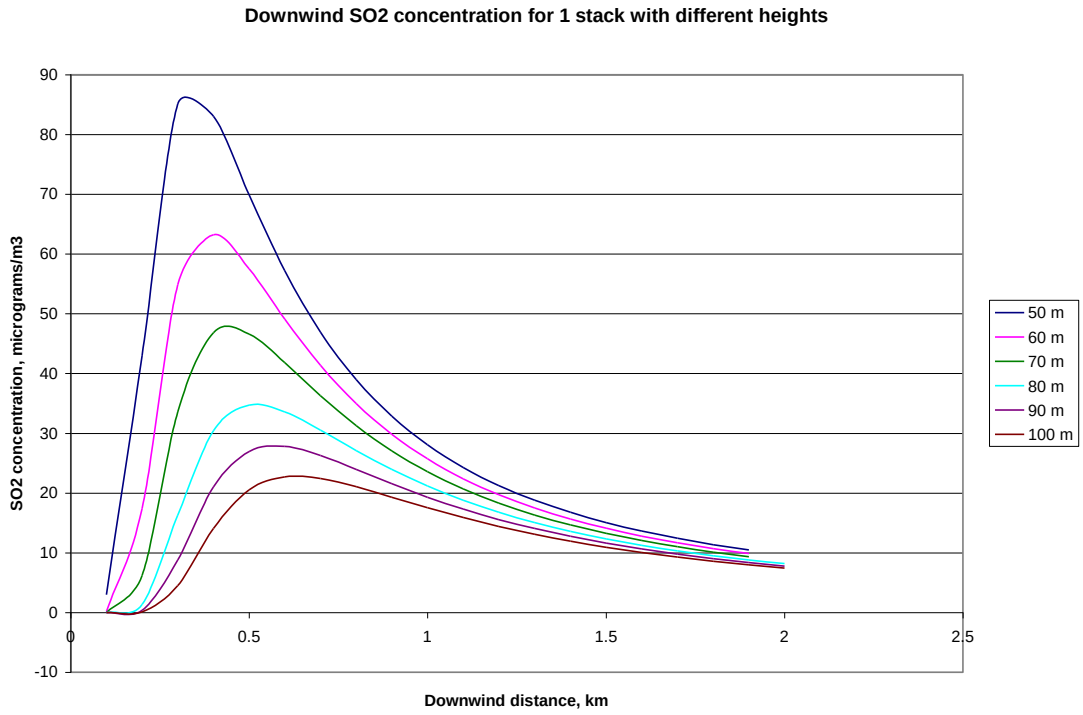

Fig. 4.26 Centerline ground level concentration of SO_2 for different stack heights

The data in the above table are concentration of pollutants at downwind distances from the stack. It can be seen that concentration level at ground level decreases with stack height.

4.3 Effect of 3 stacks with a set location but different stack height on the SO_2 dispersion profile

HAWA is used to simulate the SO_2 dispersion profile form three elevated point source (stack) at different location (L-shaped configuration) with different stack height. As before, 400 receptor points are used and are at ground level.

4.3.1 Meteorology Data

The data used in Table 4.6 are reasonable estimate of meteorological data of a normal Malaysian atmospheric condition.

Table 4.6 Meteorology data 2

Parameter	**Value**
Pasquill-Gifford Stability Class	Neutral (D)
Wind velocity	2 m/s
Wind direction	3.142 rad
Averaging time	10 min
Atmospheric pressure	1000 mb
Mixing height	6000 m
Height wind is recorded	10 m
Terrain type	Urban
Stack tip downwash	Enabled

4.3.2 Emission data

The following data in Table 4.7 are similar for all three stacks with the only difference being the location of the stacks, height of the stacks,

Table 4.7 Emission data 2

Parameter	**Value**
Stack inner diameter	5 m

Flue gas temperature	450 K
Mass flowrate of pollutant SO_2	5 g/s
Half-life of pollutant SO_2	14400 s

4.3.3 Stacks aligned with the x-axis

The first sets of results generated by HAWA are based on the data above with the location of the stacks according to the Table 4.8. The stacks are 500 m apart on the left and right of the center stack. The effect of all three stacks, aligned with the x-axis, to the surroundings can be seen by the contour and 3-dimensional plot of the results in Fig. 4.27 and Fig. 4.28. The stack heights of each stack are shown in Table 4.9.

Table 4.8 Stacks location 2

Stack	**X (km)**	**Y (km)**	**Z (km)**
Stack 1	-0.5	0	0
Stack 2	0	0	0
Stack 3	0.5	0	0

The stack heights are changed to describe the effect of stack height to pollutant concentration distribution to the surroundings and are shown by Fig. 4.27 to Fig. 4.36.

Table 4.9 Stack height for 3 stacks 1

Stack 1	**Stack 2**	**Stack 3**
100 m	50 m	50 m

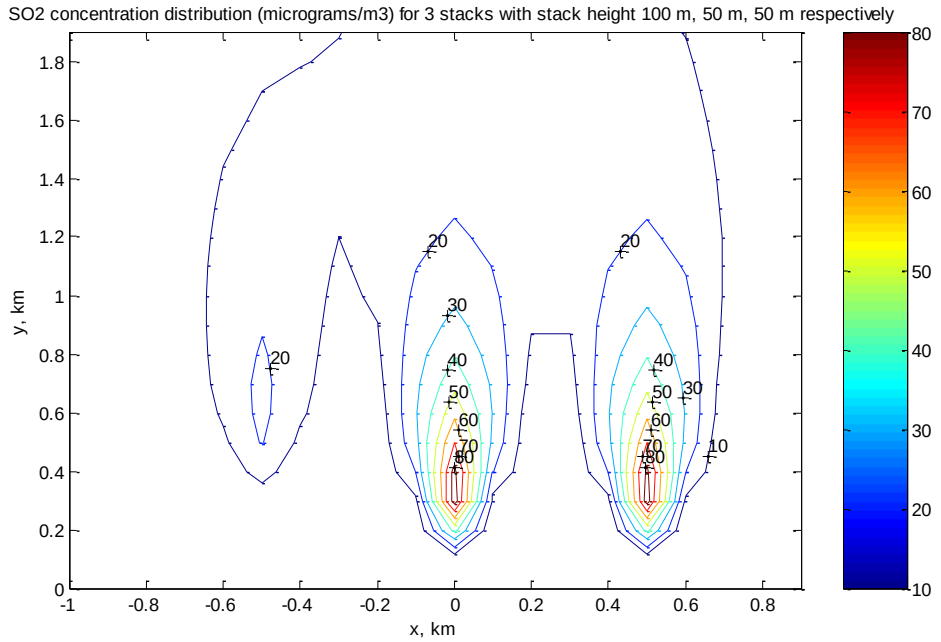

Fig. 4.27 Contour plot of SO_2 concentration distribution ($\mu g/m^3$) for 3 stacks with stack height 100 m, 50 m, 50 m respectively

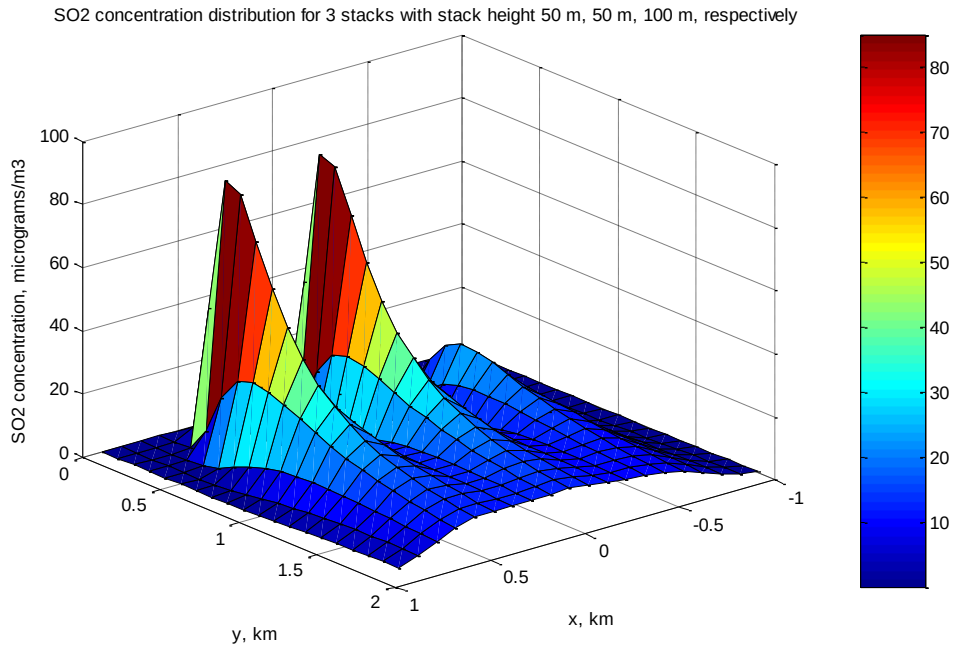

Fig. 4.28 3-D plot of SO_2 concentration distribution for 3 stacks with stack height 100 m, 50 m, 50 m respectively

Table 4.10 Stack height for 3 stacks 2

Stack 1	**Stack 2**	**Stack 3**
100 m	100 m	50 m

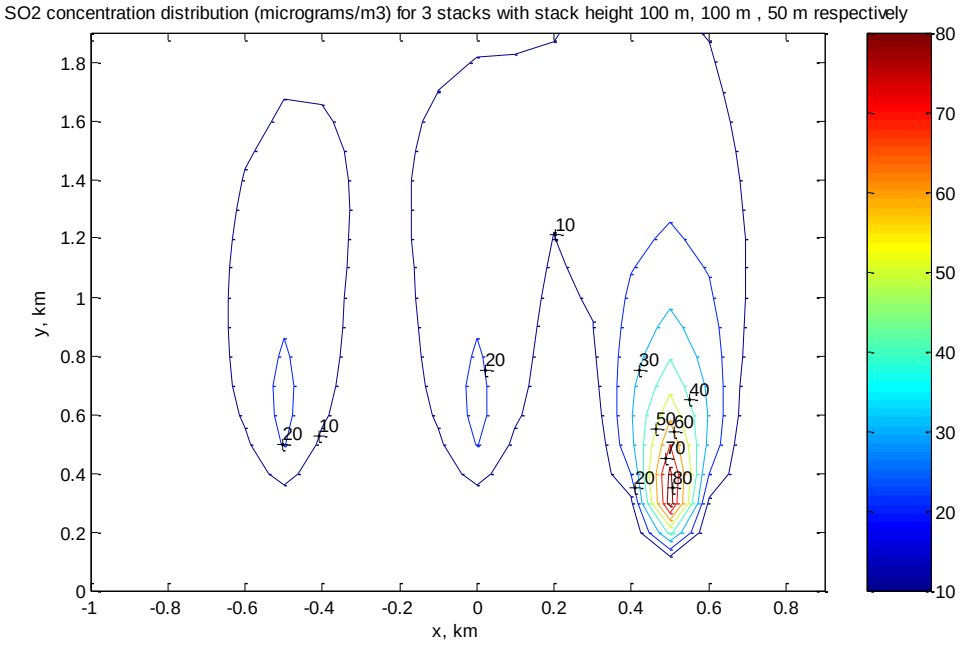

Fig. 4.29 Contour plot of SO_2 concentration distribution ($\mu g/m^3$) for 3 stacks with stack height 100 m, 100 m, 50 m respectively

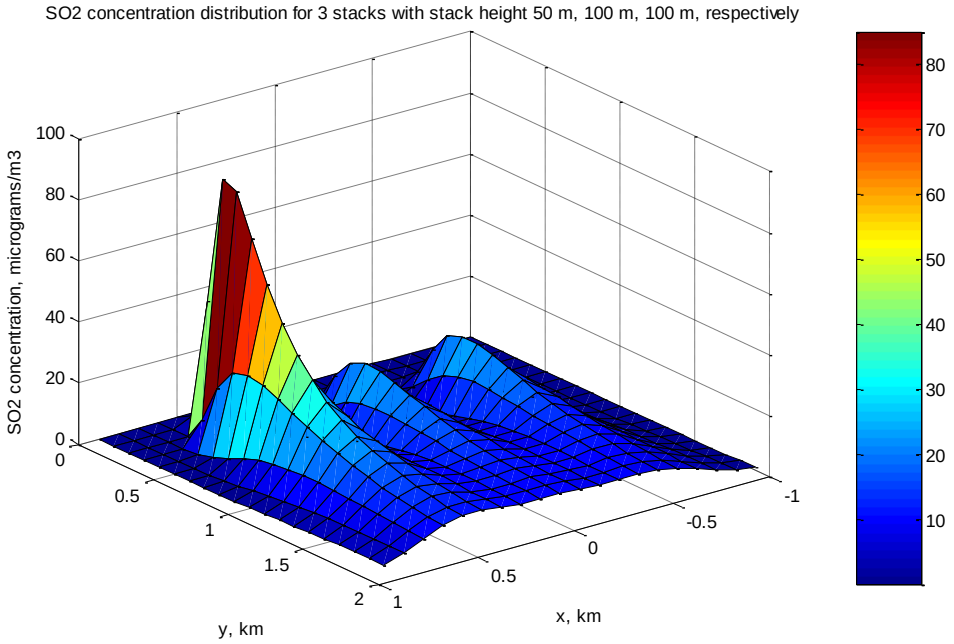

Fig. 4.30 3-D plot of SO_2 concentration distribution for 3 stacks with stack height 100 m, 100 m, 50 m respectively

Table 4.11 Stack height for 3 stacks 3

Stack 1	**Stack 2**	**Stack 3**
100 m	50 m	100 m

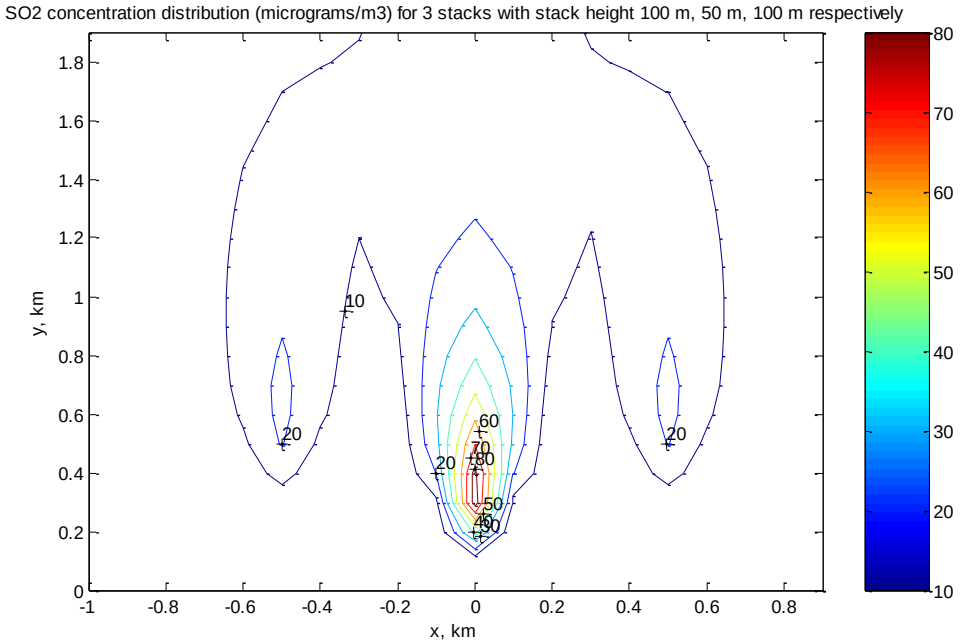

Fig. 4.31 Contour plot of SO_2 concentration distribution ($\mu g/m^3$) for 3 stacks with stack height 100 m, 50 m, 100 m respectively

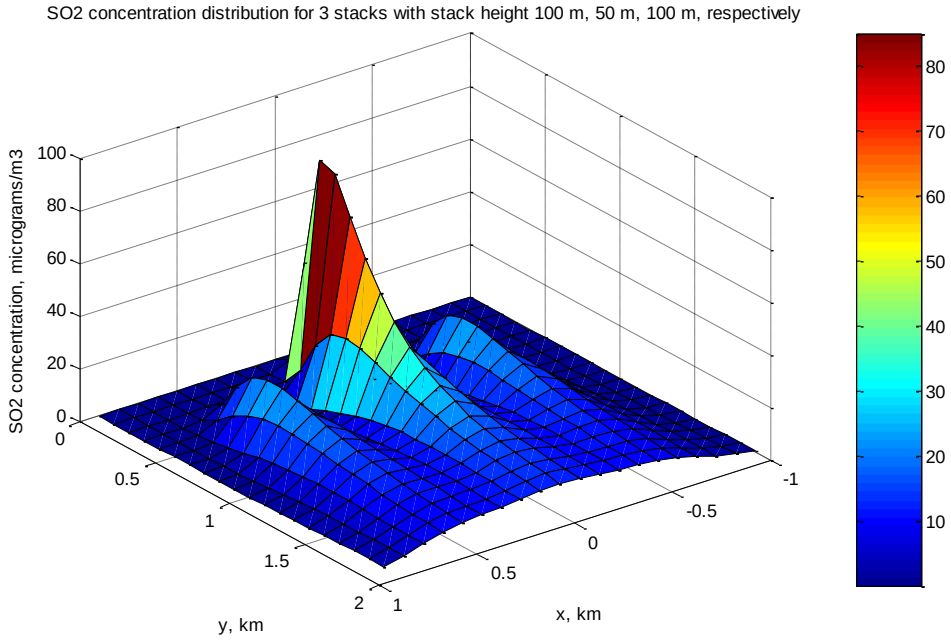

Fig. 4.32 3-D plot of SO_2 concentration distribution for 3 stacks with stack height 100 m, 50 m, 100 m respectively

Table 4.12 Stack height for 3 stacks 4

Stack 1	**Stack 2**	**Stack 3**
50 m	50 m	50 m

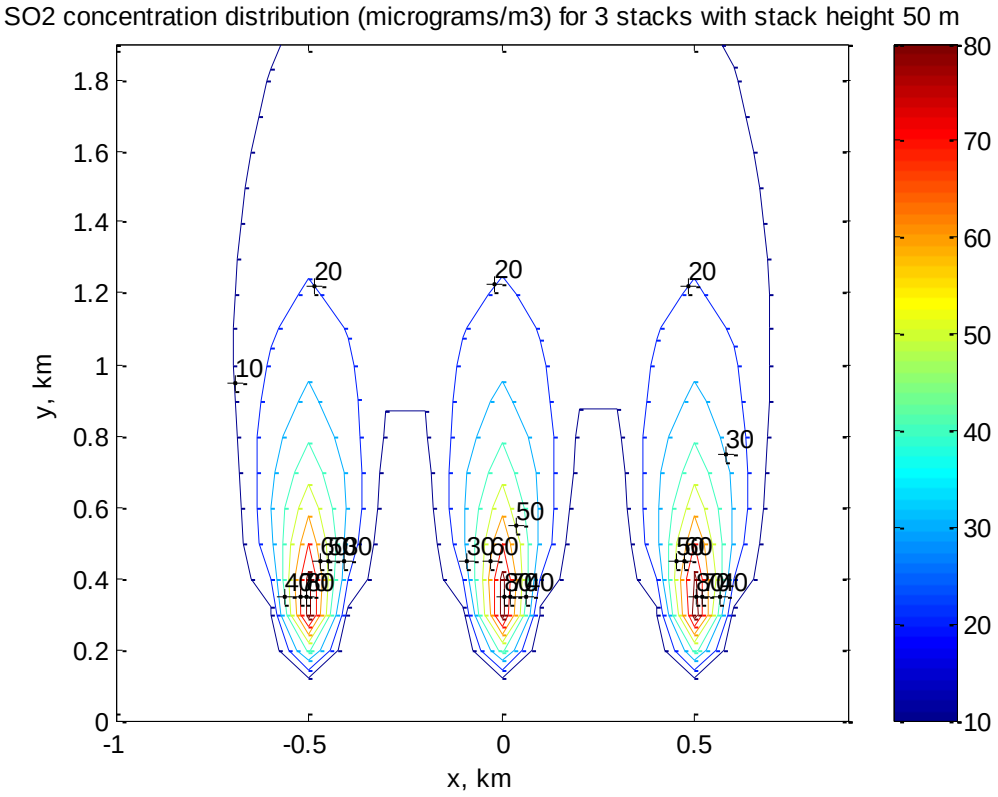

Fig. 4.33 Contour plot of SO_2 concentration distribution ($\mu g/m^3$) for 3 stacks with stack height 50 m

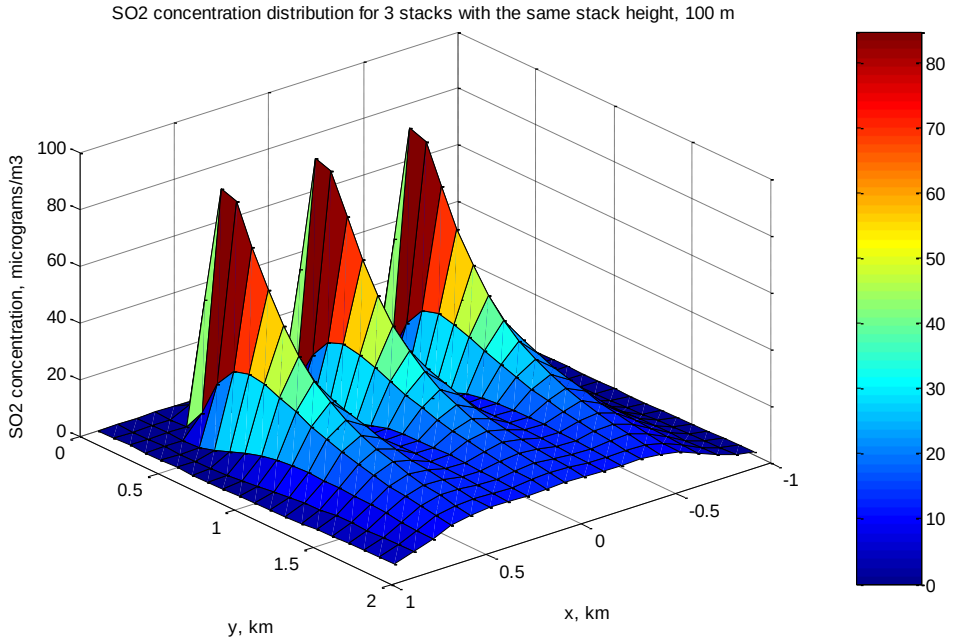

Fig. 4.34 3-D plot of SO_2 concentration distribution for 3 stacks with stack height 50 m

Table 4.13 Stack height for 3 stacks 5

Stack 1	**Stack 2**	**Stack 3**
100 m	100 m	100 m

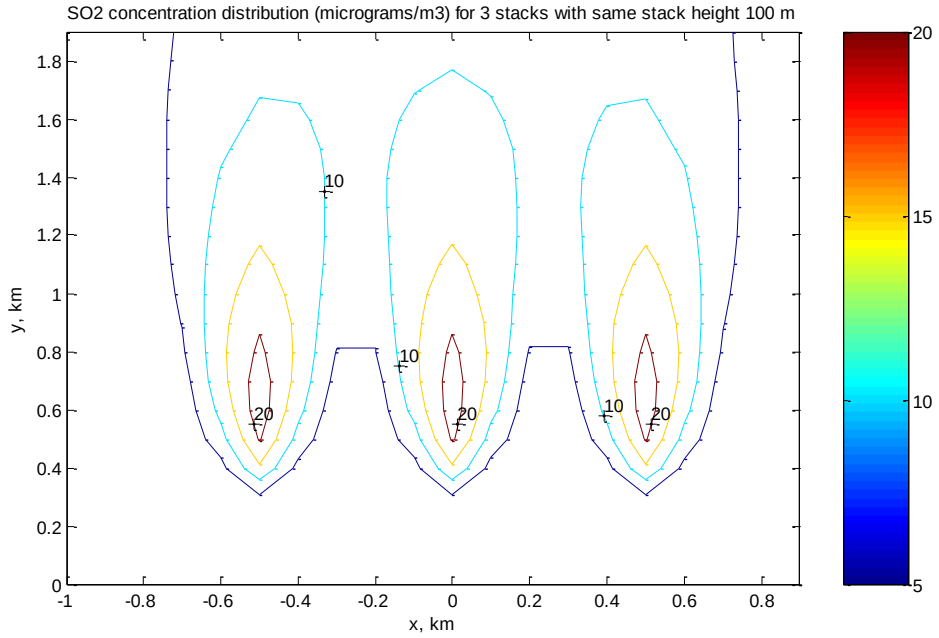

Fig. 4.35 Contour plot of SO_2 concentration distribution ($\mu g/m^3$) for 3 stacks with stack height 100 m

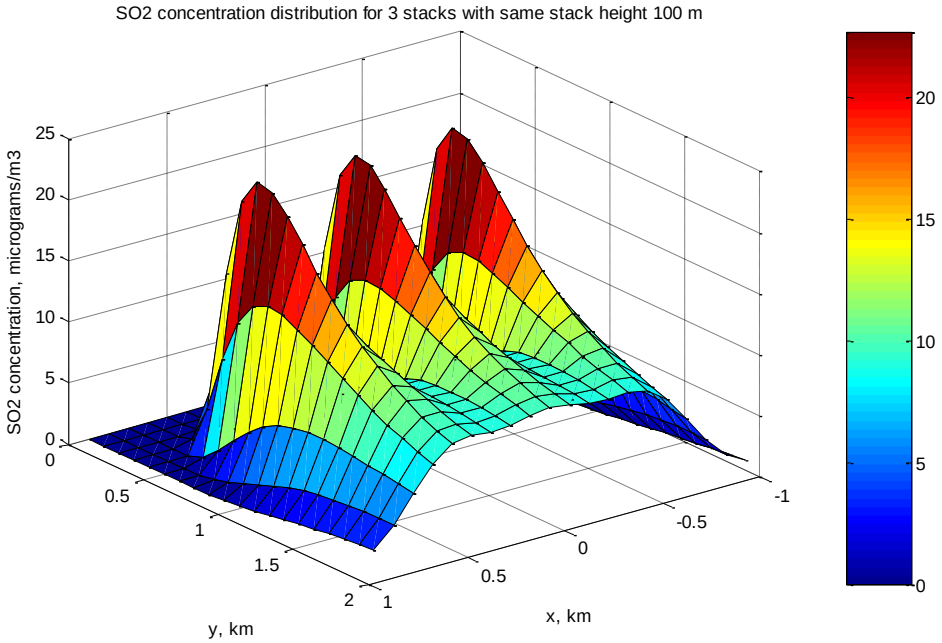

Fig. 4.36 3-D plot of SO_2 concentration distribution for 3 stacks with stack height 100 m

4.3.4 Stacks aligned with the y-axis

The stacks are aligned with y-axis to show the effect of the environment directly downwind to this type of stack configuration. The stacks are positioned 500 m in front and behind the center stack. The results are shown by Fig. 4.37 to Fig. 4.50.

Table 4.14 Stack location 3

Stack	**X (km)**	**Y (km)**	**Z (km)**
Stack 1	0	0.5	0
Stack 2	0	0	0
Stack 3	0	-0.5	0

Table 4.15 Stack height for 3 stacks 5

Stack 1	**Stack 2**	**Stack 3**
50 m	50 m	50 m

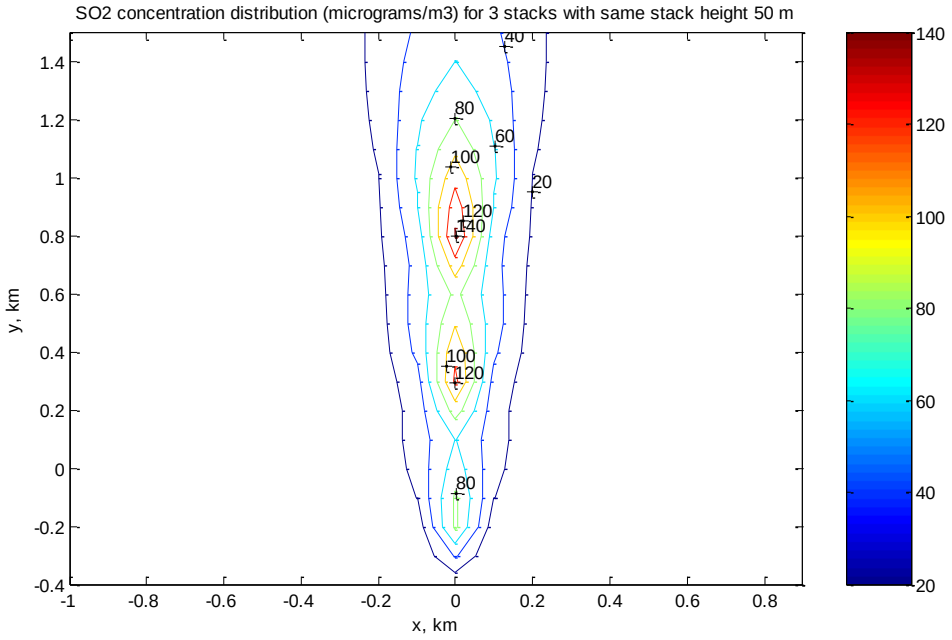

Fig. 4.37 Contour plot of SO_2 concentration distribution ($\mu g/m^3$) for 3 stacks with stack height 50 m

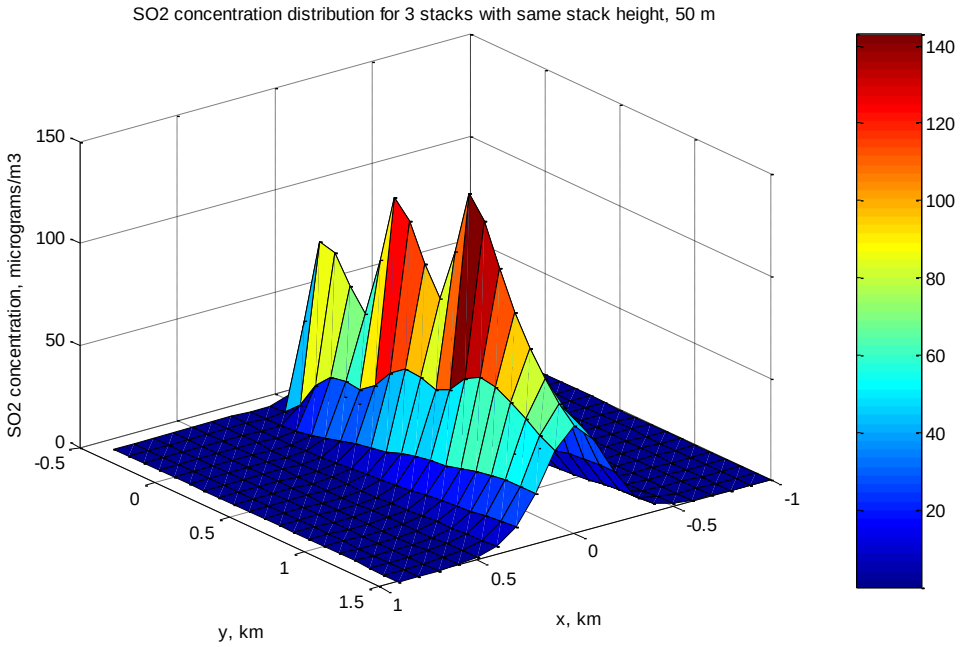

Fig. 4.38 3-D plot of SO_2 concentration distribution for 3 stacks with stack height 50 m

Table 4.16 Stack height for 3 stacks 6

Stack 1	**Stack 2**	**Stack 3**
100 m	50 m	50 m

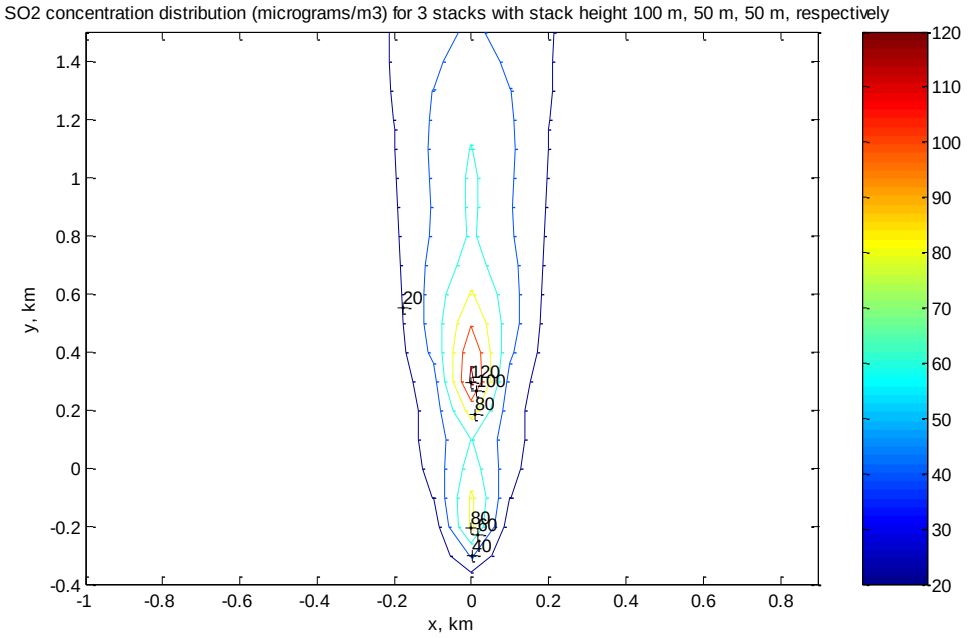

Fig. 4.39 Contour plot of SO_2 concentration distribution ($\mu g/m^3$) for 3 stacks with stack height 100 m, 50 m, 50 m respectively

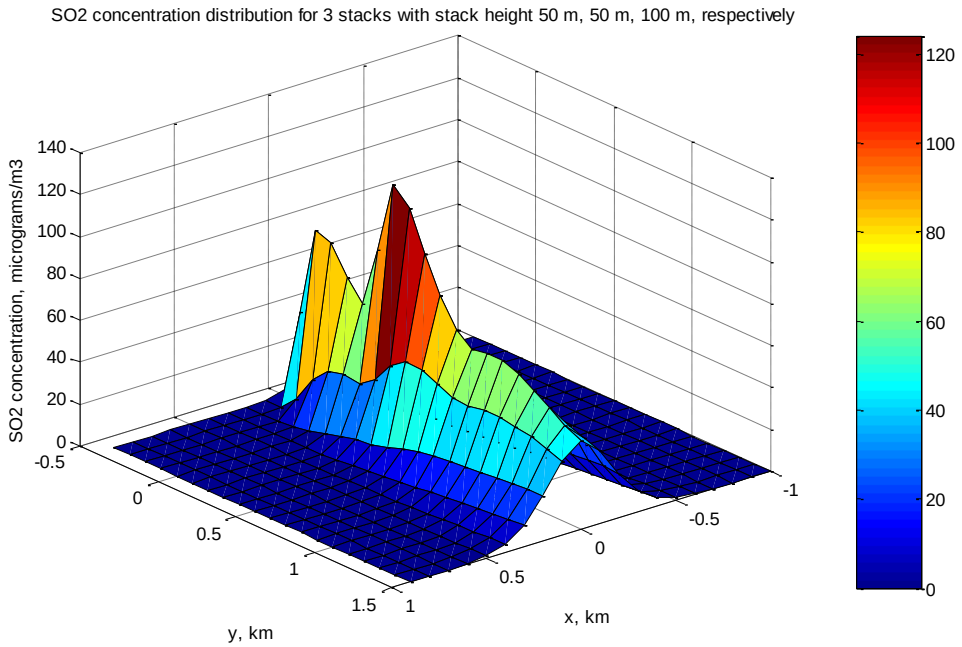

Fig. 4.40 3-D plot of SO_2 concentration distribution for 3 stacks with stack height 100 m, 50 m, 50 m respectively

Table 4.17 Stack height for 3 stacks 7

Stack 1	**Stack 2**	**Stack 3**
50 m	100 m	50 m

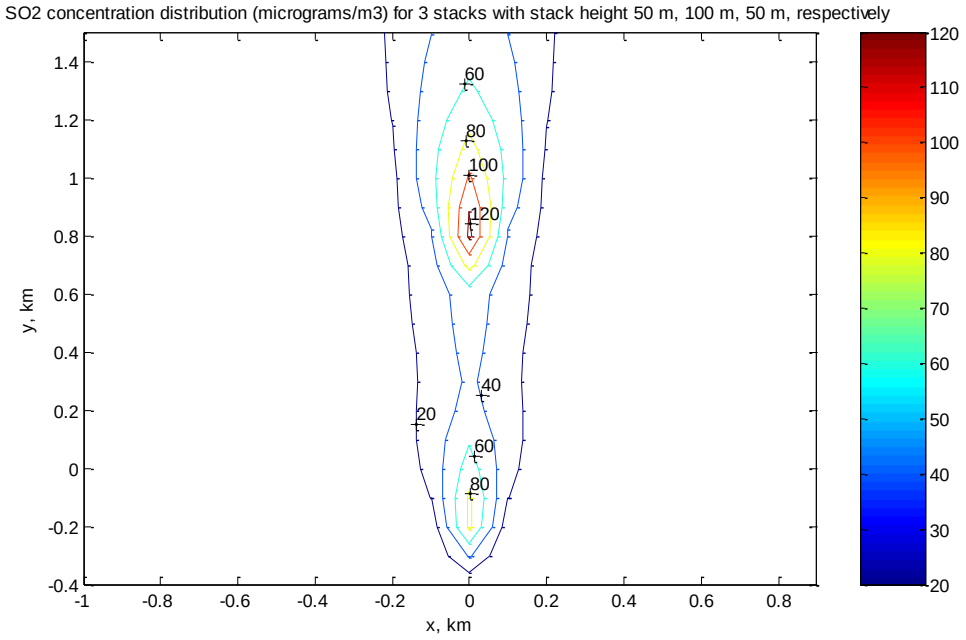

Fig. 4.41 Contour plot of SO_2 concentration distribution ($\mu g/m^3$) for 3 stacks with stack height 50 m, 100 m, 50 m respectively

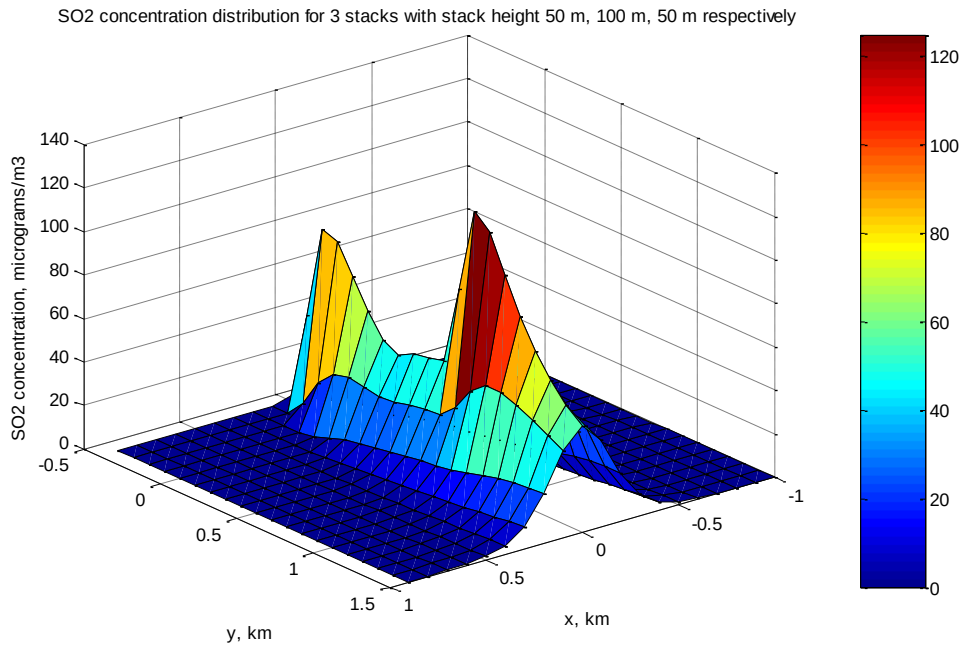

Fig. 4.42 3-D plot of SO_2 concentration distribution for 3 stacks with stack height 50 m, 100 m, 50 m respectively

Table 4.18 Stack height for 3 stacks 8

Stack 1	**Stack 2**	**Stack 3**
50 m	50 m	100 m

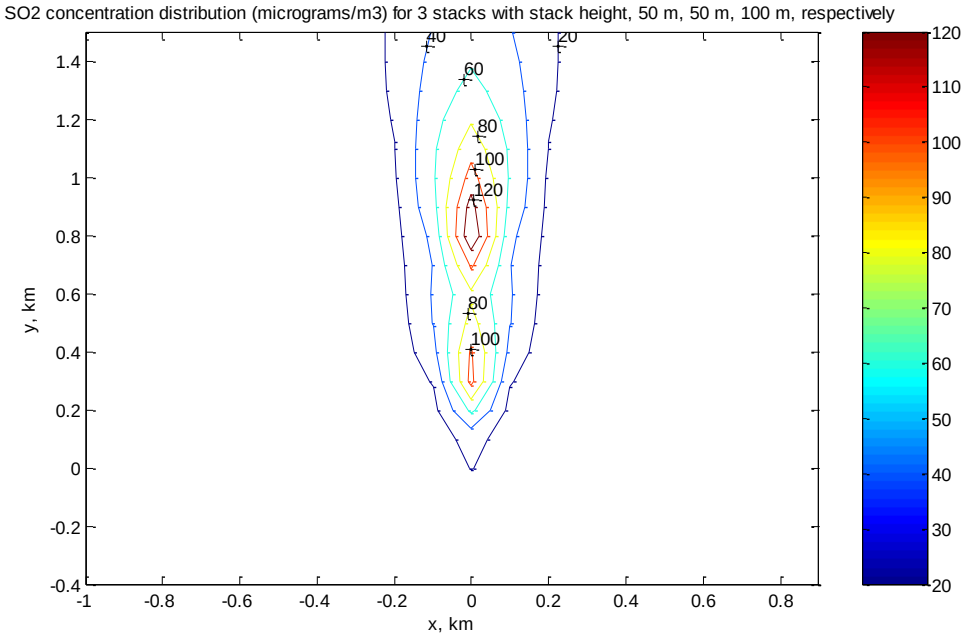

Fig. 4.43 Contour plot of SO_2 concentration distribution ($\mu g/m^3$) for 3 stacks with stack height 50 m, 50 m, 100 m respectively

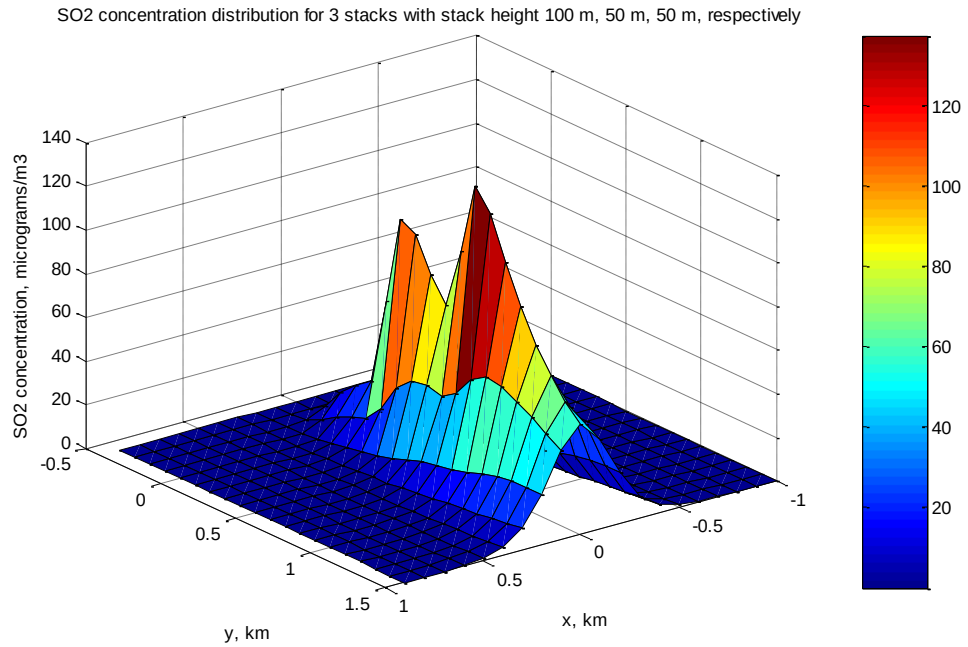

Fig. 4.44 3-D plot of SO_2 concentration distribution for 3 stacks with stack height 50 m, 50 m, 100 m respectively

Table 4.19 Stack height for 3 stacks 9

Stack 1	**Stack 2**	**Stack 3**
100 m	100 m	50 m

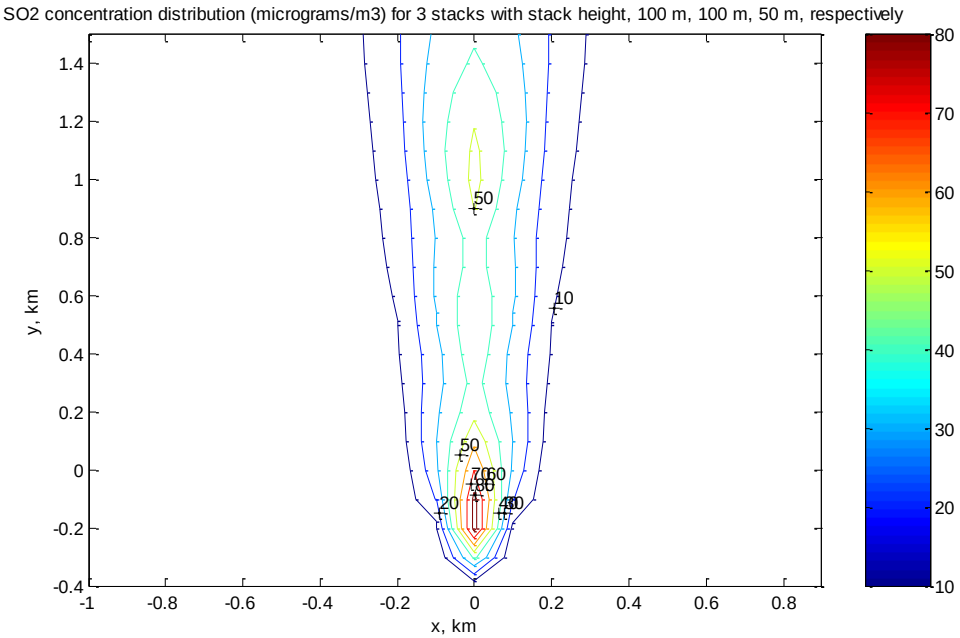

Fig. 4.45 Contour plot of SO_2 concentration distribution ($\mu g/m^3$) for 3 stacks with stack height 100 m, 100 m, 50 m respectively

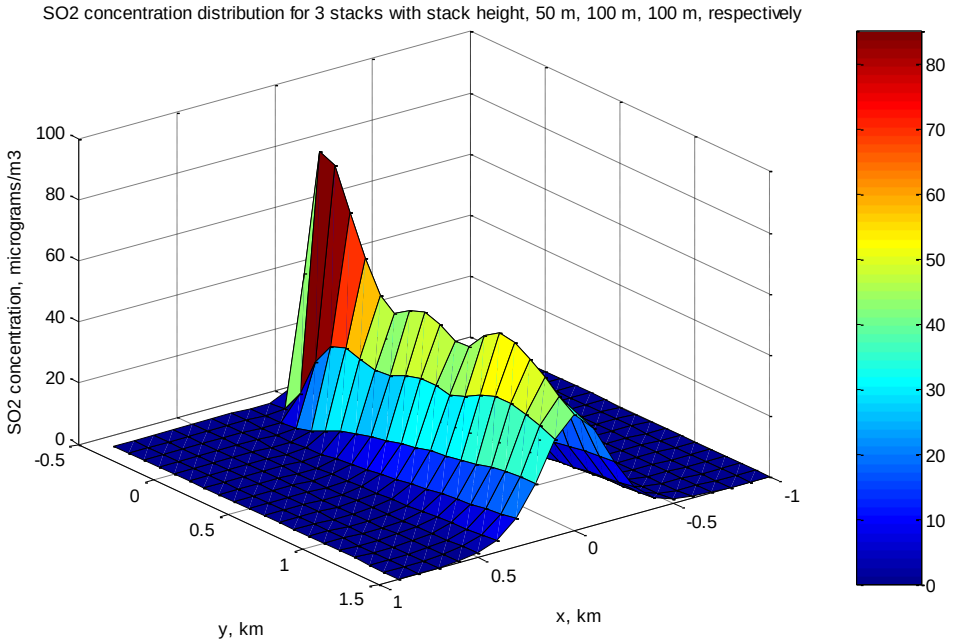

Fig. 4.46 3-D plot of SO_2 concentration distribution for 3 stacks with stack height 100 m, 100 m, 50 m respectively

Table 4.20 Stack height for 3 stacks 10

Stack 1	**Stack 2**	**Stack 3**
100 m	50 m	100 m

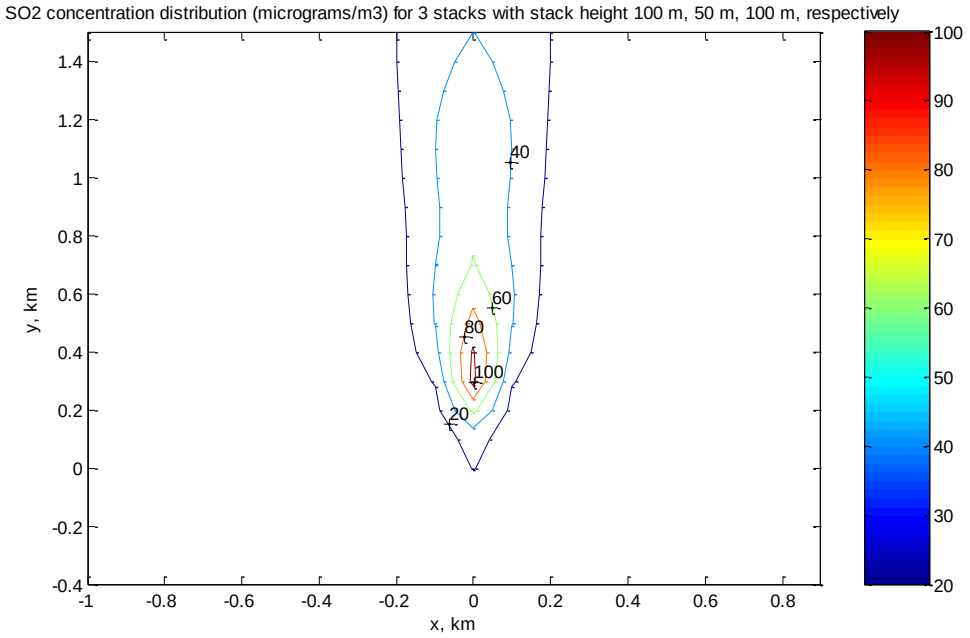

Fig. 4.47 Contour plot of SO_2 concentration distribution ($\mu g/m^3$) for 3 stacks with stack height 100 m, 50 m, 100 m respectively

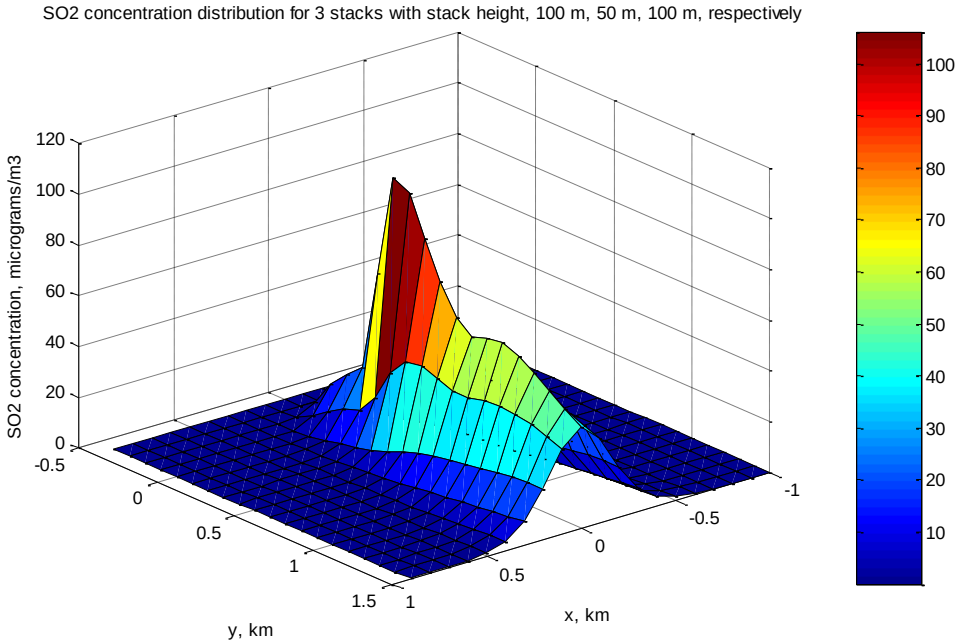

Fig. 4.48 3-D plot of SO_2 concentration distribution for 3 stacks with stack height 100 m, 50 m, 100 m respectively

Table 4.21 Stack height for 3 stacks 11

Stack 1	**Stack 2**	**Stack 3**
100 m	100 m	100 m

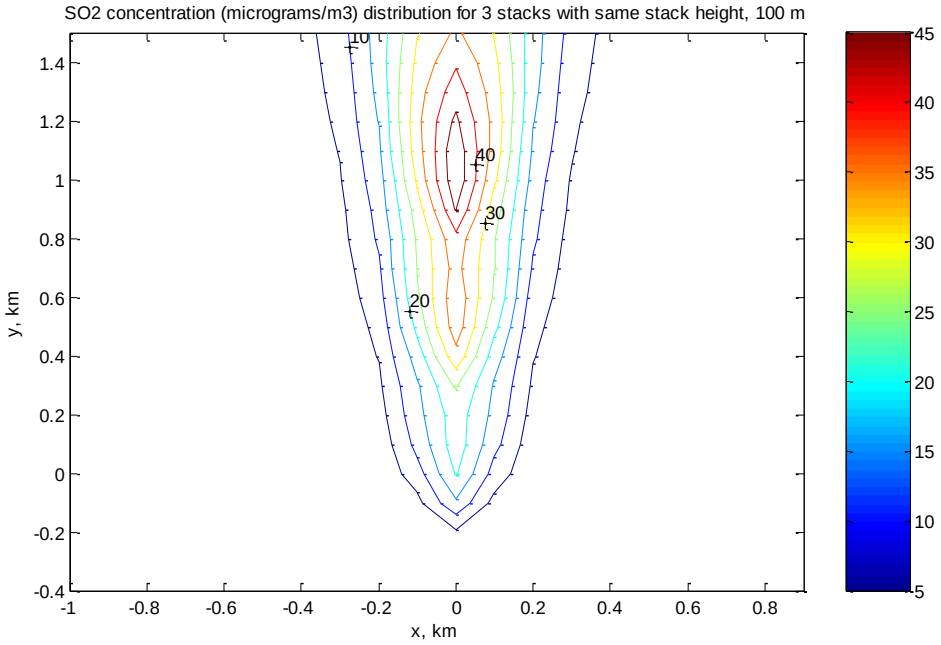

Fig. 4.49 Contour plot of SO_2 concentration distribution ($\mu g/m^3$) for 3 stacks with stack height 100 m

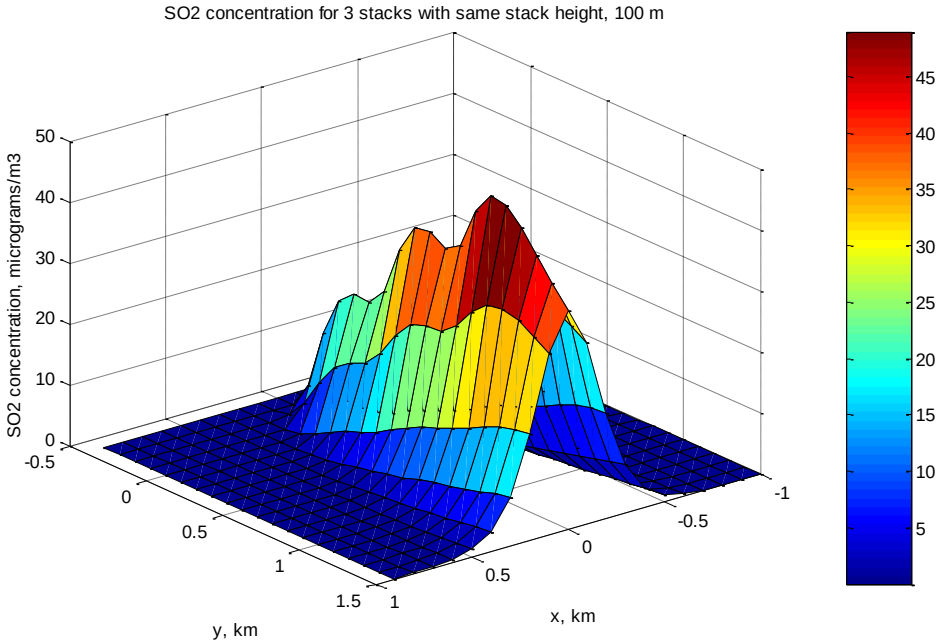

Fig. 4.50 3-D plot of SO_2 concentration distribution for 3 stacks with stack height 100 m

4.3.5 Stacks of L-shaped configuration with different stack height

The stacks are arranged in an L-shaped configuration to show the effect of the environment directly downwind to this type of stack formation. The stacks are positioned 500 m in front and right of the center stack. The results are shown by Fig. 4.51 to Fig. 4.66.

Table 4.22 Stack location 4

Stack	**X (km)**	**Y (km)**	**Z (km)**
Stack 1	0	0.5	0
Stack 2	0	0	0
Stack 3	0.5	0	0

Table 4.23 Stack height for 3 stacks 12

Stack 1	**Stack 2**	**Stack 3**
50 m	50 m	50 m

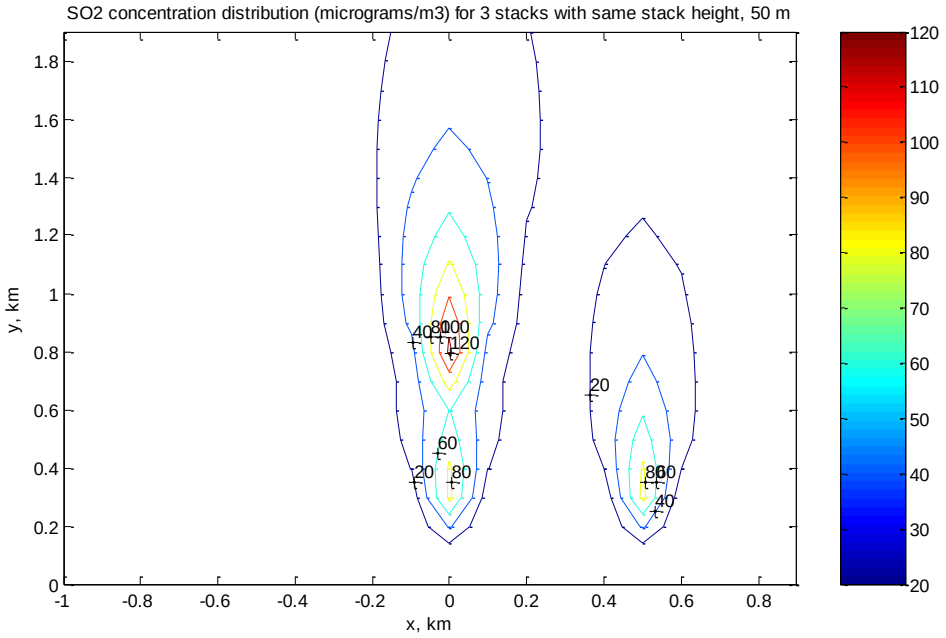

Fig. 4.51 Contour plot of SO_2 concentration distribution ($\mu g/m^3$) for 3 stacks with stack height 50 m

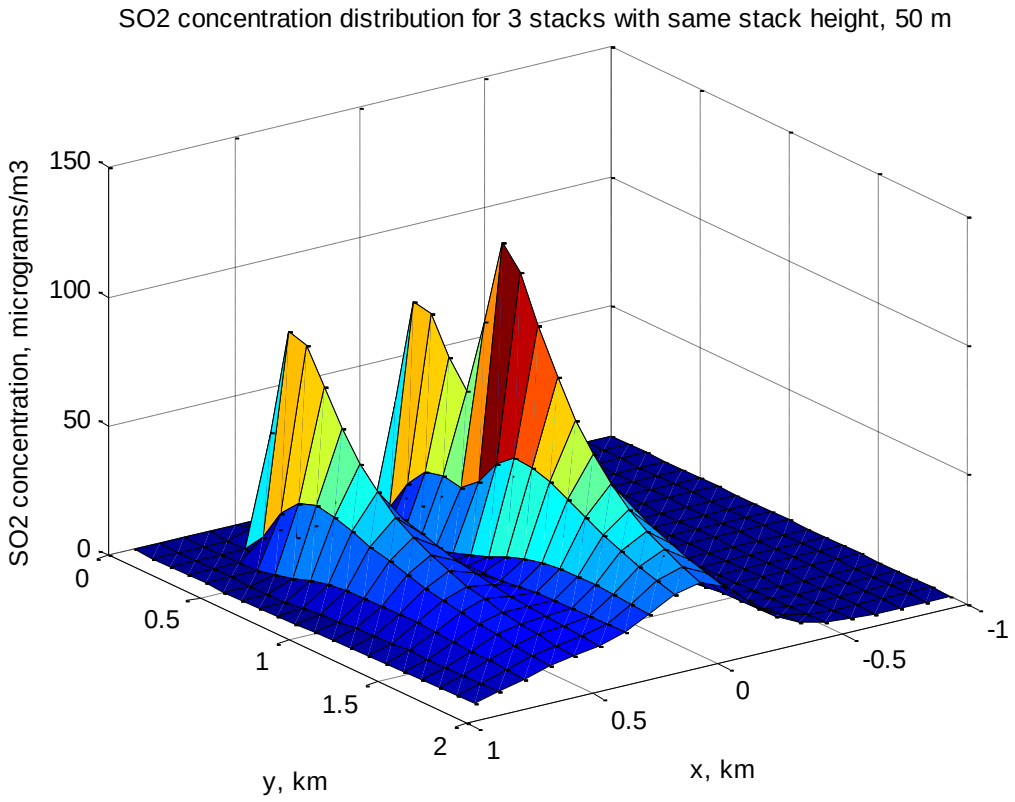

Fig. 4.52 3-D plot of SO_2 concentration distribution for 3 stacks with stack height 50 m

Table 4.24 Stack height for 3 stacks 13

Stack 1	**Stack 2**	**Stack 3**
100 m	100 m	100 m

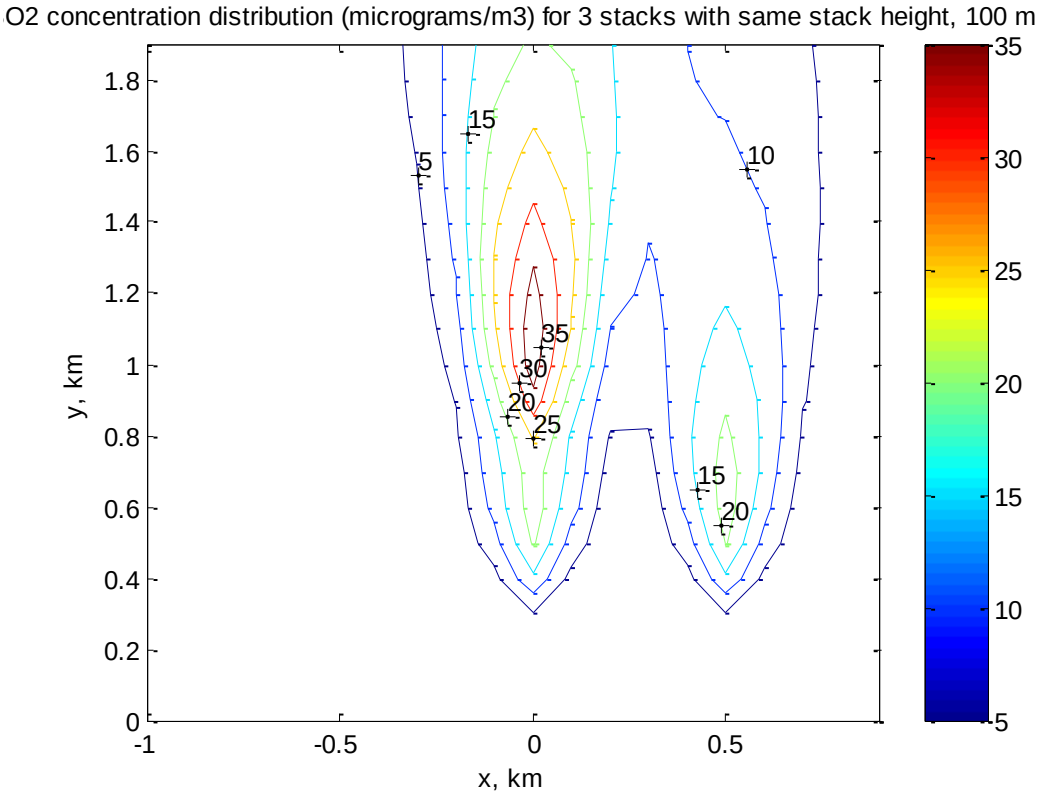

Fig. 4.53 Contour plot of SO_2 concentration distribution ($\mu g/m^3$) for 3 stacks with stack height 100 m

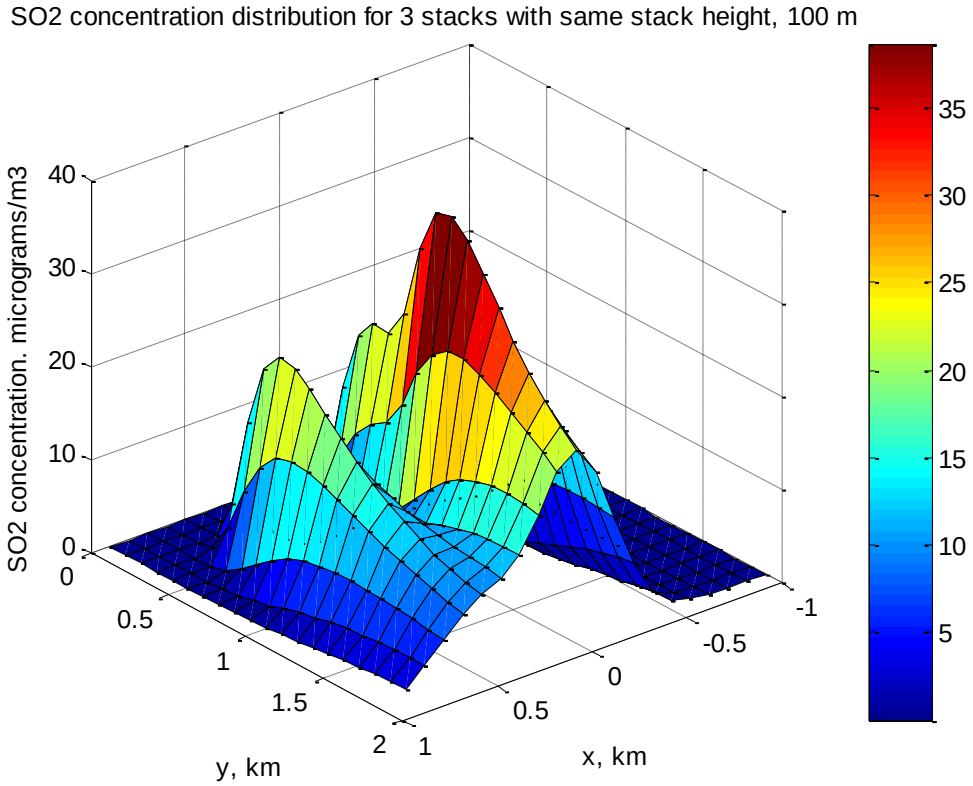

Fig. 4.54 3-D plot of SO_2 concentration distribution for 3 stacks with stack height 100 m

Table 4.25 Stack height for 3 stacks 14

Stack 1	**Stack 2**	**Stack 3**
50 m	100 m	50 m

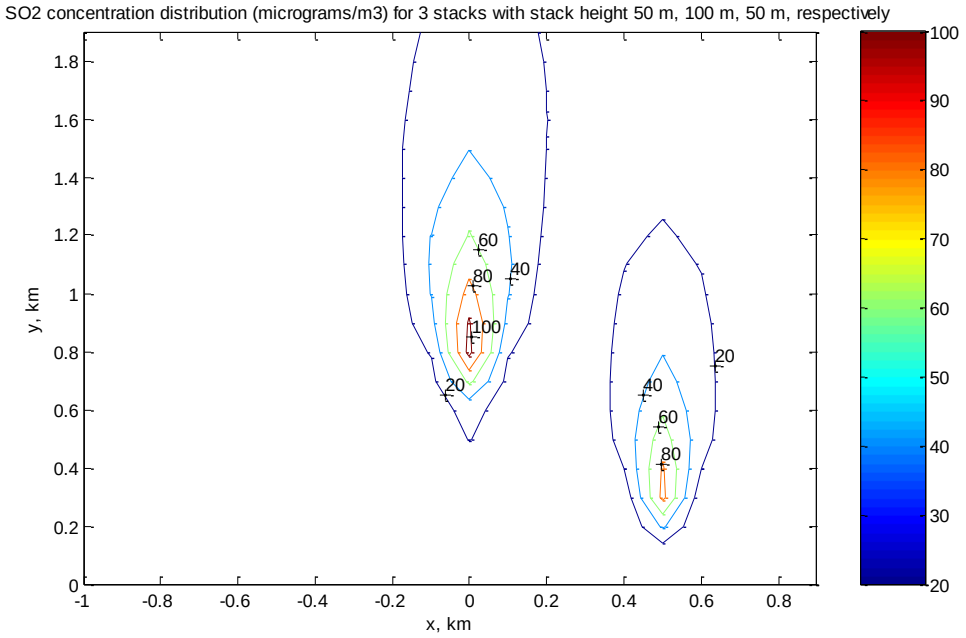

Fig. 4.55 Contour plot of SO_2 concentration distribution ($\mu g/m^3$) for 3 stacks with stack height 50 m, 100 m, 50 m respectively

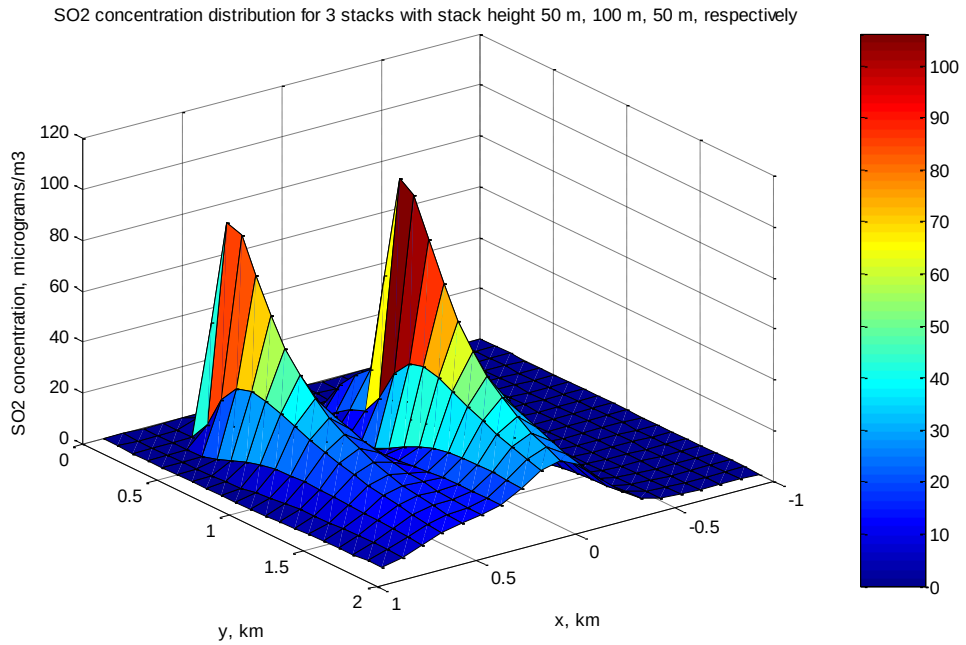

Fig. 4.56 3-D plot of SO_2 concentration distribution for 3 stacks with stack height 50 m, 100 m, 50 m respectively

Table 4.26 Stack height for 3 stacks 15

Stack 1	**Stack 2**	**Stack 3**
100 m	50 m	100 m

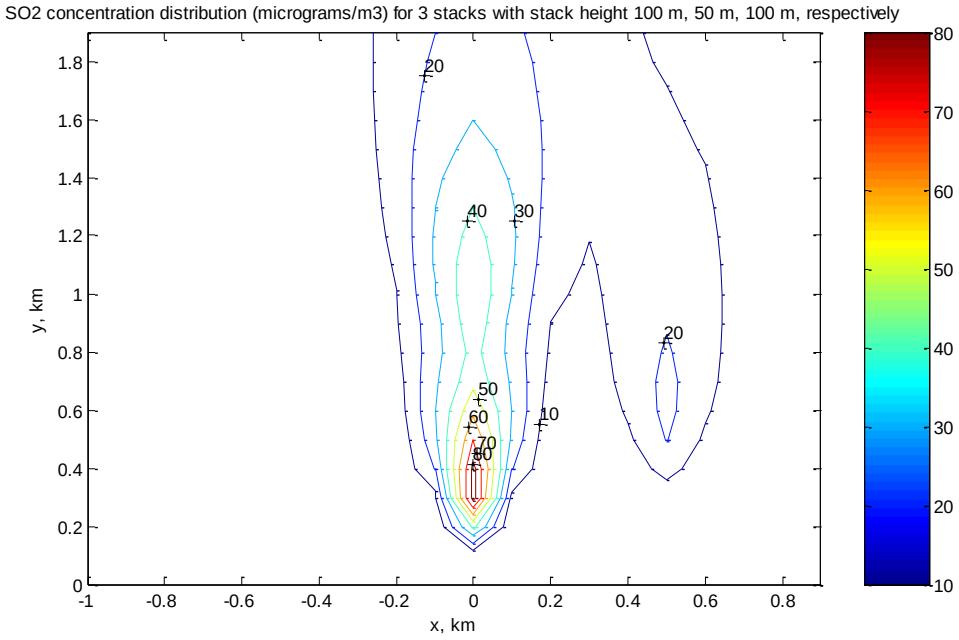

Fig. 4.57 Contour plot of SO_2 concentration distribution ($\mu g/m^3$) for 3 stacks with stack height 100 m, 50 m, 100 m respectively

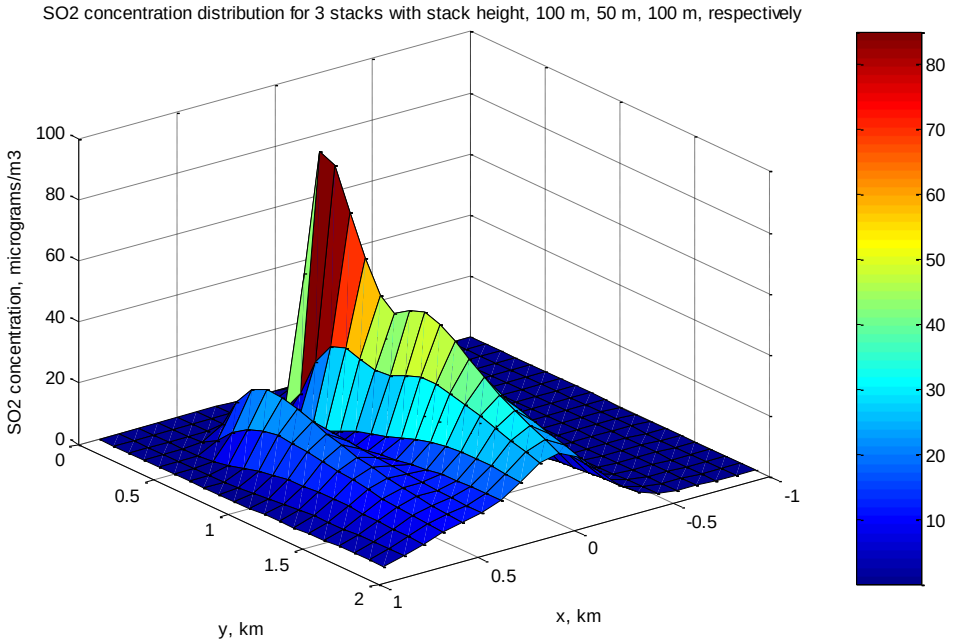

Fig. 4.58 3-D plot of SO_2 concentration distribution for 3 stacks with stack height 100 m, 50 m, 100 m respectively

Table 4.27 Stack height for 3 stacks 16

Stack 1	**Stack 2**	**Stack 3**
100 m	100 m	50 m

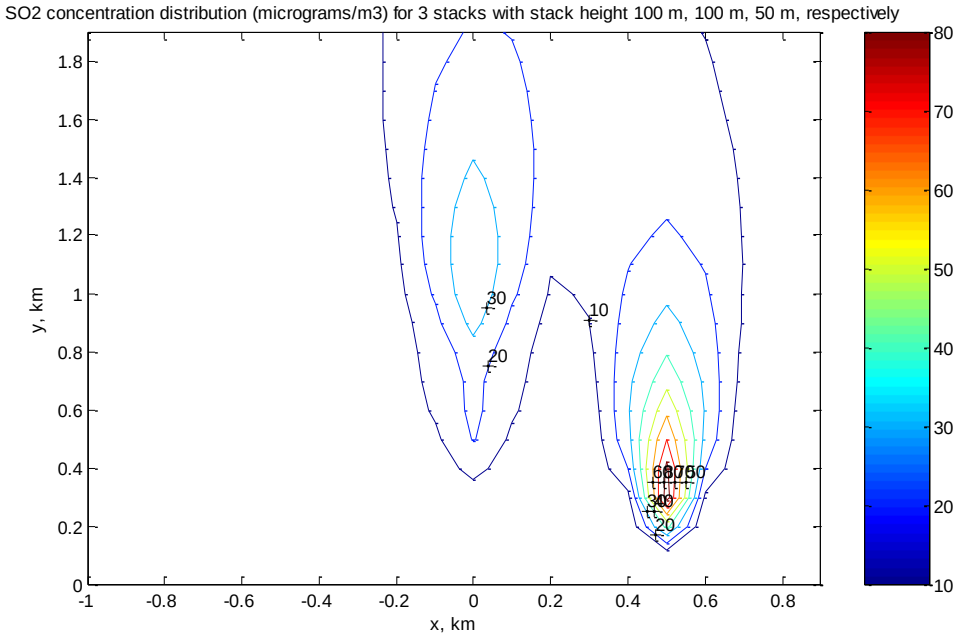

Fig. 4.59 Contour plot of SO_2 concentration distribution ($\mu g/m^3$) for 3 stacks with stack height 100 m, 100 m, 50 m respectively

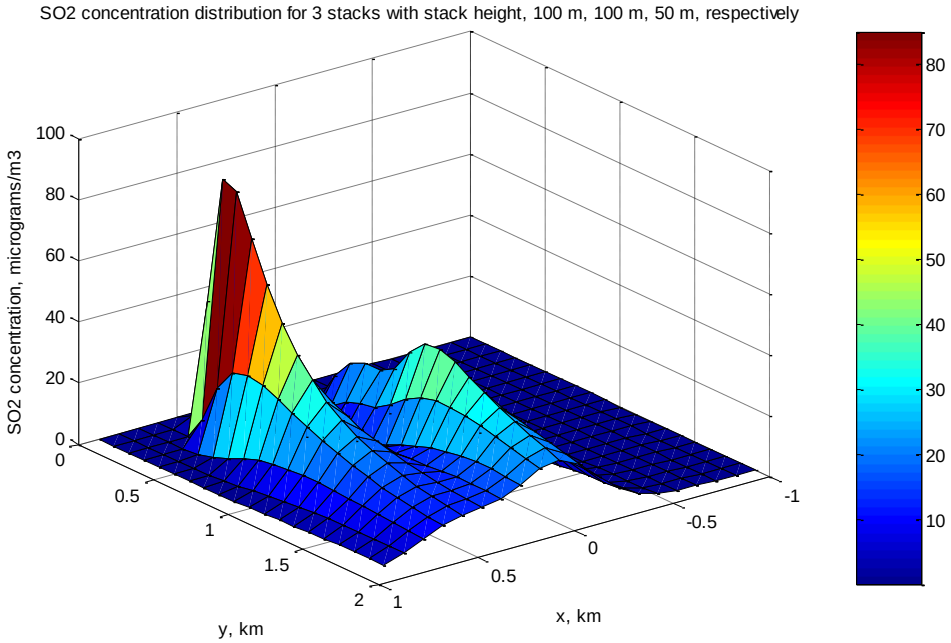

Fig. 4.60 3-D plot of SO_2 concentration distribution for 3 stacks with stack height 100 m, 100 m, 50 m respectively

Table 4.28 Stack height for 3 stacks 17

Stack 1	**Stack 2**	**Stack 3**
50 m	50 m	100 m

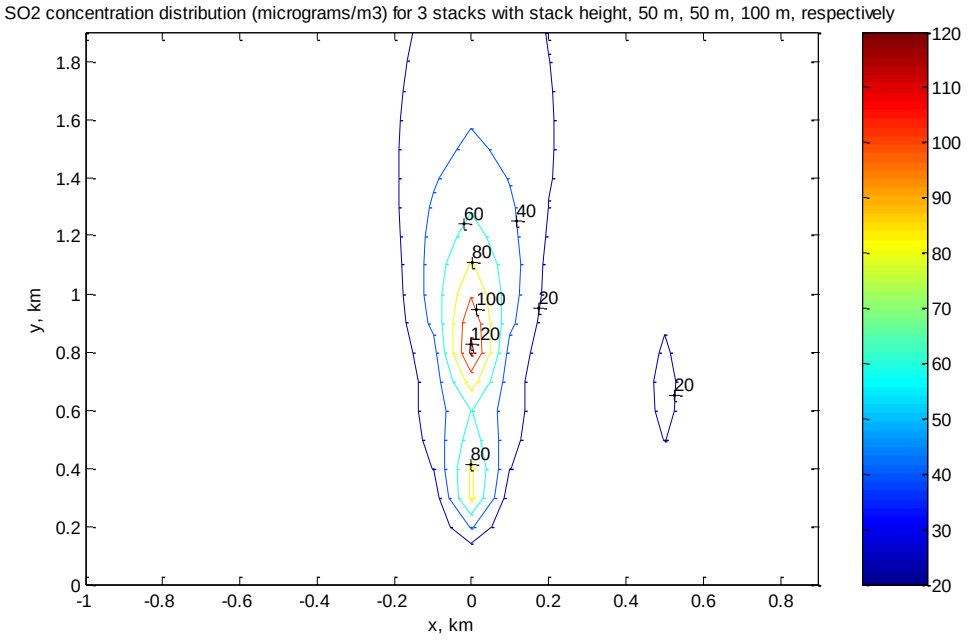

Fig. 4.61 Contour plot of SO_2 concentration distribution ($\mu g/m^3$) for 3 stacks with stack height 50 m, 50 m, 100 m respectively

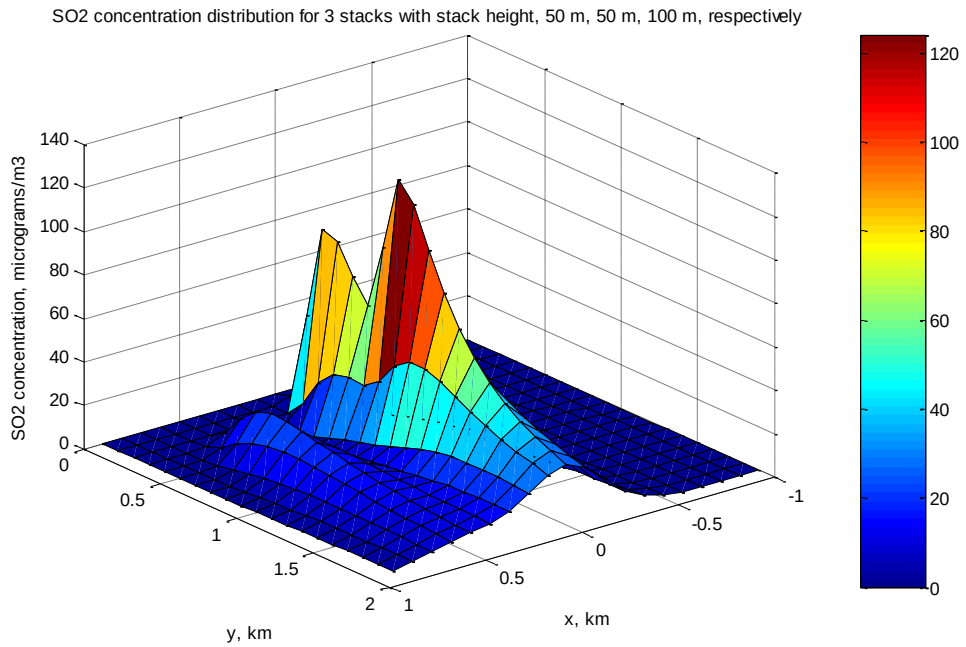

Fig. 4.62 3-D plot of SO_2 concentration distribution for 3 stacks with stack height 50 m, 50 m, 100 m respectively

Table 4.29 Stack height for 3 stacks 18

Stack 1	**Stack 2**	**Stack 3**
50 m	100 m	100 m

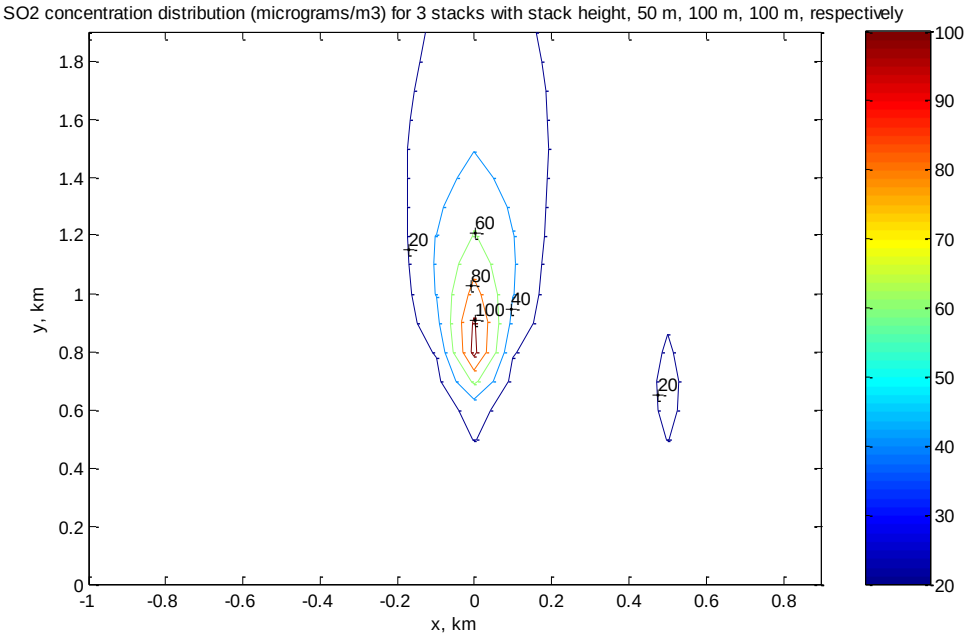

Fig. 4.63 Contour plot of SO_2 concentration distribution ($\mu g/m^3$) for 3 stacks with stack height 50 m, 100 m, 100 m respectively

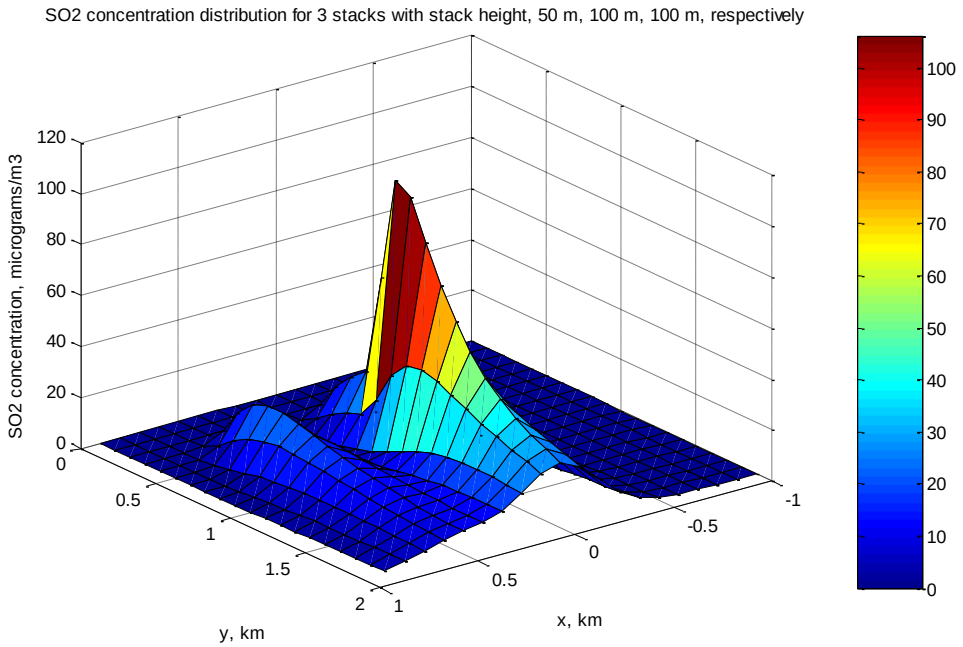

Fig. 4.64 3-D plot of SO_2 concentration distribution for 3 stacks with stack height 50 m, 100 m, 100 m respectively

Table 4.30 Stack height for 3 stacks 19

Stack 1	**Stack 2**	**Stack 3**
100 m	50 m	50 m

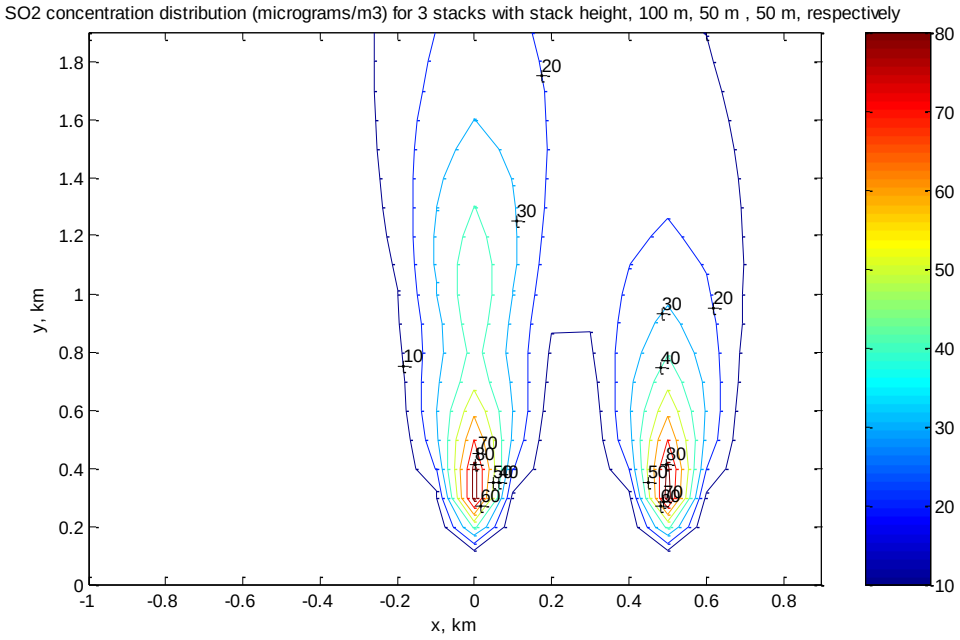

Fig. 4.65 Contour plot of SO_2 concentration distribution (µg/m^3) for 3 stacks with stack height 100 m, 50 m, 50 m respectively

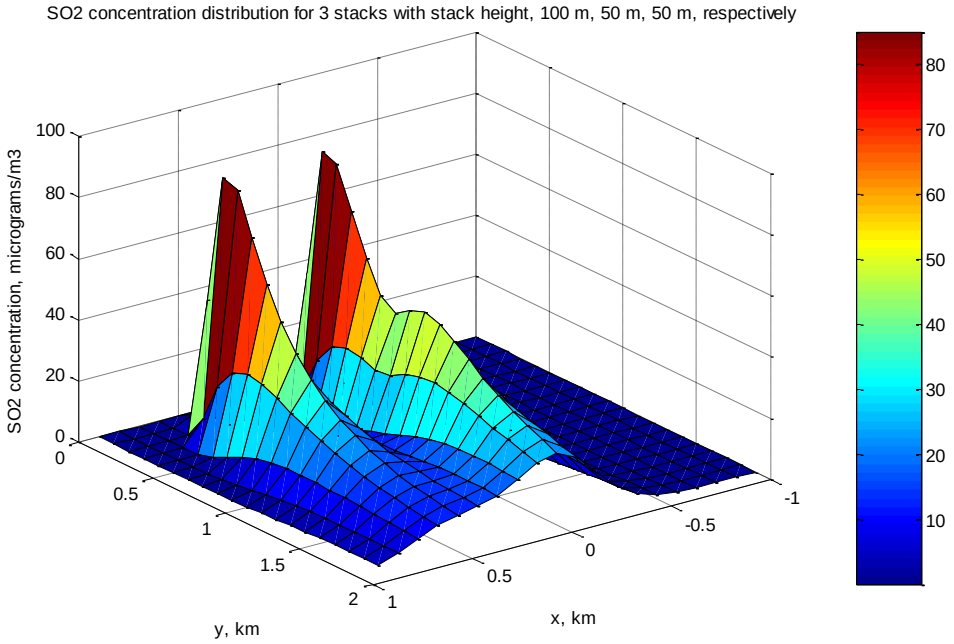

Fig. 4.66 3-D plot of SO_2 concentration distribution for 3 stacks with stack height 100 m, 50 m, 50 m respectively

4.3.6 Effect of building height on SO_2 dispersion profile

The emission and meteorology data are the same as previous section with an addition of building height and building width parameter. The Schulman-Scire plume rise and building downwash option are also enabled.

Table 4.31 Stack location and height with building width

Parameter	**Value**
Stack height	50 m
Stack location: x-coordinate	0
Stack location: y-coordinate	0
Building width	100 m

4.3.6.1 Building height 100 m

The dispersion profile of SO2 with building height 100 m are shown in Fig. 4.67 and Fig. 4.68.

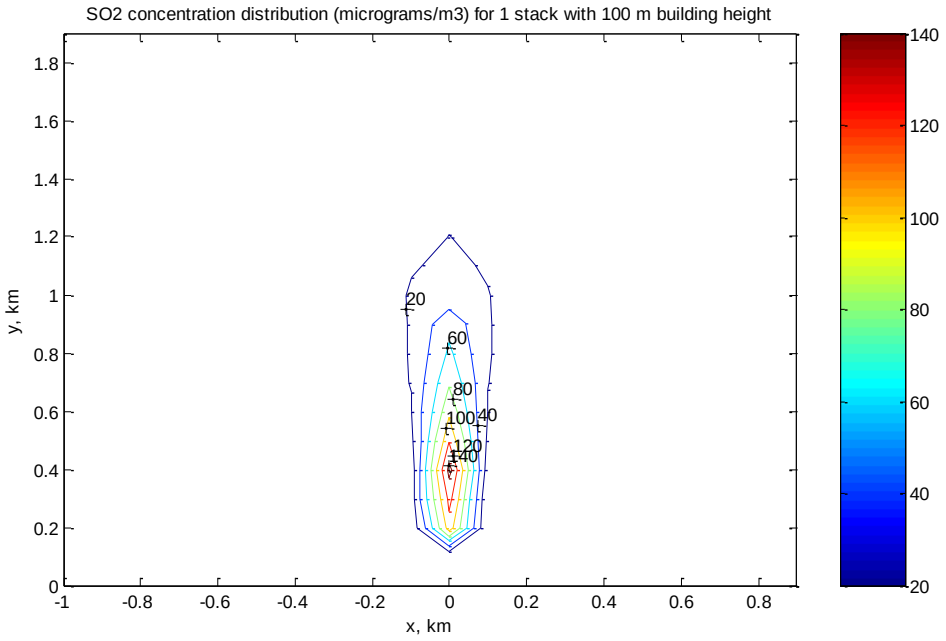

Fig. 4.67 Contour plot of SO_2 concentration distribution ($\mu g/m^3$) for 1 stack with 100 m building height

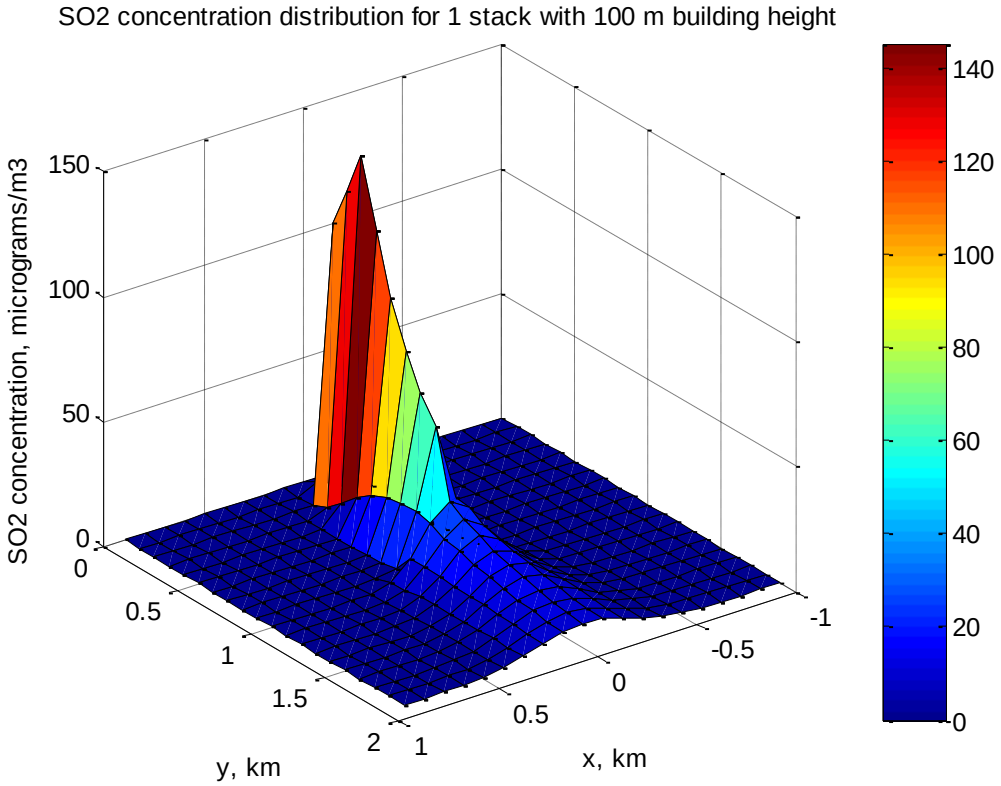

Fig. 4.68 3-D plot of SO_2 concentration distribution for 1 stack with 100 m building height

4.3.6.2 Building height 80 m

The dispersion profile of SO2 with building height 80 m are shown in Fig. 4.69 and Fig. 4.70.

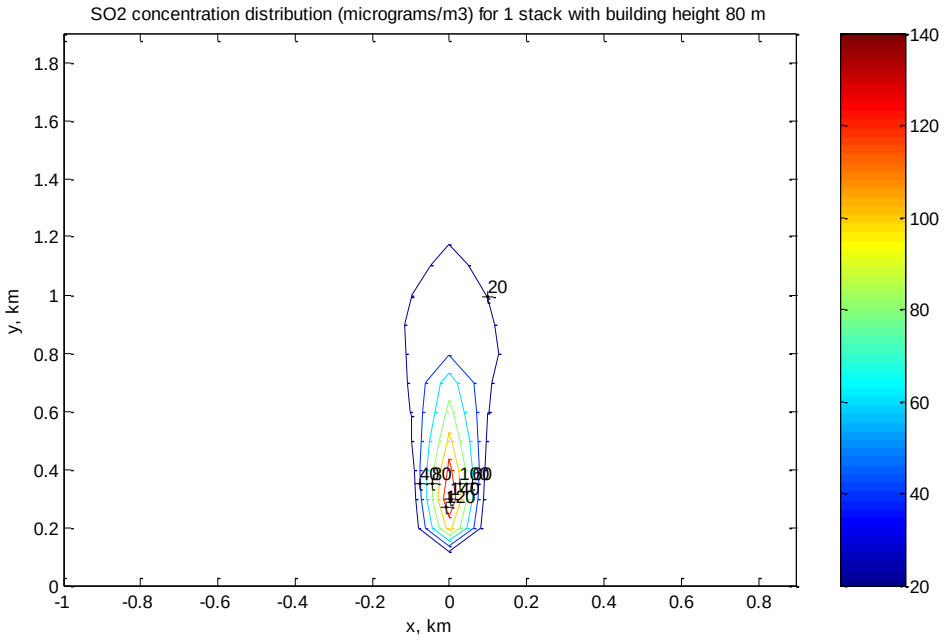

Fig. 4.69 Contour plot of SO_2 concentration distribution ($\mu g/m^3$) for 1 stack with 80 m building height

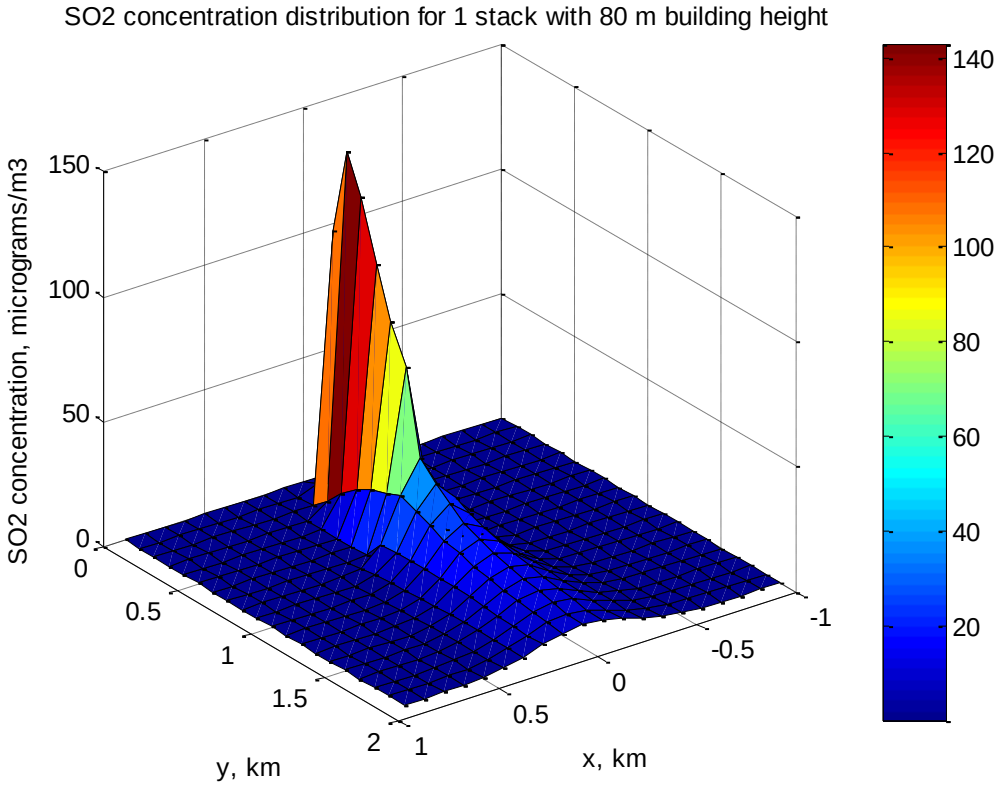

Fig. 4.70 3-D plot of SO_2 concentration distribution ($\mu g/m^3$) for 1 stack with 80 m building height

4.3.6.3 Building height 60 m

The dispersion profile of SO2 with building height 60 m are shown in Fig. 4.71 and Fig. 4.72.

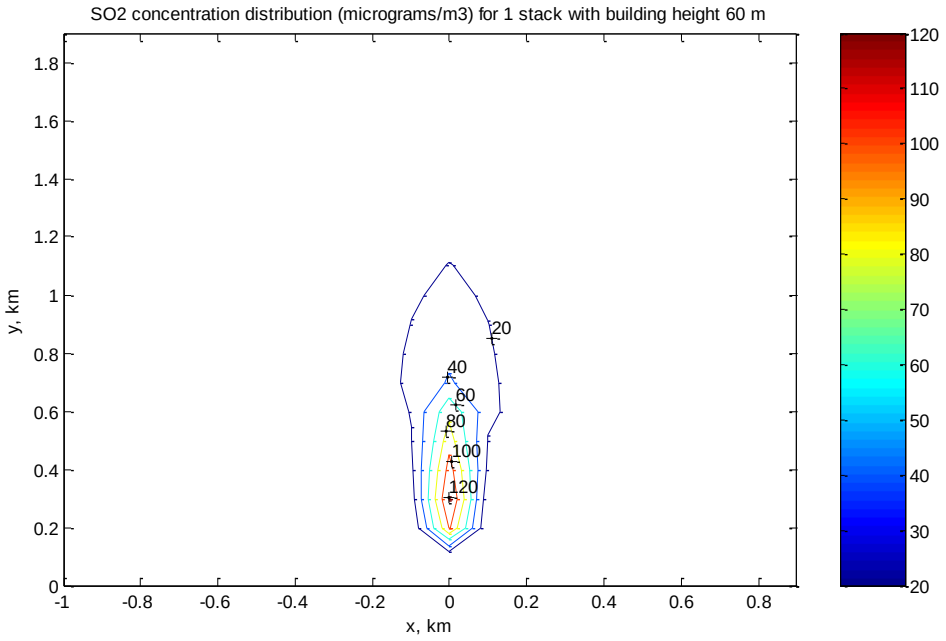

Fig. 4.71 Contour plot of SO_2 concentration distribution ($\mu g/m^3$) for 1 stack with 60 m building height

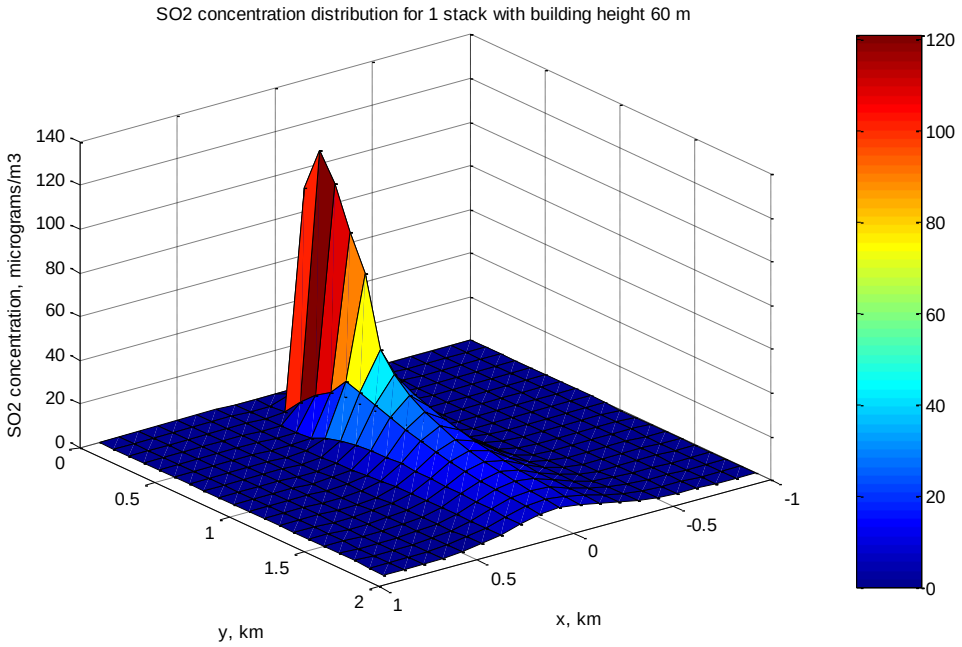

Fig. 4.72 3-D plot of SO_2 concentration distribution for 1 stack with 60 m building height

4.3.6.4 Building height 40 m

The dispersion profile of SO2 with building height 40 m are shown in Fig. 4.73 and Fig. 4.74.

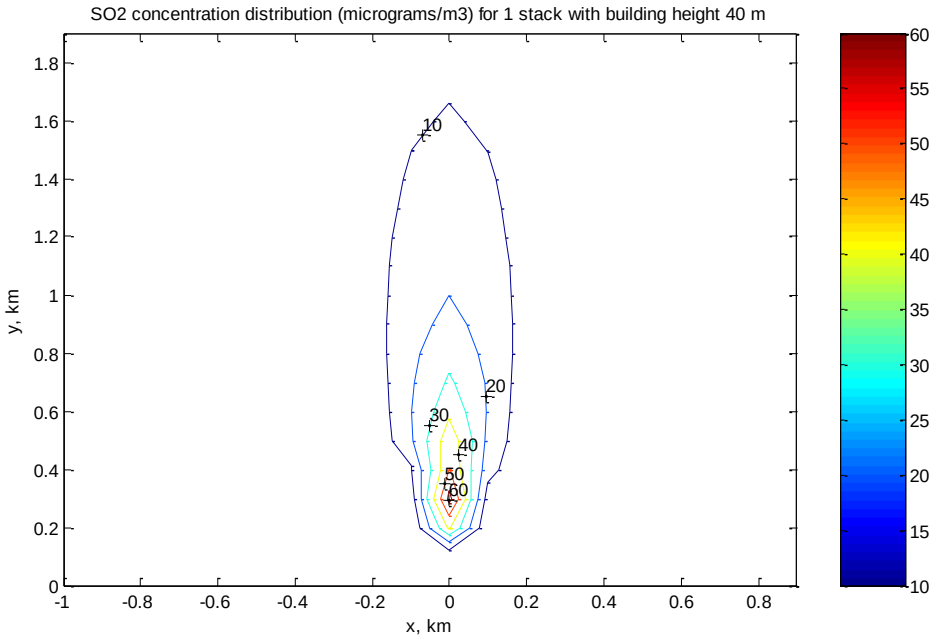

Fig. 4.73 Contour plot of SO_2 concentration distribution ($\mu g/m^3$) for 1 stack with 40 m building height

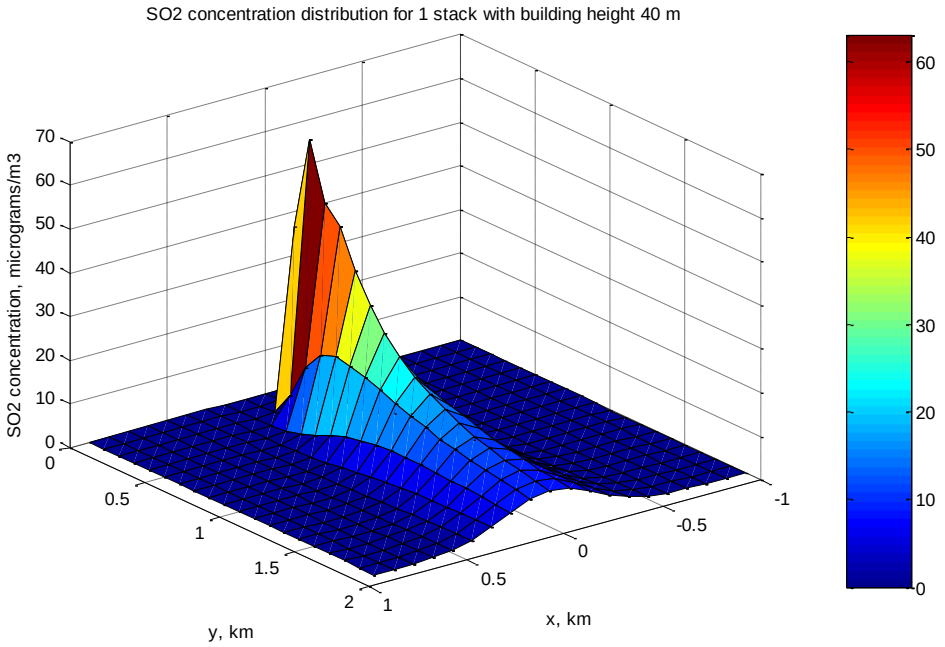

Fig. 4.74 3-D plot of SO_2 concentration distribution for 1 stack with 40 m building height

4.3.6.5 Building height 20 m

The dispersion profile of SO2 with building height 20 m are shown in Fig. 4.75 and Fig. 4.76.

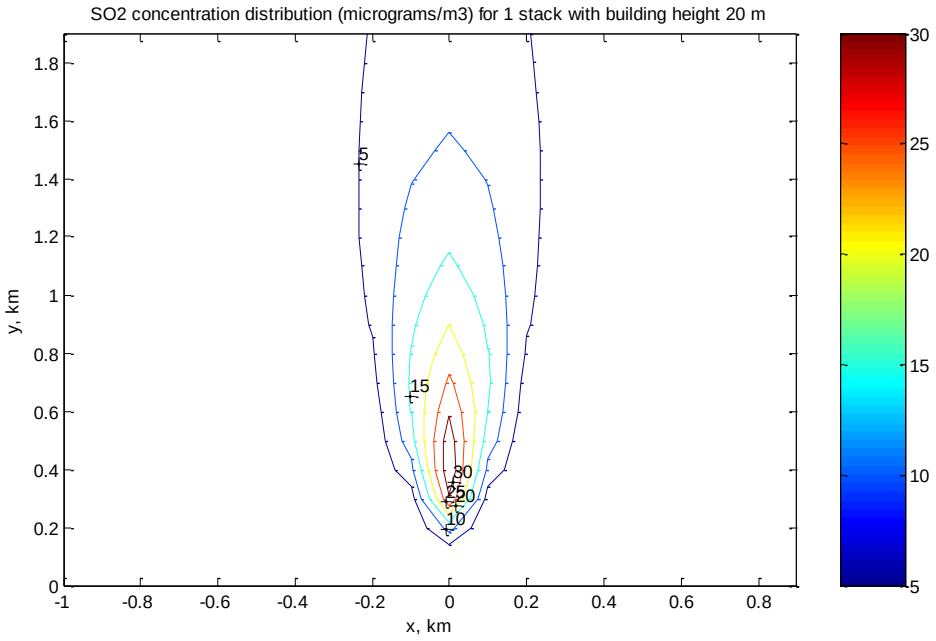

Fig. 4.75 Contour plot of SO_2 concentration distribution ($\mu g/m^3$) for 1 stack with 20 m building height

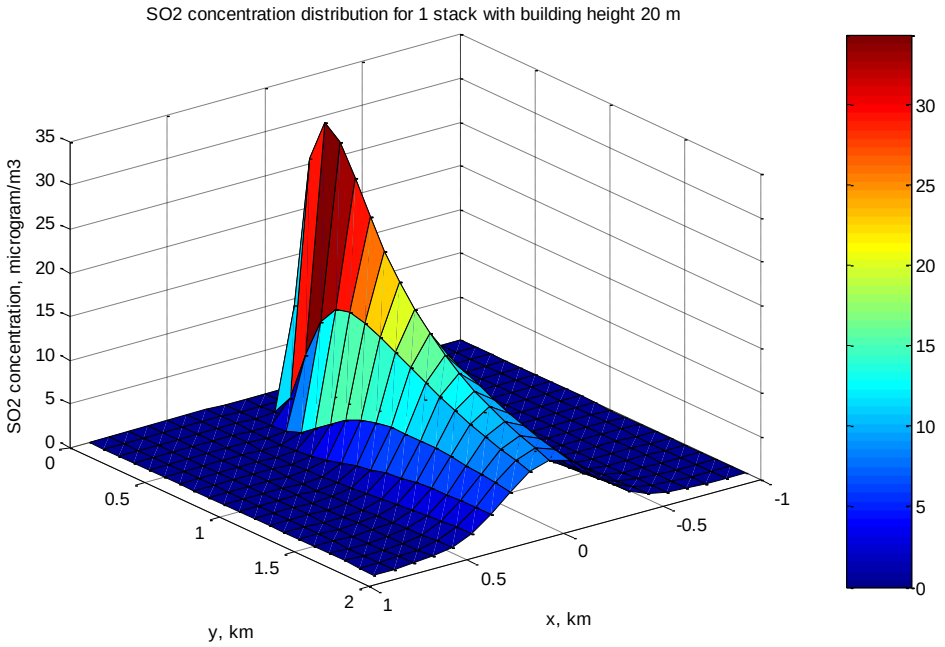

Fig. 4.76 3-D plot of SO_2 concentration distribution for 1 stack with 20 m building height

4.4 24-hour average dispersion profile of SO_2 for one stack

SO2 dispersion profile in hourly changing wind speed and direction for 24 hours is studied. Other meteorology and emission data remains constant.

4.4.1 Meteorology data

Table 4.32 Meteorology data 3

Parameter	**Value**
Pasquill-Gifford Stability Class	Neutral (D)
Averaging time	10 min
Atmospheric pressure	1000 mb
Mixing height	6000 m
Height wind is recorded	10 m
Terrain type	Urban
Stack tip downwash	Enabled

4.4.2 Emission data

Table 4.33 Emission data 3

Parameter	**Value**
Stack inner diameter	5 m
Flue gas temperature	450 K
Mass flowrate of pollutant SO_2	5 g/s
Half-life of pollutant SO_2	14400 s

The wind velocity and wind direction varies based on data collected from Perkhidmatan Kajicuaca Malaysia weather station at Butterworth for the date 1st of January 2001 from 1.00 am to 12 am.

Table 4.34 Wind direction and speed for every hour data collected from Perkhidmatan Kajicuaca Malaysia weather station at Butterworth for the date 1st of January 2001 from 1.00 am to 12 am

Hour	**Wind direction (radian)**	**Wind speed (m/s)**
1	1.571	0.8
2	0.698	0.6
3	1.222	0.9
4	1.746	0.9
5	1.369	0.9
6	1.222	1.0
7	6.248	0.3
8	1.222	1.7
9	1.047	2.1
10	1.222	1.1
11	0.698	1.3
12	5.062	3.1
13	5.237	5.1
14	5.237	5.1
15	5.237	4.8
16	5.586	3.9
17	5.760	1.9
18	1.396	2.3
19	1.571	2.4
20	0.698	1.4
21	1.222	1.2
22	5.935	1.2
23	6.248	2.6
24	0.349	1.7

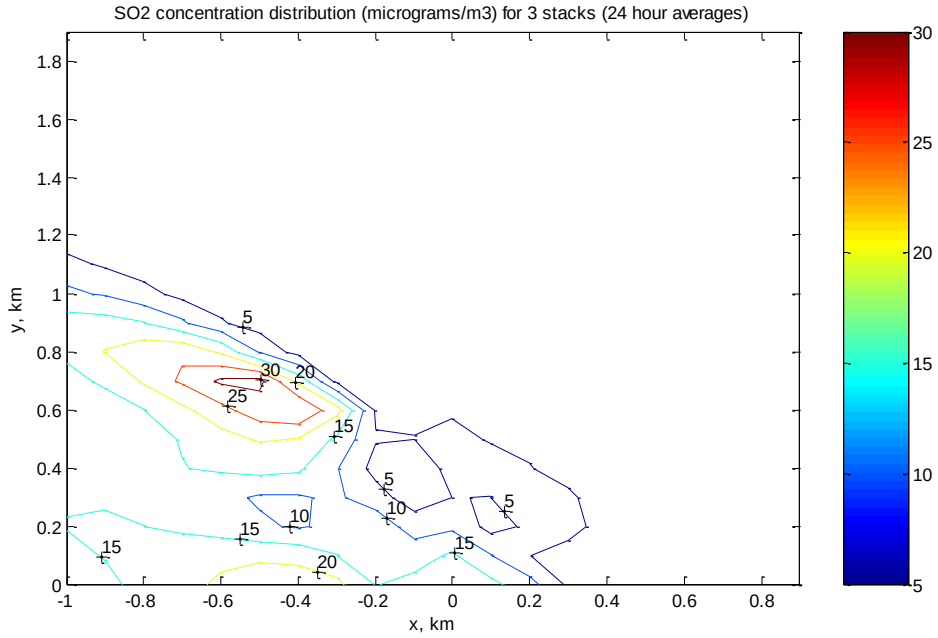

Fig. 4.77 Contour plot of SO_2 concentration distribution ($\mu g/m^3$) for 1 stack (24 hour averages)

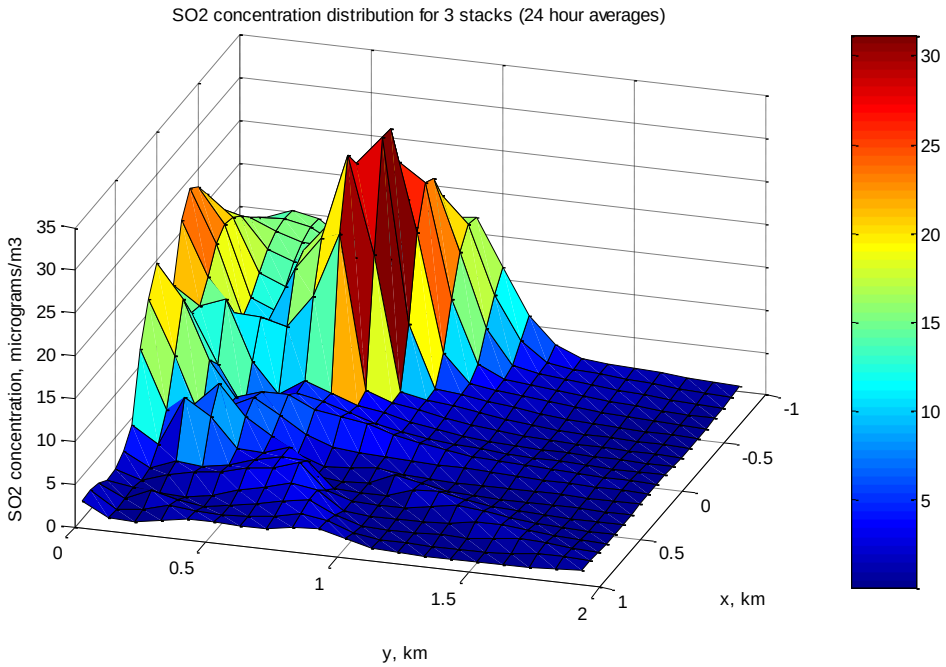

Fig. 4.78 3-D plot of SO_2 concentration distribution for 1 stack (24 hour averages)

4.5 Effect of dry deposition of particulates with 30 µm diameter and 300 g/cm^3 density on dispersion profile

Emission and meteorology data remains constant with the addition of enabled dry deposition option and particulate density and diameter.

Table 4.35 Particle density and diameter

Parameter	**Value**
Particulate density	300 g/cm^3
Particulate diameter	30 µm

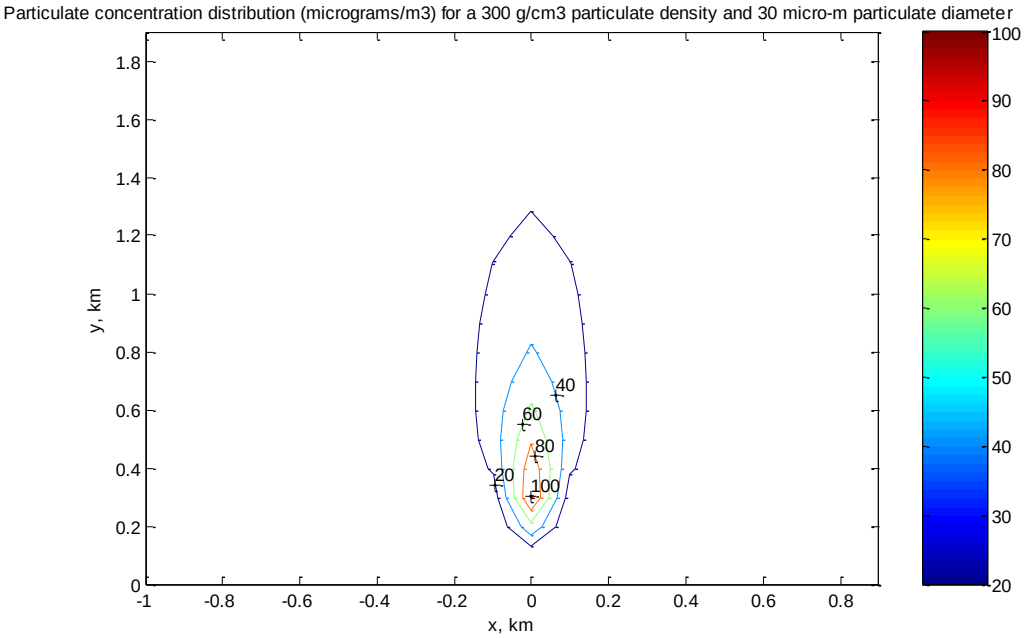

Fig. 4.79 Contour plot of particulate concentration (µg/m^3) distribution for a 300 g/cm3 particulate density and 30 µm particulate diameter

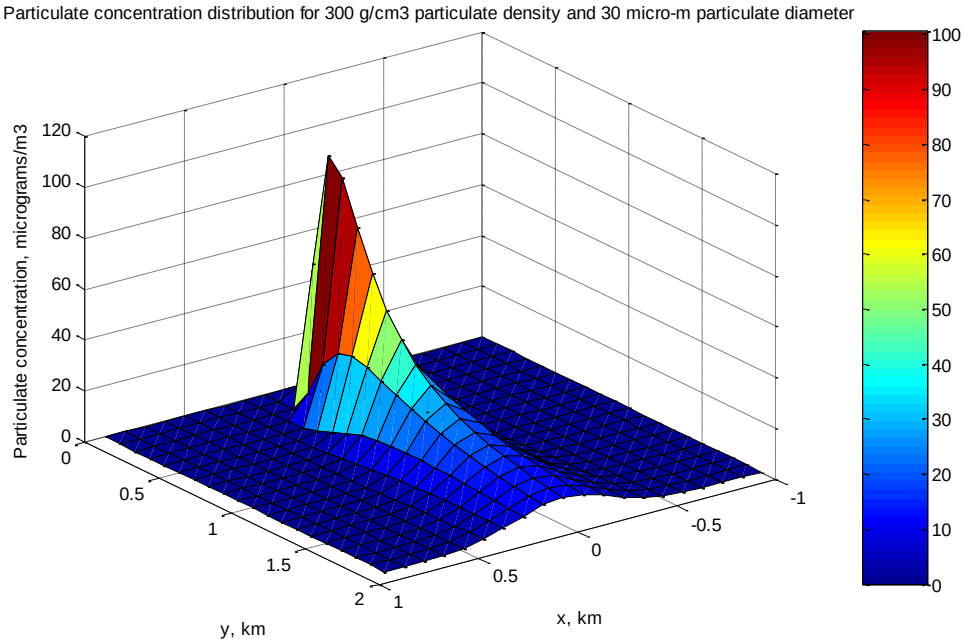

Fig. 4.80 3-D plot of particulate concentration distribution for a 300 g/cm3 particulate density and 30 µm particulate diameter

5.0 OVERALL DISCUSSION

HAWA is not without limitations. It is imperative to be aware of the limitations so that HAWA can be used properly. The limitations of this model includes,

1. Only valid beyond 100 meters.
2. Not valid for winds below 1 ms^{-1} (EPA suggested setting the wind speed to $1ms^{-1}$ in cases where the wind is below this level).
3. Not suitable for extreme meteorological conditions.

Longer average times increases the accuracy of the model compared to shorter average times. Although HAWA can calculate one run at a time and generate one text file and .m file with each run, there is a way to calculate up to any amount of average time desired. Each run requires new input of meteorology and emission data. Using the Matlab file generated, each 'z' value in the .m file is added with the next 'z' value for how many hour averages that the user decided. The sum is then divided by the amount of 'z' value that has been added to get the specific hour averages that the user desired. This means that the .m file would be required to be edited.

The "Save as Matlab file…" command automatically creates a .m file that could be loaded up to Matlab 6.0. It is required to input the minimum and maximum x coordinates with the minimum and maximum y coordinate with the distance between each point in the "Grid" window. The distance between maximum and minimum x and y coordinate must be the same length or the .m file would not be constructed properly. HAWA may need some time in generating the .m file so it is suggested to leave it to calculate without performing other commands until it has finish or it will freeze and would force to shut down or develop an unfinished .m file.

Naturally, HAWA calculates slower with increasing receptor points due to the large amount of equations to run through just by calculating one receptor point. HAWA is particularly slow when displaying the results of the calculation on screen in text form when displaying large amount of receptor points (e.g. more than 100 receptor points). This is because every time the screen scrolls down, each point would be calculated

again. I recommend using the "Save as text file…" command to automatically generate a text file with the same data displayed on screen, except that it is faster.

It is important to input appropriate meteorology and emission data from each of the point sources for HAWA to provide reasonable estimate of the pollutant dispersion. This was stressed by many air pollution modelers in attempting to simulate the pollution dispersion. Inaccurate meteorology and emission data will result in serious misjudgment of the actual impact of the sources to the environment.

It is recommended by the EPA to have at least 5 years worth of hourly meteorological data from off site weather station or 1 year of hourly meteorological data on site to conduct impact assessment of sources (modeling). Maximum load and half load source emission data are also suggested.

5.1 Discussion

In the previous chapter, a number of runs were conducted to show the ability of HAWA to simulate air pollutant dispersion for different type of stack location and atmospheric condition. It can be seen from the results that the pollutant dispersion for different stability class (ranging from very unstable to stable) would present a different type of dispersion profile.

5.1.1 Pasquill-Gifford stability classes

Very unstable (or Pasquill-Gifford stability class A) atmospheric condition would result in higher maximum pollutant concentration in close proximity to the source. As the result of this, it is the most undesired atmospheric condition. The main reason of emission of pollutants is the hope of maximum dispersion of pollutant in the atmosphere. This would lower concentration of the pollutants in the environment. Average and strong north or south wind describe the unstable (very unstable to slightly unstable) atmosphere condition. This condition is rare at night or day.

Moderately unstable (Pasquill-Gifford stability class B) atmospheric condition, in reference to the result in the previous section, has the same dispersion profile as stability class A. This is due to the fact that the

dispersion parameter equations are similar for both stability classes A and B for urban terrain. Dispersion parameters describe the behavior of the atmosphere and are essential in determining the type of air pollutant dispersion profile.

Slightly unstable (Pasquill-Gifford stability class C) atmospheric condition allows better dispersion of pollutants from point sources. Maximum pollutant concentrations are lower compared to the 2 previous stability class with it occurring further away from the source. This dispersion profile has lower average concentration downwind from the source.

Neutral (Pasquill-Gifford stability class D) atmospheric condition is the preferred stability class used when modeling the impact of sources to the environment in absence of complete meteorological data. This is because it is frequent with less strong winds during day or night. The result show better dispersion profile of the pollutants, thus lower maximum concentration further from the source.

Slightly stable and stable (Pasquill-Gifford stability class E and F) atmospheric conditions are almost identical because of the same dispersion parameter equations used for urban terrain. Stable atmospheric conditions occur during low or calm winds that may be north-south wind or even east wind. This condition would produce maximum pollutant concentration dispersion.

5.1.2 Stack height

From the results in the previous section, it can be seen that the higher the stack is, the lesser the maximum ground-level concentration. Stacks are needed to be designed to be able to contribute less than allowable ground-level pollutant concentration at all meteorological condition. Minimum stack height is needed to ensure that the latter is followed and at the same time cost effective.

5.1.3 Stacks aligned with the x-axis

The stacks' height greatly influences the dispersion profile. The dispersion of pollutants, where the stacks are 50 m high, is identical with the dispersion of one stack for distances below 1200 m away from the

stacks. Further this point, the pollutants from all 3 stacks start to combine, making the region with 10 $\mu g/m^3$ pollutants large. For stacks that are all 100 m, pollutants from each stack start to combine at 1200 m but with lower concentration (5 $\mu g/m^3$). Stack combination of a stack with 100 m stack height and 2 stacks with 50 m stack height, shows that 100 m stack does not effect the pollutant dispersion of the other 2 shorter stacks.

5.1.4 Stacks aligned with the y-axis

Stacks aligned with the y-axis also demonstrate the effect of stack height on pollutant dispersion. The lowest concentration of pollutants for this type of stack configuration is 5 $\mu g/m^3$ and ranges up to 45 $\mu g/m^3$, where the stacks are all 100 m tall. Naturally, the highest pollutant concentration occurs when the stacks are all 50 m tall from 20 $\mu g/m^3$ to 140 $\mu g/m^3$.

5.1.5 Stacks with L-shaped configuration with different stack height

Stack height of 50 m for all stack has a highest concentration of 120 $\mu g/m^3$ and lowest concentration at 20 $\mu g/m^3$. Stack height of 100 m for all stack, on the other hand, has a highest concentration of 35 $\mu g/m^3$ and lowest at 5 $\mu g/m^3$. In-line 2 stacks with 50 m stack height will cause relatively high maximum concentration downwind compared to other stack configurations

5.1.6 Effect of building height on SO_2 dispersion profile

It can be seen from the results that the higher the building, the more affected the plume would be caused by the building. The highest maximum concentration is at 140 $\mu g/m^3$ from building height of 100 m to 80 m. The building causes the pollutants to retain longer in the region between the stack and building causing pollutant build up. By 60 m building height, the plume downwind at 800 m would not be affected by the building (maximum concentration at 120 $\mu g/m^3$). The plume is furthermore not influence by the building (40 m building height) at 400 m from the stack maximum concentration at 60 $\mu g/m^3$). Finally, at 20 m building height, the building has no influence on the plume maximum concentration at 30 $\mu g/m^3$) because it is too short compared to the stack height (50 m).

5.1.7 24-hour average dispersion profile of SO2 for one stack

Actual wind data collected from Butterworth weather station shows that wind speed and direction are never constant in real life situation. Wind plays an important role in determining the pollutant dispersion. One stack emitting SO2 is modeled based on the actual wind data mentioned above to produce a 24-hour (data recorded each hour for 24 hours and divided by 24) average dispersion of pollutants. It can be seen that wind is more inclined coming from the south-east resulting in higher pollutant concentration north-west of the stack. Highest pollutant concentration recorded in this direction at 30 $\mu g/m^3$ (x-coordinate: 0.8, y-coordinate: -0.5).

5.1.8 Effect of dry deposition of particulates with 30 µm diameter and 300 g/cm^3 density on dispersion profile

Larger or heavier particles would descend down to ground-level faster compared to gases or lighter particles (below 20 µm). Large or heavy particles are categorized as particles that are bigger than 20 µm. Particulates of 30 µm diameter and 300 g/cm^3 density would result in maximum ground-level concentration of 100 $\mu g/m^3$ at a close distance from the stack (300 m).

6.0 CONCLUSION

A program capable of modeling air pollution dispersion has been successfully designed and implemented as the objective of this study intended. A program that is able to model using a Gaussian-based equation with factors accounting for stack tip downwash, building downwash, dry deposition, wet deposition, and rural or urban terrain.

This program called HAWA is based on the equation used in Industrial Source Complex 3 developed by EPA using FORTRAN language. HAWA is much easier to use compared to ISC3 where a little computer programming knowledge and complex data input are needed.

6.1 Case study

The case study conducted with the results shown in chapter 4 shows the capability of HAWA being able to model different type of atmospheric conditions, stack configuration, varying stack height, different building heights, and particulate emissions. The mentioned parameters are important for the users to be able to decide on the best stack configuration or stack design that will not affect the surrounding atmospheric pollution condition.

Different atmospheric condition case study using Pasquill-Gifford stability class, displays that the unstable condition (high winds, strong solar radiation striking ground) will cause maximum ground level concentration very close in proximity with the source. Stable condition (calm winds, weak solar radiation), will disperse the pollutants in a larger area resulting in lower ground level concentration further away from the source. Stable condition is predominant in normal Malaysian weather. It is used in absence of precise meteorological data or impact assessment (worst case scenario).

Based on the results, higher the stack height will result in lower the maximum ground level concentration. The stack designer will need to determine the best stack height which is cost efficient as well as following the guideline in ground level concentration of pollutants permitted by Department of Environment of Malaysia (DOE).

Different stack height and different stack configuration will ultimately yield different dispersion profile of pollutants. Based on 3 stack configuration, 50 m stack height for all 3 stacks will likely cause the highest ground level concentration of pollutants while 100 m stack for all 3 stacks will cause the lowest. Logically, the concentration of the stack behind of a directly upwind stack will add up to the pollutants emitted by the stack in front resulting in higher concentration downwind. It is advisable then to have a stack configuration where the either of the inline stack higher than the other stack or both stack designed using the best stack height. All 3 stacks in-line will cause the highest ground level concentration, so this type of stack configuration is undesirable.

Tall buildings downwind of source can cause a turbulent region (wake region) in the plume causing high ground-level concentration of pollutants. It must be noted that Gaussian-based equations are not suited to model accurately the dispersion profile of pollutants in turbulent regions. According to the results, building height is needed to be lower than stack height, so that the plume is not affected by the building. At least about 20 m building height below stack height is required to avoid causing wake regions. Rule of thumb of most stack designer is to design the stack to have a stack height of at least 2.5 times the height of the highest building close to the stack. More accurately, the criteria to determine whether a plume is affected by building wakes is when the plume height to building height ratio is less than or equal to 1.2.

Impact assessment of a source to the surrounding environment requires hourly meteorology data that extends up to 5 years (off-site data) or 1 year (on-site data) so that all meteorology conditions of a given site can be determined. This is because of the need to determine the worst meteorology condition that will cause the worst air pollution dispersion scenario for that particular source. Only this way will the model depict the real impact of a source to environment. Longer averaging time will give better estimates of the concentration of the pollutants.

REFERENCES

Atkinson, D. G., Bailey, D. T., & Irwin, J. S. (1997). Improvements to the EPA industrial source complex model. *Journal of Applied Meteorology*. **36**, 1088 – 1095.

Bowman, W. A. (1334). Maximum ground-level concentrations with downwash. *Journal of the Air & Waste Management Association*. **44**, 1124 – 1128.

Brunner, C. R. (1985). *Hazardous Air Emissions from Incineration*. Reston Va.

Canepa, E., Modesti, F., & Ratto, C. F. (2000). Evaluation of the SAFE_AIR code against air pollution field and laboratory experiments. *Atmospheric Environment*. **34**(28), 4805 – 4818.

Carslaw, D. C. & Beevers, S. D. (2002). Dispersion modeling considerations for transient emissions from elevated point sources. *Atmospheric Environment*. **36**(18), 3021 - 3029.

Cheremisinoff, P. N. ed. (1989). *Encyclopedia of Environmental Control Technology, Volume 2 Air Pollution Control*. Houston, TX: Gulf Publishing Company.

Cooper, C. D. & Alley, F. C. (1994). *Air Pollution Control A Design Approach*, 2nd ed. Prospect Height, Illinois: Waveland Press, Inc.

Davidson, M. J., Snyder, W. H., & Lawson, R. E. Jr. (1996). Wind tunnel simulations of plume dispersion through groups of obstacles. *Atmospheric Environment*. **30**(22), 3715 – 3731.

Davidson, M. J., Mylne, K. R., & Jones, C. D. (1995). Plume dispersion through large groups of obstacles – a field investigation. *Atmospheric Environment*. **29**(22), 3245 – 3256.

European Process Safety Centre (1999). *Atmospheric Dispersion*. UK: Institution of Chemical Engineers.

Gregory, K. (2002*). Special Edition Using Visual C++ .Net*. Indianapolis, Indiana: Que Publishing.

Griffin, L. R. & Rutherford, T. L. (1994). Comparison of air dispersion modeling results with ambient air sampling data: a case study at Tacoma Landfill, a national priorities list site. *Environmental Progress*. **13**, 155 – 162.

Hales, J. M. (2002). Wet removal of pollutants from Gaussian plumes: Basic linear equations and computational approaches. Journal *of Applied Meteorology*. **41**(9), 905 – 918.

Hanly, J. R. (1996). *Essential C++ for Engineers and Scientists*. Reading, Massachusetts: Addison-Wesley.

Ishikawa, Y. & Sada, K. (2002). An atmospheric dispersion model for the environment impact assessment of thermal power plants in Japan – a method for evaluating topographical effects. *Journal of the Air & Waste Management Association*. **52**(3), 313 – 323.

Jin, A. & Chang, S. (1996). Field estimation of standard deviations for 3D Gaussian model. *Journal of Environmental Engineering*. **122**, 660-662.

Jin, H. & Raman S. (1996). Dispersion of an elevated release in a coastal region. *Journal of Applied Meteorology*. **35**, 1611 -1624.

Kumar, A., Madasu, R., & Mahurkar, A. (1995). A review of AIRSCAPE program for the ISC2 model. *Environmental Progress*. **14**, M13 – M15.

Levy, J. I. & Spengler, J. D. (2002). Modeling the benefits of power plant emission controls in Massachusetts. *Journal of the Air & Management Association*. **52**(1), 5 – 18.

Macdonald, R. W., Griffiths, R. F., & Hall, D. J. (1998). A comparison study of results from scaled field and wind tunnel modeling of dispersion in arrays of obstacles. *Atmospheric Environment*. **32**(22), 3845 – 3862.

Macdonald, R. W., Griffiths, R. F., & Hall, D. J. (1997). Field experiments of dispersion through regular arrays of cubic structures. *Atmospheric Environment*. **31**(6), 783 - 795.

Mavroidis, I., Griffiths, R. F., & Jones, C. D. (1999). Experimental investigation of the residence of contaminants in the wake of an obstacle under different stability conditions. *Atmospheric Environment*. **33**(6), 939 – 949.

Oh, H. S. & Ghim, Y. S. (2001). Numerical study of atmospheric dispersion of a substance released from an industrial complex in the southern coast of Korea. *Atmospheric Environment*. **35**(18), 3103 – 3111.

Patrick, D. R. ed. (1994). *Toxic Air Pollution Handbook*. New York: Van Nostrand Reinhold.

Rafson, H. J. ed. (1998). *Odor and VOC Control Handbook*. New York: McGraw-Hill.

Raza, S. S. & Avila R. R. (2002). A comparison of direct gamma dose rates from a stationary Gaussian plume using different models. *Nuclear Technology*. **138**, 211 – 216.

Rege, M. A. & Tock, R. W. (1996). Estimation of point-source emissions of hydrogen sulfide and ammonia using a modified Pasquill-Gifford approach. Atmospheric Environment. **30**(18), 3181 – 3195.

Roberts, P. T. *et. al* (1994). Wind-tunnel studies of roughness effects in gas dispersion. *Atmospheric Environment*. **28**(11), 1861 – 1870.

Schulman, L. L., Strimaitis, D. G., & Scire, J. S. (2000). Development and evaluation of the PRIME plume rise and building downwash model. *Journal of the Air & Waste Management Association*. **50**(3), 378 – 390.

Schwede, D. B. & Paumier, J. O. (1997). Sensitivity of the Industrial Source Complex model to input deposition parameters. *Journal of Applied Meteorology*. **36**, 1096 – 1106.

Seika, M. *et. al* (1998). Ambient background model (ABM): development of an urban Gaussian dispersion model and its application to London. *Atmospheric Environment*. **32**(11), 1881 – 1891.

Seinfeld, J. H. (1975). *Air Pollution, Physical and Chemical Fundamentals*. New York: McGraw-Hill Book Company.

Singh, S., Fulker, M. J., & Marshall, G. (1994). A wind-tunnel examination of the variation of sigma Y and sigma Z with selected parameters. Atmospheric Environment. 28(11), 1837 – 1848.

Sharan, M., Yadav, A. K., & Singh, M. P. (1996). A mathematical model for the dispersion of air pollutants in low wind conditions. *Atmospheric Environment*. **30**(8), 1209 – 1220.

Sharan, M., Yadav, A. K., & Singh, M. P. (1995). Comparison of sigma schemes for estimation of air pollutant dispersion in low winds. *Atmospheric Environment*. **29**(16), 2051 – 2059.

Stern, A. C. (1976). *Air Pollution, Volume I Air Pollutants, Their Transformation and Transport*, 3rd ed. New York: Academic Press.

Stern, A. C. ed. (1977). *Air Pollution, Volume II The Effects of Air Pollution*, 3rd ed. New York: Academic Press.

Straja, S. (1994). The importance of the pollutant dispersion along the nominal wind direction. *Atmospheric Environment*. **28**(2), 371 – 374.

Strauss, W. ed. (1971). *Air Pollution Control, Part I*. Victoria, Australia: Wiley-Interscience.

U.S. Environmental Protection Agency (1987), *Guideline on Air Quality Models, Revised*. Research Triangle Park, NC: U.S Environmental Protection Agency.

U.S. Environmental Protection Agency (1992). *Screening Procedures for Estimating the Air Quality Impact of Stationary Sources, Revised*. Research Triangle Park, NC: U.S Environmental Protection Agency.

U.S. Environmental Protection Agency (1992). *Protocol for Determining the Best Performing Model*. Research Triangle Park, NC: U.S Environmental Protection Agency.

U.S. Environmental Protection Agency (1995). *User's Guide for the Industrial Source Complex (ISC3) Dispersion Models, Volume II – Description of Model Algorithms*. Research Triangle Park, NC: U.S Environmental Protection Agency.

Venkatesan, R., Mathiyarasu, R., & Somayaji, K. M. (2002). A study of atmospheric dispersion of radionuclides at a coastal site using a modified Gaussian model and a mesoscale sea breeze model. *Atmospheric Environment*. **36**(18), 2933 – 2942.

Venkatesan et. al (2001). A complex terrain dispersion model for regulatory applications. *Atmospheric Environment*. **35**(24), 4211 – 4221.

Wang, I. T. (1996). Determination of transport wind speed in the Gaussian plume diffusion equation for low-lying point sources. *Atmospheric Environment*. **30**(4), 661 – 665.

Wark, K. & Warner, C. F. (1976). *Air Pollution, The Origin and Control*. New York: IEP A Dun-Donnelley Publisher.